UNIVERSIDADE DA BEIRA INTERIOR
Engenharia

Aircraft Attitude Tracking using a Model Reference Adaptive Control

(versão corrigida após defesa)

Emanuel da Costa Castanho

Dissertação para obtenção do Grau de Mestre em
Engenharia Aeronáutica
(ciclo de estudos integrado)

Orientador: Prof. Doutor Kouamana Bousson

Covilhã, janeiro de 2020

Dedication

To my parents, Eduardo Castanho and Virgínia Costa, for helping me both emotionally and financially even miles away. The fact that they believed in my learning potential was essential in order to achieve this long academic journey.

To my two sisters, Marina and Teresa, for all their support.

To all my other family members and friends for always being willing to help me.

Acknowledgments

First, I would like to thank my academic supervisor Dr. Kouamana Bousson for suggesting me a very interesting, yet challenging, dissertation theme. His knowledge sharing, motivational speeches, as well as his humor and respect for the students were a great help to keep the focus and the calm during the realization of this thesis.

Secondly, I am grateful to all the educational establishments and professors who, over the years, have helped me in some way to build my intellectual personality, allowing me to be where I am today.

Finally, I would like to thank some colleagues for sharing useful engineering and aeronautical information.

Resumo

O controlo de voo de aeronaves é um assunto importante e interessante, no qual uma ampla gama de habilidades e esforços de engenharia são alinhados, a fim de projetar um controlador capaz de garantir estabilidade, evitar ocorrência de falhas e em certos casos contribuir para um voo completamente autónomo. Durante o voo, uma aeronave apresenta um movimento tridimensional combinado que pode ser decomposto em um movimento simétrico ou longitudinal no eixo de arfagem e um movimento assimétrico ou latero-direcional nos eixos de rolamento e guinada.

Na presente dissertação é efetuado o controlo da atitude de uma aeronave, em que um controlo adaptativo por modelo de referência (MRAC) discreto com algoritmo de traço constante é aplicado a um *F-4C Phantom*, cujo modelo é obtido por identificação de sistema através de dados gerados pelas equações de estado linearizadas para o caso longitudinal e latero-direcional. O objetivo é testar o desempenho desse tipo de controlo durante condições específicas de voo.

No caso longitudinal, a aeronave é assumida como sendo um sistema de única entrada e única saída (SISO) e são realizadas simulações para dois exemplos de dados de ângulo de arfagem, nos quais duas expressões para o controlador (clássica e penalizada) são aplicadas em cada exemplo para comparar o seu desempenho.

No caso latero-direcional, a aeronave é assumida como sendo um sistema de múltipla entrada e múltipla saída (MIMO) com número de entradas igual ao de saídas, em que o algoritmo do MRAC deve ser modificado de modo a descrever um processo de desacoplamento. Foram realizadas simulações para verificar se o controlador é capaz de lidar com a relação de acoplamento entre variáveis, como velocidade lateral, ângulo de rolamento, ângulo de *aileron* e ângulo do leme de direção.

O tipo de controlo adaptativo estudado apresentou bons resultados nos dois casos de estudo, seguindo o sinal de referência sem discrepâncias. A escolha das condições iniciais da simulação também é analisada nesta dissertação a fim de evitar saturação dos atuadores.

Palavras-chave

Atitude da aeronave, controlo adaptativo, desacoplamento, MRAC, tempo discreto.

Abstract

A discrete-time explicit Model Reference Adaptive Control (MRAC) with constant trace algorithm is applied to a linearized aircraft model during longitudinal and lateral-directional motions in order to test the performance of this type of control during specific flight conditions. The model was obtained through system identification with data generated from the linearized state equations of the F-4C.

In the longitudinal case the aircraft behaves like a Single-Input-Single-Output (SISO) system and simulations are performed for two examples of pitch angle data, in which two expressions for the control (classic and penalized) are applied in each example to compare their performance.

In the lateral-directional case the airplane behaves like a Multi-Input-Multi-Output (MIMO) system with equal number of inputs and outputs and the MRAC control law must be modified to describe a decoupling process. Simulations are performed in order to verify if the controller is able to handle the coupling relation between some variables, such as lateral velocity, roll angle, aileron angle and rudder angle.

The adaptive control in both study cases and for the chosen initial conditions showed good tracking when following the reference output, presenting no drift problems. The choice of the initial simulation conditions is also analyzed, in order to prevent actuator saturation.

Keywords

Adaptive control, aircraft attitude, decoupling, discrete-time, MRAC.

Contents

List of Figures

List of Tables

Nomenclature

Symbols	Description	System of Units
A	System matrix	[−]
$\hat{a}, \hat{b}, \hat{c}, \hat{d}, \hat{e}, \hat{f}, \hat{g}, \hat{h}$	Set of adaptive weights (they are time-varying)	[−]
B	Input matrix	[−]
C	Output matrix	[−]
d	Time delay	[−]
F	Adaptation gain matrix	[−]
I	Identity matrix	[−]
J	Cost function	[−]
k	Time instant, non-dimensional	[−]
m	Dimension of the state-space	[−]
n	Fixed length of the rectangular window method	[−]
N	Sensor noise vector	[−]
p	Roll rate perturbation	[rad/s]
$\hat{p}$	Estimation parameter vector	[−]
q	Pitch rate perturbation	[rad/s]
r	Yaw rate perturbation	[rad/s]
t	Time	[s]
u	Longitudinal velocity perturbation	[m/s]
u_p	Plant input	[−]
v	Lateral velocity perturbation	[m/s]
w	Vertical velocity perturbation	[m/s]
x	State vector	[−]
y_p	Plant output	[−]
Greek Letters	**Description**	**System of Units**
γ	Weighting coefficient	[−]
Δ	Controllability matrix	[−]
ε^*	“Augmented” filtered plant-model error	[−]
ζ	Rudder angle perturbation	[rad]
η	Elevator angle perturbation	[rad]
θ	Pitch angle perturbation	[rad]
Θ	Observability matrix	[−]
Λ	Eigenvalue	[−]
λ_1, λ_2	Coefficients to obtain different types of adaptation algorithms	[−]
ξ	Aileron angle perturbation	[rad]
φ	Roll angle perturbation	[rad]
Φ	Plant variable vector	[−]
ψ	Yaw angle perturbation	[rad]
Others	**Description**	**System of Units**
$(_{ref})$	Subscript to denote a reference signal	[−]
$(^T)$	Superscript to denote a transposed vector/matrix	[−]
Re	Real part	[−]
$tr[]$	Trace	[−]

List of Acronyms

CG	Centre of Gravity
FCS	Flight Control System
LTI	Linear Time-Invariant
MIMO	Multi-Input-Multi-Output
MIT	Massachusetts Institute of Technology
MRAC	Model Reference Adaptive Control
MRAS	Model Reference Adaptive System
NASA	National Aeronautics and Space Administration
PID	Proportional-Integral-Derivative
SISO	Single-Input-Single-Output
STR	Self-Tuning Regulator
U.S.	United States
UAV	Unmanned Aerial Vehicle
USAF	United States Air Force

Chapter 1 – Introduction

1.1 System of Axes and Notation

An aircraft has six degrees of freedom, being their motion described in terms of force, moment, linear and angular velocities and attitude. The attitude is defined as the angular orientation of generalized body axes with respect to earth axes [1].

In order to obtain coherent results and analyzes in the final sections of this dissertation, the system of axes considered and the positive notation of the angles for the control surfaces are shown in Figure 1.1.

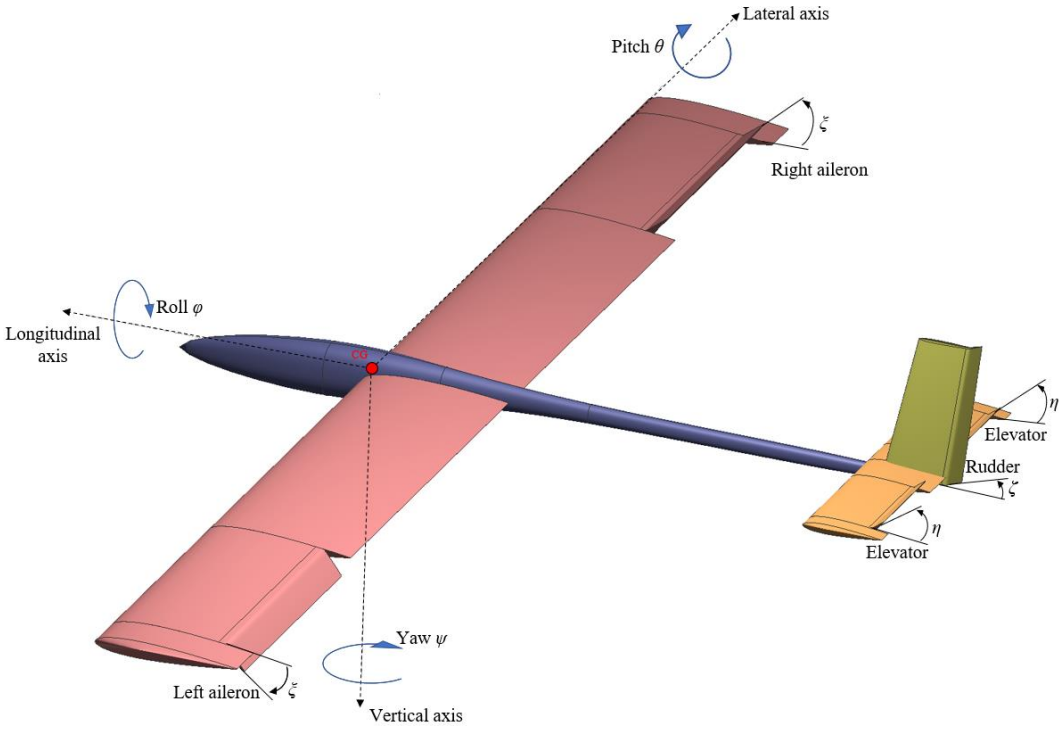

Figure 1.1 – Generalized body axis and positive notation.

Since the ailerons act differentially, ξ is considered as the mean value of the two surface angles [1].

1.2 Adaptive Flight Control

Flight vehicles, such as civilian and military aircraft, are designed to strictly follow airworthiness codes and regulations. Flight control systems are fundamental to ensure the maneuverability of the aircraft during its entire mission, being those manufactured based on modern control theory that offers a huge number of various designs and techniques [2].

Modern FCSs allow to introduce the concept of "family", where flying different aircraft can be made almost the same for pilots, reducing pilot training costs. FCSs also help control the open-loop instability characteristic of some military aircraft, which is related to agility and high-performance [3].

An aircraft is a non-linear dynamic system that changes significantly with speed, altitude, angle of attack, fuel consumption, among other factors, and in some particular cases may be subject to structural damage and component failure [4]. During its mission, the autopilot may be subject to regimes (specified by speed and altitude) in which the aircraft can be approximated by a linear system, however this only guarantees local stability. It can be said that the autopilot must adapt to almost all conditions, so it is necessary a controller that offers good results when large uncertainties are present or when the dynamics of the system are not fully known [5], [6].

Adaptive control is useful in a practical engineering environment and is a good option to design autopilots, as it requires only a limited knowledge of the plant structure [7]. It can adjust its own operation behavior in response to unpredictable changes in the dynamics of the plant or in the operating environment [3]. This type of controller differentiates from the other types because of its adaptation mechanisms, where an online estimation of the uncertainties is done and the controller adapts their own parameters to produce an input to anticipate, minimize, or overcome the undesirable deviations from the targeted specifications [8], [9].

Adaptive controllers work to overcome slowly time varying changes of any parameters of a particular system, while fixed-gain controllers are only suitable for time-invariant systems. Furthermore, modern LTI robust controllers and other fixed-gain controllers may decay in performance due to uncertain conditions. Also, robust controllers performance may not be better than adaptive control when subjected to constant or slow varying parameters [5].

Most industrial processes in the aerospace/aeronautic sector are complex and not well understood. For instance, in some cases when an aircraft is developed and modifications are necessary, a wind tunnel might be an expensive option in terms of schedule and budget, instead an adaptive control can be retrofitted into the existing production FCS, reducing costs [6].

Adaptive controllers are normally designed using methods based on Lyapunov stability theory [10] and the way the parameter estimator is combined with the control law leads to two different approaches. The first one is indirect adaptive control or explicit adaptive control, in this approach the plant parameters are constantly estimated and used to calculate the controller parameters so that the plant can mimic the behavior of the explicit plant model. The second approach is direct adaptive control or implicit adaptive control, here an implicit plant model is parameterized directly in terms of controller parameters, that is without intermediate calculations involving plant parameter estimates [5], [11].

Two important adaptive control schemes in flight control can be built from the two approaches previously mentioned. The first one is gain-scheduling and the second one is model reference adaptive control.

Gain-scheduling is the most used method for handling parameter variations in flight control systems since it is usual for an aircraft to have acceptable flying qualities at many points in its flight envelopes [12]. In this type of control, the Mach number and the altitude are measured by sensors and stored as scheduling variables in a look-up table, then the scheme detects the operating point and chooses the corresponding value from the table to change the controller [4], [11]. Although some authors consider that gain-scheduling systems are not fully adaptive, the truth is that this type of control presents satisfactory results [13]. There are, however, flight missions where gain-scheduling cannot provide good results, such as when an aircraft has just released a significant quantity of payload or when is performing rapid maneuvers [12].

The MRAC is the basis of this dissertation, thus the next subsection is focused on this type of control.

1.2.1 The Model Reference Adaptive Control (MRAC)

MRAC is a possible new flight control technology for aerospace vehicles in the near future [14]. This controller can be built using a direct or an indirect approach [11] and was originally proposed to solve performance specifications. The desired performance of the system is given in terms of a reference model that determines how the process output ideally should respond to an external command signal. The structure of a MRAC system includes a plant with a known structure but unknown parameters, reference model, adaptive law and controller. The adaptive law adjusts the controller's parameters based on the tracking error between the outputs of the plant and the reference model to ensure good results [4].

Although many physical systems exhibit non-linear characteristics, most MRAC design methods assume that the control problem is linear [15]. The MRAC system has a feedback loop composed of the plant and the controller and another feedback loop that changes the

controller parameters. A typical model reference adaptive control system block diagram based on [14] is shown in Figure 1.2.

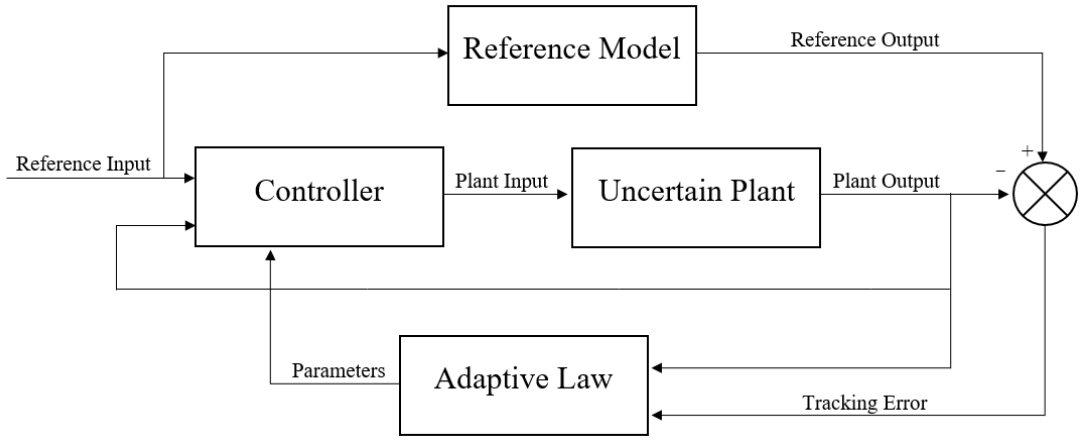

Figure 1.2 – Typical MRAC scheme.

The MRAC is one of the most popular types of adaptive control [15]. Its design for MIMO plant models with multiple sensors and actuators is more complex than in the SISO case, because of the coupling between inputs and outputs. However, as in the SISO case, the design of a MRAC for a MIMO plant can be achieved by combining a control law with an adaptive law [11].

The MRAC can be used in some situations to avoid gain-scheduling and other methods, that might be time consuming, costly and labor intensive [16].

1.3 Historical Overview

The implementation of adaptive control on aircraft flight has undergone several changes over the years. In this section a brief historical introduction will be made, where the most important dates are mentioned.

The development of adaptive control emerged in the early 1950s with the aerospace industry due to the design of autopilots for aircraft that operated in a wide flight envelope, with a large range of speeds and altitudes [17].

Due to drastic changes in flight conditions it was found that ordinary constant-gain and linear feedback control only worked well in one operating condition of the whole flight regime, so a more sophisticated controller was needed. After a significant research and development, gain-scheduling control was accepted as a suitable technique for FCSs, since there was few information available about the non-linearity of adaptive control [4], [14].

In 1951, researchers successfully developed a self-optimizing controller for the combustion engine of an aircraft, and a flight test was successfully conducted. In 1958, it was proposed the concept of a MRAS and the corresponding architecture became known as the MRAC. This

led to a design rule known as “MIT rule” by Whitaker [5], [17], however this controller had some stability problems. The MRAC was an idea from the early work on flight control that had an important impact on the adaptive control discipline.

The early 1960s began very well in terms of adaptive control theory and implementation. It was shown the applications of dynamic programming in adaptive controls [18] and it was introduced the state-space system representation as well as the use of Lyapunov stability for general control systems [9]. There were also important results in stochastic control theory and developments in system identification [4].

In 1967, an intense period of research ended dramatically with a hypersonic flight tested by NASA, in which one of the three X-15 aircraft crashed, killing the test pilot Michael J. Adams. The X-15 (Figure 1.3) was using the Honeywell’s MH-96 self-oscillating adaptive controller, which had already been used in several missiles [14], [18]. Although it was an isolated case, the fatal failure of the adaptive control in combination with the success of gain-scheduling based on air data sensors casted some doubts on fully adaptation systems in practical applications, such as aircraft flight.

Figure 1.3 - North American X-15 number 3 [19].

Research in adaptive control resurged in the 1970s, where Lyapunov stability theory was established as a foundation for model reference adaptive control and different estimation schemes were combined with various design methods. Many successful applications for MRAC and STR were reported, however theoretical results were still limited [4], [14], [18]. In 1977, the first design of a MRAC for discrete-time SISO systems in input-output form was proposed by Ionescu and Monopoli [20].

In the early 1980s, adaptive controllers started to be commercialized because of the rapid progress in microelectronics. Between the 1980s and early 1990s the robustness of adaptive controllers was addressed and studies on non-linearity with results on “feedback linearization” led to an increased understanding of adaptive control [4], [21]. Since there, engineers have been focused upon determining the stability and robustness of MIMO designs in the presence of parameter uncertainties, leading to new methods [17]. This hard work over

the years also brought the success of the X-36 aircraft (Figure 1.4) test flight which used onboard adaptive control [23].

Figure 1.4 – McDonnell Douglas X-36 [22].

In the 1990s it was introduced some concepts about neural networks as a mechanism for adaptation and, until the present, they are still being studied and applied [24].

NASA and other researchers have already contributed a lot to adaptive control technology development and research in this matter is still ongoing. UAV flight experiments regarding new adaptive controllers have been made, increasing the confidence in model reference adaptive control as a possible new flight control technology for aerospace vehicles in the near future [14].

Although the study of adaptive control has recently provided good experimental results in the aerospace industry, new problems arisen concerning the creation of the L_1-AC in 2006-2011, where the method's proofs and claimed advantages were putted into question in 2013-2014 [9], [25]. The adaptive control discipline is a constantly changing field.

1.4 Main Objectives

The aerospace industry has always been an inspiration for the design of controllers leading to a great variety of them, as it was mention in the previous section. With the recent widely spread of UAVs and increasing demands on performance and reliability for autopilots during complex missions [26], adaptive control theory should be used in order to ensure satisfactory results [8], being the MRAC a possible future option.

A literature review on the field of adaptive control shows that different types of MRAC with different aeronautical applications, such as reconfigurable flight control for airplanes that suffered structural damage [27], [28] or combat aircraft that are considered highly non-linear systems [16], [29], have been already addressed. Also, the works from [3], [30]–[32] and [33]

include topics about adaptive decoupling control of MIMO plants and MRAC with lateral-directional analysis.

The main objective of this dissertation is to verify the tracking performance of a discrete-time explicit MRAC with constant trace algorithm applied to an example aircraft. This type of control is based on the work of Landau and Lozano [20] and other authors [34], [35], presenting very few results in the literature when applied to aircraft flight control.

The full aircraft motion is analyzed, and attitude flight data is generated using the F-4C Phantom's linearized equations of motion. In the longitudinal motion case, the aircraft is assumed to be a SISO system where a classic control and a penalized one are compared in terms of operation. In the lateral-directional motion case, the aircraft is assumed to be a MIMO system and the MRAC design is slightly modified to decouple the relation between the inputs and outputs of the plant. In the first motion case, two different reference signals are used and in the last motion case, the data was generated using sensor noise.

1.5 Layout

This thesis is divided into a total of six chapters in order to provide an easy and intuitive reading:

Current Chapter - Theoretical concepts related to adaptive control are given, as well as important axes notation and main objectives of the study. A brief historical review is presented with the most important dates related to flight control in the aeronautic industry. Finally, the layout is given.

Chapter 2 - The problem is identified and explained for both motion cases. The ideal situation in contrast to reality is presented, establishing the basis for the next chapter.

Chapter 3 - It describes the MRAC algorithm in three parts. The first part is about the adaptation mechanism, the second one introduces the fundamental requirements that a system needs to fulfill to carry on with the third part that presents the control law equations. Two types of control law, classic and penalized, will be introduced. Also, a slightly modified version of the penalized control law is presented for the decoupling process of a MIMO plant.

Chapter 4 - In this section the linear case of study is described and how the flight data was generated to be used in the creation of models with system identification. It is also checked if the F-4C Phantom meets all stability, controllability and observability requirements.

Chapter 5 - The simulation, using appropriate software, is performed for the longitudinal and lateral-directional motions, where the results are shown through graphics with the concomitant analysis.

Chapter 6 - It is composed by the principal remarks, conclusions and suggestions for future studies related to the subject.

Finally, all the used bibliography and some appendix (including two papers) with relevant information are presented.

Chapter 2 – Problem Statement

2.1 Longitudinal Motion

Every pilot wants an accurate aircraft that can be effectively controlled during the path between its point of departure and its destination. However, the path of any aircraft is never completely stable without control. In order to fly a straight and level route, continuously controlling adjustments must be made, either through a human pilot or by an automatic FCS. Small corrections during several hours of flight can be exhausting for a pilot, so automatic control is a good flight implementation [12].

Usually, for study purposes and under specific conditions, a plant can be described by a set of LTI differential equations with the following state-space form:

$$\begin{aligned} \dot{x}(t) &= Ax(t) + Bu_p(t) \\ y_p(t) &= Cx(t) + N(t) \end{aligned} \tag{2.1}$$

In this longitudinal motion study, the plant is an airplane with input ($u_p \in \mathbb{R}$): elevator angle; and output ($y_p \in \mathbb{R}$): pitch angle. The engine thrust is held constant and the other output variables are not analyzed. In Figure 2.1, this paragraph is translated schematically.

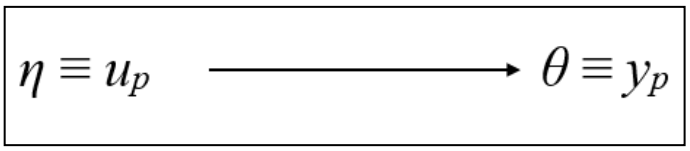

Figure 2.1 - Direct relation between variables.

Where, at each time instant, the longitudinal model is given by:

$$y_p(k) = \hat{p}^T(k-1) \cdot \Phi(k-1) \tag{2.2}$$

with:

$$\hat{p}_0^T(k) = [\hat{b}_1(k), ..., \hat{b}_{n-1}(k), \hat{a}_0(k), ..., \hat{a}_{n-1}(k)] \tag{2.3}$$

$$\hat{p}^T(k) = [\hat{b}_0(k); \hat{p}_0^T(k)] \tag{2.4}$$

$$\Phi_0^T(k) = [u_p(k-1), ..., u_p(k-n+1), y_p(k), ..., y_p(k-n+1)] \tag{2.5}$$

$$\Phi^T(k) = [u_p(k); \Phi_0^T(k)] \tag{2.6}$$

Given the measurements (Φ_0), the parameter vector should be estimated, and the appropriate control determined so that it tracks the desired reference. Since the plant has only one input and one output, this problem can be considered as SISO, being the solution presented in chapter 3 through a control algorithm. This algorithm is based on the MRAC scheme for SISO plants from Landau and Lozano [20].

2.2 Lateral-Directional Motion

The ideal situation in terms of aircraft control during lateral-directional flight is that ailerons are only responsible for rolling and the rudder is only responsible for yaw, consequently changing the lateral velocity. However, in reality there is a coupling relation between those variables.

Most control systems for industrial processes are designed for SISO plants, this is acceptable only if the coupling relations between inputs and outputs are weak. Nevertheless, there are many MIMO processes that have strong coupling relations that cannot be disregarded when designing a controller. Thus, it may be desirable to design a controller with decoupling to control the multiple outputs individually [32]. This is a MIMO problem with high coupling, in which a PID and classical control methods are impractical to yield acceptable results, although being very effective when dealing with SISO systems [3], [8].

Applying a specific type of MRAC to a MIMO system is a very interesting problem since, although several adaptive controllers have been introduced in the past few years, only some of these schemes deal with the problem of decoupled control [31].

In this lateral-directional motion study, the plant is an airplane with inputs ($u_p \in \mathbb{R}^2$): aileron angle and rudder angle; and outputs ($y_p \in \mathbb{R}^2$): roll angle and lateral velocity. In Figure 2.2, it can be seen the coupling relation between the different variables of the plant, where the superscripts *1* and *2* are used to distinguish between the two relations.

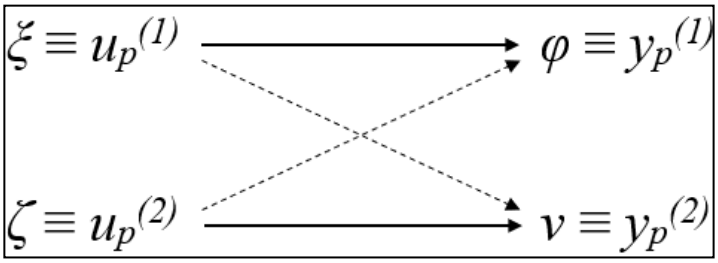

Figure 2.2 - Coupling relation between variables.

Where, at each time instant, the lateral-directional model is given by:

$$y_p^{(1)}(k) = \hat{p}^{(1)T}(k-1) \cdot \Phi^{(1)}(k-1) \tag{2.7}$$

$$y_p^{(2)}(k) = \hat{p}^{(2)T}(k-1) \cdot \Phi^{(2)}(k-1) \tag{2.8}$$

$\hat{p}(k)$ and $\Phi(k)$ must translate the decoupling process of the relation between the multi-variables of the plant. Therefore, one has the following formats:

$$\hat{p}_0^{(1)T}(k) = [\hat{d}_1(k),...,\hat{d}_{n-1}(k),\hat{e}_0(k),...,\hat{e}_{n-1}(k),\hat{c}_0(k),...,\hat{c}_{n-1}(k)] \tag{2.9}$$

$$\hat{p}^{(1)T}(k) = [\hat{d}_0(k); \hat{p}_0^{(1)T}(k)] \tag{2.10}$$

$$\Phi_0^{(1)T}(k) = [u_p^{(1)}(k-1),...,u_p^{(1)}(k-n+1),u_p^{(2)}(k-1),...,u_p^{(2)}(k-n), y_p^{(1)}(k),..., y_p^{(1)}(k-n+1)] \tag{2.11}$$

$$\Phi^{(1)T}(k) = [u_p^{(1)}(k); \Phi_0^{(1)T}(k)] \tag{2.12}$$

$$\hat{p}_0^{(2)T}(k) = [\hat{g}_1(k),..., \hat{g}_{n-1}(k),\hat{h}_0(k),...,\hat{h}_{n-1}(k), \hat{f}_0(k),..., \hat{f}_{n-1}(k)] \tag{2.13}$$

$$\hat{p}^{(2)T}(k) = [\hat{g}_0(k); \hat{p}_0^{(2)T}(k)] \tag{2.14}$$

$$\Phi_0^{(2)T}(k) = [u_p^{(2)}(k-1),...,u_p^{(2)}(k-n+1),u_p^{(1)}(k-1),...,u_p^{(1)}(k-n), y_p^{(2)}(k),..., y_p^{(2)}(k-n+1)] \tag{2.15}$$

$$\Phi^{(2)T}(k) = [u_p^{(2)}(k); \Phi_0^{(2)T}(k)] \tag{2.16}$$

Given the measurements ($\Phi_0^{(1)}$ and $\Phi_0^{(2)}$), the parameter vectors should be estimated, and the appropriate controls determined so that they track the desired references. The following section presents the algorithm that intends to solve the referred problem. This algorithm is based on the MRAC scheme for SISO plants from Landau and Lozano [20], being the penalized control law extended for MIMO plants.

Chapter 3 – The MRAC Algorithm

3.1 Adaptive Law

The adaptation algorithm is coupled with the control algorithm [36] and the most important requirement when designing an adaptive law is to achieve asymptotic tracking of a known reference signal with good stability [21]. The MRAC technique allows to easily incorporate considerations of decoupling in the adaptive design [28], so this algorithm is valid for a SISO and a MIMO plant.

The parameter estimation problem is dynamic and uses real-time measured data signals to identify linear model parameter estimates [4], [37], [38]. The adaptation mechanism is described next by a set of equations that estimate process parameters.

$$\hat{p}(k) = \hat{p}(k-1) + F(k-1)\cdot\Phi(k-d)\cdot\varepsilon^{*}(k) \tag{3.1}$$

with:

$$F(k) = \frac{1}{\lambda_1(k)}\times\left[F(k-1) - \frac{F(k-1)\cdot\Phi(k-d)\cdot\Phi^{T}(k-d)\cdot F(k-1)}{\lambda_1(k)/\lambda_2(k) + \Phi^{T}(k-d)\cdot F(k-1)\cdot\Phi(k-d)}\right]; \qquad F(0) > 0 \tag{3.2}$$

To make the algorithm implementable an expression for ε^{*}, which depends on the parameters estimated up to $k\text{-}1$, is given as:

$$\varepsilon^{*}(k) = \frac{y_p(k) - \hat{p}^{T}(k-1)\cdot\Phi(k-d)}{1 + \Phi^{T}(k-d)\cdot F(k-1)\cdot\Phi(k-d)} \tag{3.3}$$

To complete the introduction of this algorithm, one needs to choose the correct values of $\lambda_1(k)$ and $\lambda_2(k)$. The constant trace algorithm [34] is used, where the ratio between $\lambda_1(k)$ and $\lambda_2(k)$ is maintained equal to 1, while λ_1 is adjusted at each time step according to:

$$\lambda_1(k) = \frac{tr\left[F(k-1) - \dfrac{F(k-1)\cdot\Phi(k-d)\cdot\Phi^{T}(k-d)\cdot F(k-1)}{1 + \Phi^{T}(k-d)\cdot F(k-1)\cdot\Phi(k-d)}\right]}{tr\left[F(0)\right]} \tag{3.4}$$

with:

$$0 < \lambda_1(k) \leq 1;\ 0 < \lambda_2(k) < 2 \quad \forall k \tag{3.5}$$

The parameter estimates are calculated at each time sample when new measured data are available, thus the above algorithm requires that some of the data points be stored. This recursive nature avoids reprocessing old data, ensuring an efficient operation and better results [39].

Real-time parameter estimation involves adjustment of some variables, such as the variable n, to decide how long into the past the data memory will extend. This is important because, in the context of aircraft flight, there are periods of low or no excitation where the control and state variables are almost constant, leading to numerical problems for some methods when noise is present [4], [37].

Note that, during the execution of the algorithm for a MIMO plant one must use the adaptive law two times, one to update $\hat{p}^{(1)}(k)$ and another to update $\hat{p}^{(2)}(k)$.

3.2 Stability, Controllability and Observability

Before designing a control law, it is necessary to verify that the system to be studied has the requirements regarding stability, controllability and observability. In order to define these concepts, one must consider a system described by a set of equations as (2.1).

3.2.1 Dynamic Stability

There are essentially three methods to verify if a system is stable or not:

- Analysis of eigenvalues;
- Use of Lyapunov's stability theorem;
- Use of Jane Cronin's theorem.

In the present dissertation, only the first method is used in which the system from (2.1), considering $u_p=0$, is dynamically stable around equilibrium if and only if all eigenvalues of A have negative real parts, $Re(\Lambda)<0$. If there is an eigenvalue with positive real part, then the system is unstable.

If all the eigenvalues have non-positive real parts and at least one of them have a zero real part, then the matrix A is a critical matrix and the equilibrium of the system can be marginally stable [40].

3.2.2 Controllability of Dynamic Systems

The system from (2.1) is said to be controllable if it is possible by means of an unconstrained controller to guide the physical system between two arbitrarily specified states in a finite period of time [41].

With the characterization by Kalman [40], it is possible to find if a dynamic system is controllable using the controllability matrix:

$$\Delta = \left[B, AB, A^2B, ..., A^{m-1}B \right] \tag{3.6}$$

The system will be controllable if and only if, the rank of the controllability matrix is m, i.e.: $rank(\Delta)=m$.

3.2.3 Observability of Dynamic Systems

The dynamic system from (2.1) is observable, if for any $t>0$, the initial state can be determined by the control input behavior and the output in the interval $[0,t]$. In other words, the system is observable if, for any sequence of state and control vectors, the current state can be determined in a finite period of time using only outputs [41].

With the characterization by Kalman [40], it is possible to find if a dynamic system is observable using the observability matrix:

$$\Theta = \begin{bmatrix} C \\ CA \\ CA^2 \\ \cdots \\ CA^{m-1} \end{bmatrix} \tag{3.7}$$

The system is observable if the rank of the observability matrix is m, i.e.: $rank(\Theta)=m$.

3.3 Control Law

While the controlled system is operating, it is important that the adaptive law updates in real-time the controller parameters, so that the control law achieves tracking stability and performance goals, matching the plant output with the reference output [4], [34], [38].

Two types of control law are introduced in this section. They will be later compared in terms of operation during the longitudinal motion, characterized by a SISO process. In the lateral-directional motion, one of the control laws will be modified to deal with a MIMO process.

The type of cost function and method of minimization determines the properties of the adaptive control scheme [11], [42]. The first control $u_p(k)$ for SISO plants is given in the adaptive case by:

$$u_p(k) = \frac{y_{ref}(k+d) - \hat{p}_0{}^T(k) \cdot \Phi_0(k)}{\hat{b}_0(k)} \tag{3.8}$$

This control will be referred to as classic control (controller 1) in this dissertation and it is based on the control presented in [20].

In [20], the full algorithm has a polynomial that does not appear in (3.8), because it was assumed to be 1. The polynomial is called C_2-polynomial and when is equal to 1 it means that the plant-model error is cancelled d steps after the control input is applied. This C_2-polynomial plays a filtering role and the adaptive control performance will depend on its choice, since it smooths the adaptation process [43].

In general, it is not known how the controller 1 will behave towards the initial conditions imposed by the simulation, being able to present the following limitations:

- Inability to be applied to non-minimum phase systems, i.e. systems whose zeros have positive real parts [44];
- Instability, even if the system is a minimum phase system, the controller itself can provide signals in which the magnitude will increase, making it impossible for the aircraft actuators to reach such values [8].

The control study cannot be subject to problems due to the previous limitations, so the following cost function is introduced:

$$J\left(u_p(k)\right) = \left(y_{ref}(k+d) - \hat{p}^T(k) \cdot \Phi(k)\right)^2 + \gamma \cdot u_p^2(k) \ , \ \gamma > 0 \tag{3.9}$$

and can be derived as:

$$\frac{dJ\left(u_p(k)\right)}{du_p(k)} = 0 \tag{3.10}$$

The expression that minimizes the solution of (3.10) is the second control $u_p(k)$ for SISO plants, which is given in the adaptive case by:

$$u_p(k) = \frac{\hat{b}_0(k) \cdot \left[y_{ref}(k+d) - \hat{p}_0^T(k) \cdot \Phi_0(k) \right]}{\gamma + \hat{b}_0^2(k)} \tag{3.11}$$

This control will be referred to as penalized control (controller 2) in this dissertation, since it presents a coefficient γ that allows to damp the magnitude of the control. See Appendix A for more information in how to obtain the second control law from the cost function.

For MIMO plants, the control law from (3.11) needs to be slightly modified in terms of variable notation. In chapter 2 (problem statement) the coupling relation between variables of the lateral-directional motion was introduced, so one needs two different variations of (3.11) for two inputs that will be later analyzed:

$$u_p^{(1)}(k) = \frac{\hat{d}_0(k) \cdot \left[y_{ref}^{(1)}(k+d) - \hat{p}_0^{(1)T}(k) \cdot \Phi_0^{(1)}(k) \right]}{\gamma^{(1)} + \hat{d}_0^2(k)} \tag{3.12}$$

$$u_p^{(2)}(k) = \frac{\hat{g}_0(k) \cdot \left[y_{ref}^{(2)}(k+d) - \hat{p}_0^{(2)T}(k) \cdot \Phi_0^{(2)}(k) \right]}{\gamma^{(2)} + \hat{g}_0^2(k)} \tag{3.13}$$

During the execution of the algorithm one must use the two variations of the second control law for the lateral-directional motion, (3.12) to update ξ and (3.13) to update ζ, since Φ uses both set of updated values.

Chapter 4 – Case of Study

4.1 The Airplane as a Linear System

The equations of motion for an aircraft are the basis of flight dynamics and are usually written in a body fixed coordinate system, providing a better understanding of flying qualities [45]. These equations are non-linear and coupled, however depending on the flight regime, the non-linear flight dynamics can be effectively approximated at the operation point by a set of linear differential equations as (2.1), ensuring local stability i.e., satisfactory results close to an equilibrium regime [8], [28].

In this dissertation, the study was conducted with the linearized motion equations of the McDonnell F-4C, nickname: Phantom (Figure 4.1).

Figure 4.1 – McDonnell Douglas F-4C Phantom II [46].

The Phantom II was first developed for U.S. Navy fleet defense. The F-4C was the first version flown by the USAF in May 1963. Initially designated F-110A, it was also the first USAF Phantom in the Vietnam war [46]–[48].

The F-4C is a tactical fighter and twin engine supersonic jet whose primary mission is air-to-air missile combat during all weather conditions [47], [49]. Some specifications of this aircraft are presented in Table 4.1 [46].

Table 4.1 – F-4C General Specifications.

Propulsion	2x General Electric J79-GE-15
Wingspan [m]	11.71
Length [m]	17.7
Height [m]	5.02
Gross mass [kg]	26308.4
Maximum speed [km/h]	2253.1
Cruising speed [km/h]	940
Service ceiling [km]	18.2
Range [km]	2816.4
Crew	Two

According to the MIL-F-8785C specification [50], the F-4 Phantom II can be included in Class IV since it is a fighter/interceptor (high maneuverability airplane). The flight conditions on this dissertation study have been chosen to provide the Phantom with Category A and Level 1 requirements. Thus, the roll performance of this aircraft is 90º (1.571rad) of roll angle in 1.3s [1], [50].

Due to the lack of data in the literature concerning the maximum deflection values for the Phantom's aileron, elevator and rudder control surfaces, it is assumed ±25º (±0.4363rad). This is an acceptable value for most aircraft, because when the control surfaces are deflected more than 20-25 degrees, flow separation tend to occur with loss of control effectiveness [51].

The airplane motion can be decomposed into a trim and a perturbed motion. The first one is when the aircraft is in an equilibrium for a steady-level flight. The perturbed motion is a small amplitude motion about the trim condition. Because the amplitudes are assumed to be small, linearization of the equations of motion can be performed [14], being fully decoupled into longitudinal symmetric motion and lateral-directional asymmetric motion [26].

The linearized equations of the F-4C for Mach 0.6 at an altitude of 10.7km are given next, according to examples 4.3 and 4.4 in the Flight Dynamics Principles book (see [1] for more information). (4.1) is the longitudinal state equation and (4.2) is the lateral-directional state equation.

$$\begin{bmatrix} \dot{u} \\ \dot{w} \\ \dot{q} \\ \dot{\theta} \end{bmatrix} = \begin{bmatrix} 7.181\times10^{-4} & 4.570\times10^{-3} & -29.072 & -9.678 \\ -0.0687 & -0.2953 & 174.868 & -1.601 \\ 1.73\times10^{-3} & -0.0105 & -0.4462 & 1.277\times10^{-3} \\ 0 & 0 & 1 & 0 \end{bmatrix} \cdot \begin{bmatrix} u \\ w \\ q \\ \theta \end{bmatrix} + \begin{bmatrix} 1.041 \\ -6.294 \\ -4.888 \\ 0 \end{bmatrix} \eta \qquad (4.1)$$

$$\begin{bmatrix} \dot{v} \\ \dot{p} \\ \dot{r} \\ \dot{\varphi} \\ \dot{\psi} \end{bmatrix} = \begin{bmatrix} -0.0565 & 29.072 & -175.610 & 9.6783 & 1.6022 \\ -0.0601 & -0.7979 & -0.2996 & 0 & 0 \\ 9.218\times10^{-3} & -0.0179 & -0.1339 & 0 & 0 \\ 0 & 1 & 0 & 0 & 0 \\ 0 & 0 & 1 & 0 & 0 \end{bmatrix} \cdot \begin{bmatrix} v \\ p \\ r \\ \varphi \\ \psi \end{bmatrix} + \begin{bmatrix} -0.2678 & 2.0092 \\ 4.6982 & 0.7703 \\ 0.0887 & -1.3575 \\ 0 & 0 \\ 0 & 0 \end{bmatrix} \cdot \begin{bmatrix} \xi \\ \zeta \end{bmatrix} \quad (4.2)$$

4.2 Stability, Controllability and Observability

Before carrying on with further sections, one must use the airplane's linearized equations of motion and the equations introduced in section 3.2 to verify if the longitudinal system and the lateral-directional system meet all the stability, controllability and observability requirements.

4.2.1 Stability

Analyzing the dynamic stability of both motions, one can verity that for the longitudinal motion all real parts of the vector of eigenvalues (4.3) are negative, thus the system is dynamically stable near the control-state. For the lateral-directional motion all real parts of the vector of eigenvalues (4.4) are negative except for the last one, which is 0. By definition the system is critical and assumed to be marginally stable (stable but not attractive) [40].

$$\Lambda Vector = \begin{bmatrix} -0.3633 + 1.3669i \\ -0.3633 - 1.3669i \\ -0.0071 + 0.0770i \\ -0.0071 - 0.0770i \end{bmatrix} \quad (4.3)$$

$$\Lambda Vector = \begin{bmatrix} -0.1363 + 1.8107i \\ -0.1363 - 1.8107i \\ -0.6747 + 0.0000i \\ -0.0409 + 0.0000i \\ 0.0000 + 0.0000i \end{bmatrix} \quad (4.4)$$

Conclusion: The whole F-4C plant is stable.

4.2.2 Controllability

For both cases, longitudinal (4.5) and lateral-directional (4.6), and in terms of state controllability, the systems are controllable i.e., it is possible to guide the system in a finite period of time to achieve a desirable state. This condition is of particular interest since it allows the pilot, or automatic control system, to recover from airplane instability that may occur due to possible disturbances.

$$\Delta = \begin{bmatrix} 1.0410 & 142.08 & -21.870 & -257.01 \\ -6.2940 & -852.97 & 643.21 & 1240.5 \\ -4.8880 & 2.2489 & 8.1922 & -10.444 \\ 0.0000 & -4.8880 & 2.2489 & 8.1922 \end{bmatrix} \tag{4.5}$$

$$rank(\Delta) = m = 4$$

$$\Delta = \begin{bmatrix} -0.2678 & 2.0092 & 121.02 & 260.67 & -53.224 & -51.754 & -366.98 & -868.03 & 263.55 & 422.75 \\ 4.6982 & 0.7703 & -3.7592 & -0.3287 & -4.2446 & -15.460 & 6.2272 & 14.732 & 17.259 & 40.570 \\ 0.0887 & -1.3575 & -0.0984 & 0.1865 & 1.1961 & 2.3838 & -0.5748 & -0.5195 & -3.4173 & -8.1956 \\ 0.0000 & 0.0000 & 4.6982 & 0.7703 & -3.7592 & -0.3287 & -4.2446 & -15.460 & 6.2272 & 14.732 \\ 0.0000 & 0.0000 & 0.0887 & -1.3575 & -0.0984 & 0.1865 & 1.1961 & 2.3838 & -0.5748 & -0.5195 \end{bmatrix} \tag{4.6}$$

$$rank(\Delta) = m = 5$$

Conclusion: The whole F-4C plant is controllable.

4.2.3 Observability

The two cases are observable, this is verified by the rank of the observability matrix being equal to the m value in each case, longitudinal (4.7) and lateral-directional (4.8). Thus, the output/observation values of the models allow a reliable estimate of the state vector within a finite period of time.

$$\Theta = \begin{bmatrix} 0.0000 & 0.0000 & 0.0000 & 1.0000 \\ 0.0000 & 0.0000 & 1.0000 & 0.0000 \\ 0.0017 & -0.0105 & -0.4462 & 0.0013 \\ -4.9334 \times 10^{-5} & 0.0078 & -1.6860 & -0.0005 \end{bmatrix} \tag{4.7}$$

$$rank(\Theta) = m = 4$$

$$\Theta = \begin{bmatrix} 1.0000 & 0.0000 & 0.0000 & 0.0000 & 0.0000 \\ 0.0000 & 0.0000 & 0.0000 & 1.0000 & 0.0000 \\ -0.0565 & 29.072 & -175.61 & 9.6783 & 1.6022 \\ 0.0000 & 1.0000 & 0.0000 & 0.0000 & 0.0000 \\ -3.3628 & -12.017 & 26.328 & -0.5468 & -0.0905 \\ -0.0601 & -0.7979 & -0.2996 & 0.0000 & 0.0000 \\ 1.1549 & -89.193 & 590.53 & -32.546 & -5.3879 \\ 0.0486 & -1.1052 & 10.833 & -0.5817 & -0.0963 \\ 10.739 & 61.627 & -260.56 & 11.178 & 1.8504 \\ 0.1635 & 1.5188 & -9.7482 & 0.4703 & 0.0778 \end{bmatrix} \tag{4.8}$$

$$rank(\Theta) = m = 5$$

Conclusion: The whole F-4C plant is observable.

4.3 Data Generation

The measurement data, that will be used for the system identification process, is generated using the Butcher's algorithm (see Appendix B) in combination with the linearized equations of the F-4C.

System identification requires data that can translate the important dynamics of the system. Thus, to obtain a good model of the system, the data set generated in the next subsections took into account [52]:

- The use of input variations that excite the system dynamics appropriately;
- The long enough measuring of data to capture important time constants;
- Data with good signal-to-noise ratio.

4.3.1 Longitudinal Motion

With (4.1) and using the following variations in η over time:

$$\eta(t) = \begin{cases} 0 & 0 \le t < 20 \\ 0.1745 & 20 \le t < 40 \\ -0.1745 & 40 \le t < 60 \\ 0 \quad if & 60 \le t < 80 \\ 0.1745 & 80 \le t < 100 \\ -0.1745 & 100 \le t < 110 \\ 0 & 110 \le t < 120 \end{cases} \tag{4.9}$$

that represents a square wave:

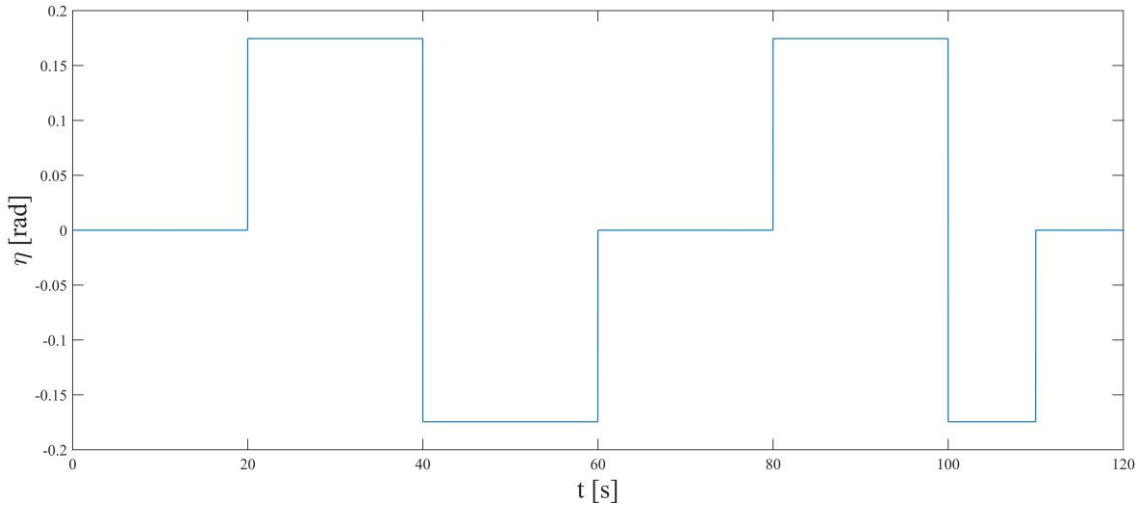

Figure 4.2 - Elevator angle perturbation over time.

and the following initial conditions:

$$x(0) = \begin{bmatrix} 5 \\ 0 \\ 0.8 \\ 0 \end{bmatrix} \tag{4.10}$$

one can apply the Butcher's algorithm with time step equal to 0.01s generating data to simulate the plant's behavior, where only the pitch angle perturbation is analyzed:

$$[\theta] = [0 \quad 0 \quad 0 \quad 1] \cdot \begin{bmatrix} u \\ w \\ q \\ \theta \end{bmatrix} + [0] \tag{4.11}$$

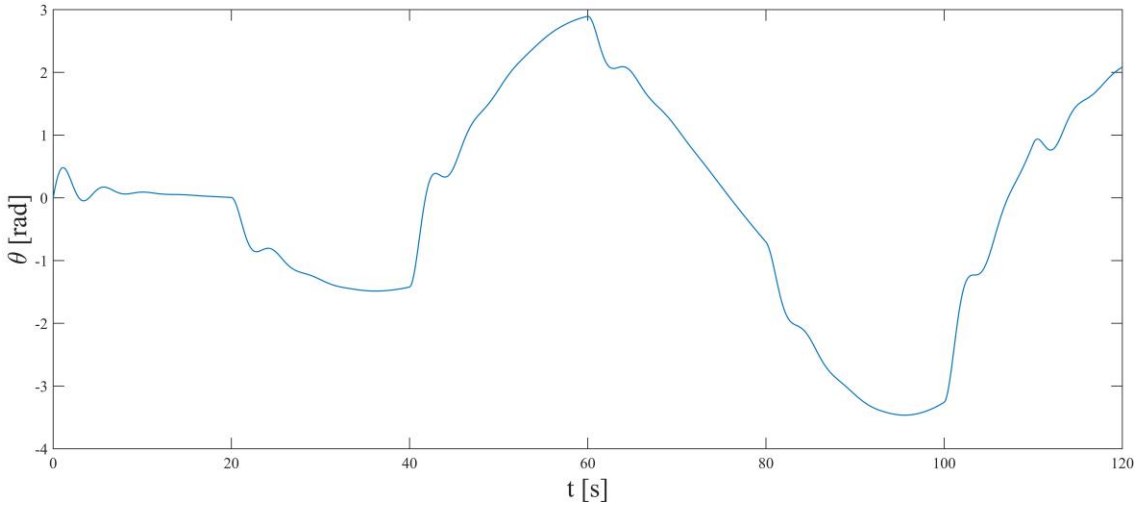

Figure 4.3 - Pitch angle perturbation generated.

The time step indicated during 120s generates a matrix in *Microsoft® Excel®* of 12000 rows (from $k=0$ to $k=11999$) and 3 columns (t, η, θ) which is important for the adaptive algorithm.

4.3.2 Lateral-Directional Motion

Using (4.2) with the following variations in ξ and ζ over time:

$$\xi(t) = \begin{cases} 0 & 0 \le t < 20 \\ 0.08727 & 20 \le t < 30 \\ -0.08727 & 30 \le t < 40 \\ 0 & if \quad 40 \le t < 60 \\ -0.08727 & 60 \le t < 80 \\ 0.08727 & 80 \le t < 100 \\ 0 & 100 \le t < 120 \end{cases} ; \quad \zeta(t) = \begin{cases} 0 & 0 \le t < 20 \\ 0.04363 & 20 \le t < 30 \\ -0.04363 & 30 \le t < 40 \\ 0 & if \quad 40 \le t < 60 \\ -0.04363 & 60 \le t < 80 \\ 0.04363 & 80 \le t < 100 \\ 0 & 100 \le t < 120 \end{cases} \tag{4.12}$$

that represents a square wave:

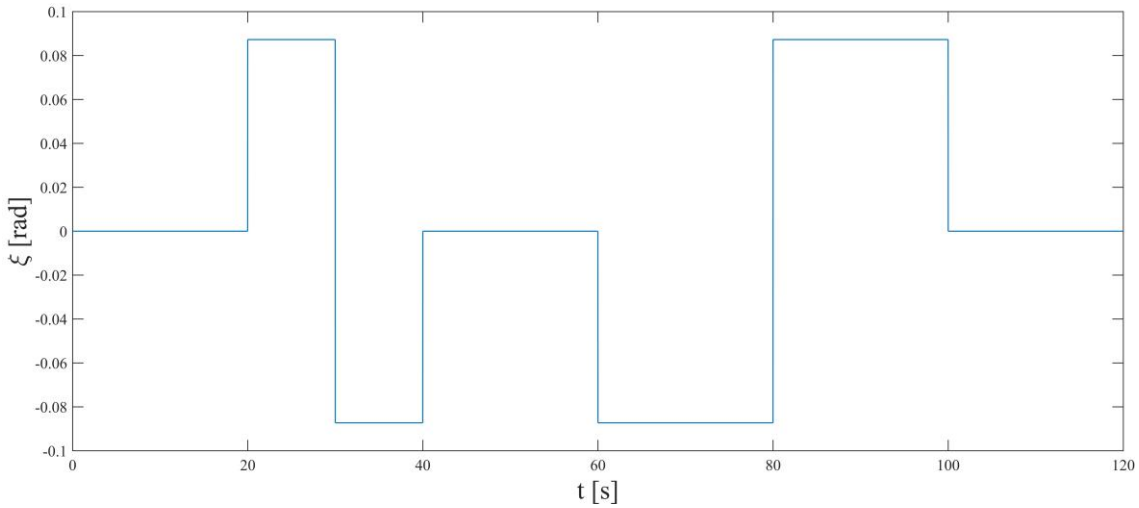

Figure 4.4 - Aileron angle perturbation over time.

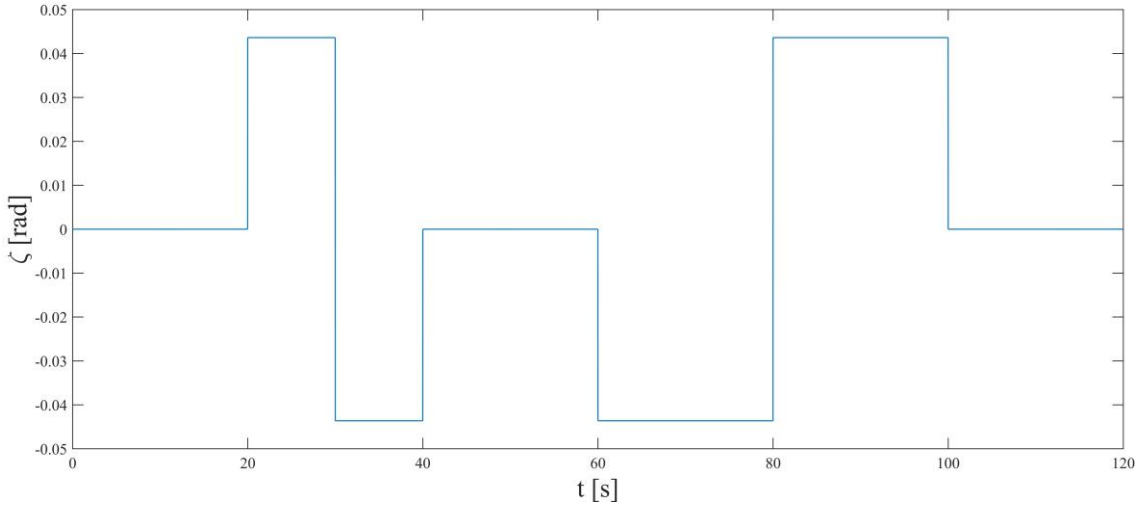

Figure 4.5 - Rudder angle perturbation over time.

and the following initial conditions:

$$x(0) = \begin{bmatrix} 1 \\ 0 \\ 0 \\ 0 \\ 0 \end{bmatrix} \tag{4.13}$$

one can apply the Butcher's algorithm with time step equal to 0.01s generating data to simulate the plant's behavior, where only the lateral velocity and roll angle perturbations are analyzed:

$$\begin{bmatrix} v \\ \varphi \end{bmatrix} = \begin{bmatrix} 1 & 0 & 0 & 0 & 0 \\ 0 & 0 & 0 & 1 & 0 \end{bmatrix} \cdot \begin{bmatrix} v \\ p \\ r \\ \varphi \\ \psi \end{bmatrix} + \begin{bmatrix} N_v \\ N_\varphi \end{bmatrix} \tag{4.14}$$

In order to obtain a more realistic set of data, the output data was corrupted with sensor noise [8], which is usually electrical [12]. N_v is 20% and N_φ is 1% of a Gaussian distribution with 0 mean and variance 1, which according to the original data set, allow to obtain graphics with slightly noise:

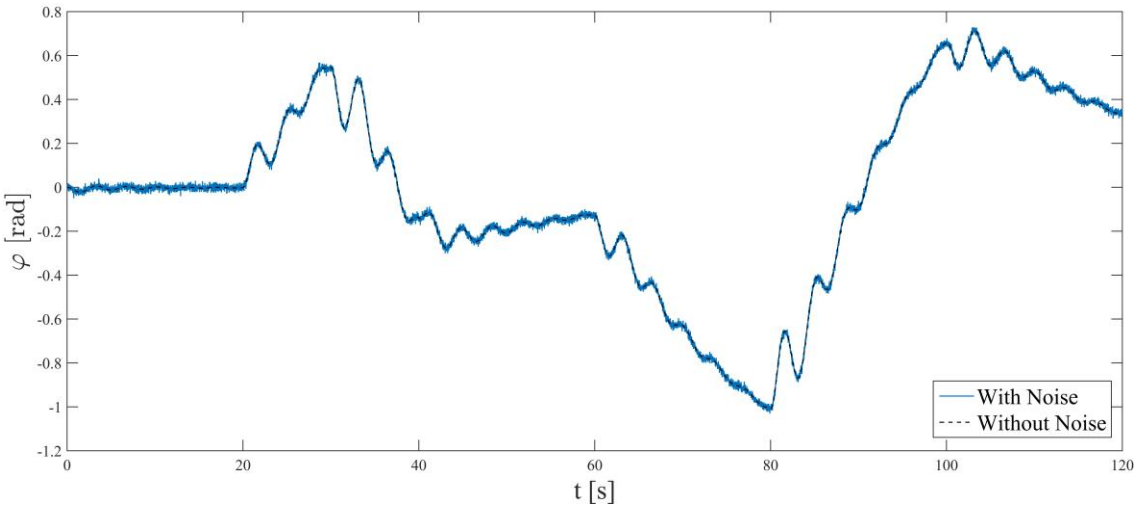

Figure 4.6 – Roll angle perturbation generated with and without noise.

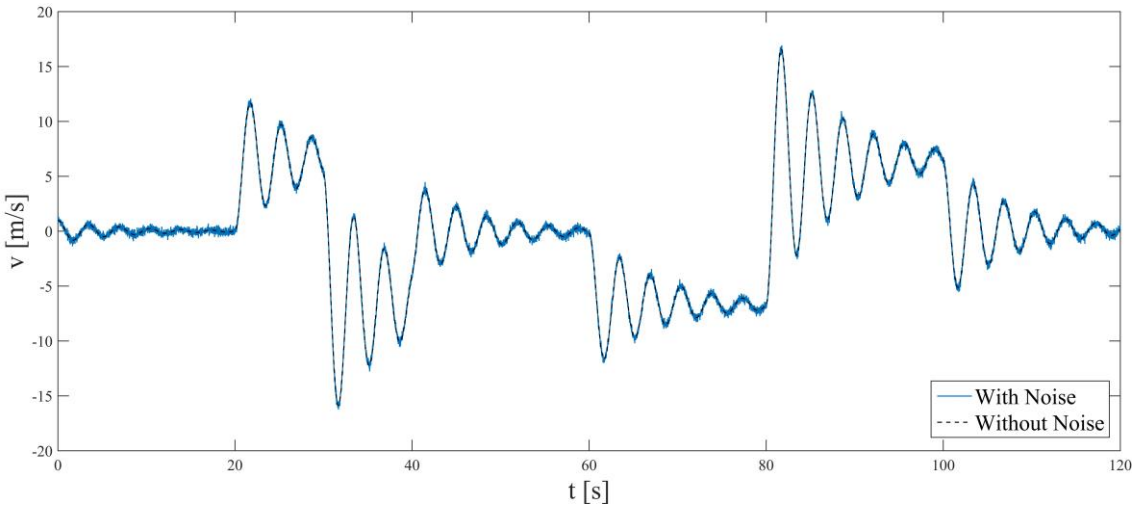

Figure 4.7 - Lateral velocity perturbation generated with and without noise.

The time step indicated during 120s generates a matrix in *Microsoft® Excel®* of 12000 rows (from $k=0$ to $k=11999$) and several columns which is important for the adaptive algorithm.

4.4 Modeling with System Identification

Linearized equations have been successfully and extensively used in stability and control analysis and also in system identification. System identification is a methodology for determining mathematical models of dynamic systems using measurement observations of the system's inputs and outputs [52], [53].

In this section, the previously generated data set in combination with the adaptation mechanism from section 3.1 are used to build mathematical models of the F-4C aircraft. The system identification process is represented schematically, where the airplane behaves well as a 3rd order system ($n=3$) for both motion cases and flight conditions. The goal of the scheme represented in Figure 4.8 is to obtain a vector of estimation parameters, in which the best estimation corresponds to $k=11999$. This vector will be used to translate the aircraft behavior in the model. It is important to know that any model is only an approximation of the actual plant, which can only reproduce some plant properties in such a way that some control design is possible [55].

The time delay of the adaptation algorithm was set as equal to 1. In order to prevent $\hat{b}_0(k) \to 0$, $\hat{d}_0(k) \to 0$ and $\hat{g}_0(k) \to 0$, the initial values of the estimation parameter vector were set as $\begin{bmatrix} 1 & 0 & 0 & 0 & 0 & 0 \end{bmatrix}$ for the longitudinal case and $\begin{bmatrix} 1 & 0 & 0 & 0 & 0 & 0 & 0 & 0 & 0 \end{bmatrix}$ for the lateral-directional case. These conditions are also valid for the controller simulation section.

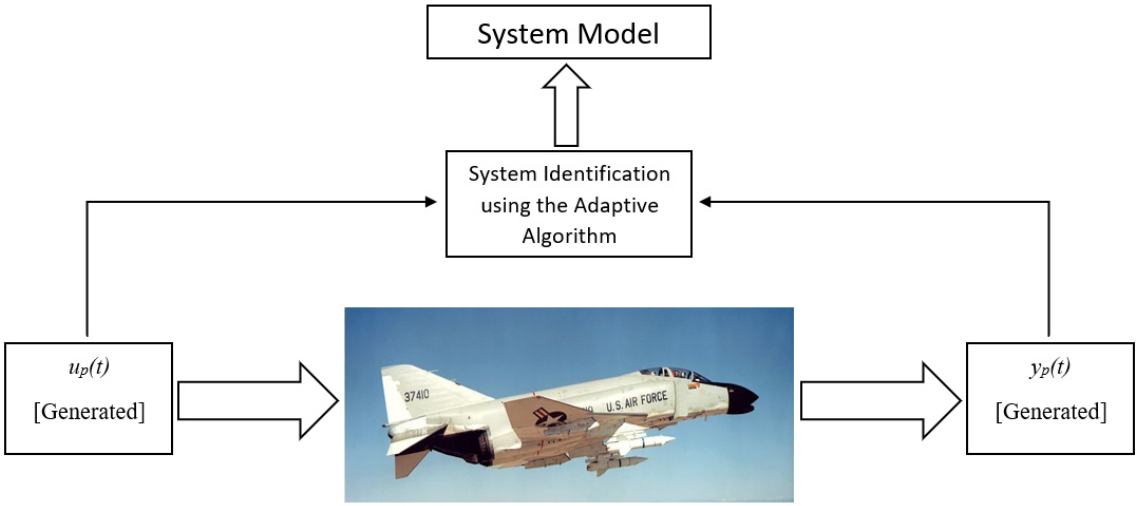

Figure 4.8 - Scheme to obtain the airplane model using generated data [54].

For the longitudinal motion, this scheme is applied using $u_p(t)$: $\eta(t)$ and $y_p(t)$: $\theta(t)$ to obtain the system model $y_p(k) = \hat{p}^T(11999) \cdot \Phi(k-1)$. For the lateral-directional motion, the scheme is applied using $u_p(t)$: $\xi(t)$; $\zeta(t)$ and $y_p(t)$: $\varphi_{noise}(t)$; $v_{noise}(t)$ to obtain the system models $y_p^{(1)}(k) = \hat{p}^{(1)T}(11999) \cdot \Phi^{(1)}(k-1)$ and $y_p^{(2)}(k) = \hat{p}^{(2)T}(11999) \cdot \Phi^{(2)}(k-1)$ that must be used simultaneously in the algorithm.

Chapter 5 – Controller Simulation: Results and Discussion

5.1 Simulation Conditions

The system models for the two cases are then used in the MRAC algorithm to behave like an approximation of the real F-4C Phantom, where the correct choice of the initial simulation conditions is essential for the precise operation of the controller. In the full algorithm, the estimation parameter vectors are updated in real-time so that the adaptive control can adjust the control law in order to track the reference output (y_{ref}) with acceptable stability. Figure 5.1 describes schematically the full MRAC simulation algorithm, where y_{ref} is a set of generated reference data to test the controller.

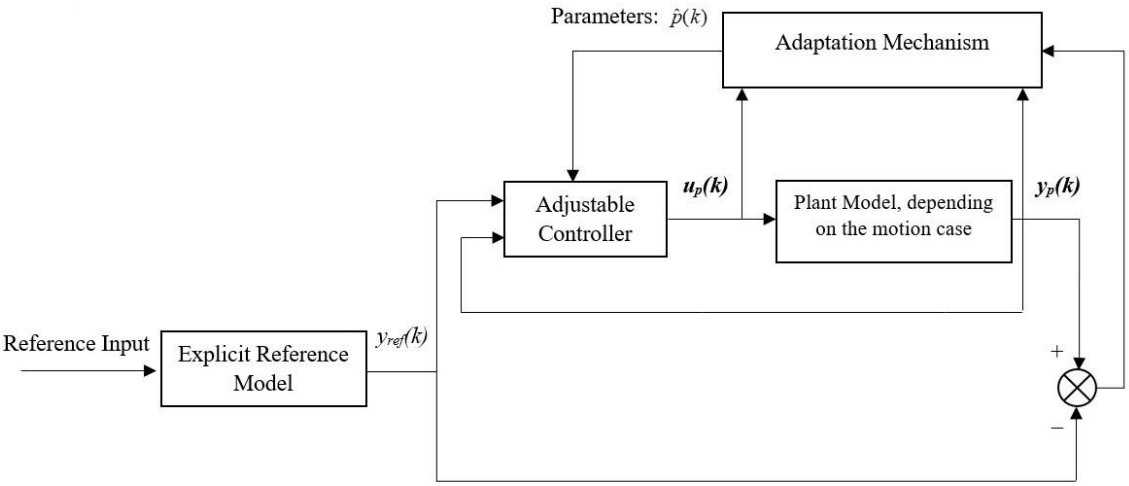

Figure 5.1 – MRAC scheme used in the simulation.

This scheme is based on the work from [13] and is applied on both simulation cases.

Sometimes when dealing with real aircraft, the implementation of an adaptive control design can be difficult because of actuator magnitude and rate saturation. Such limitations can lead to incorrect learning of the adaptive mechanism during periods of saturation [8]. In the present study, the simulation conditions were controlled to avoid a non-linear problem, since it is not the main focus of this dissertation.

5.1.1 Longitudinal Motion

This motion case is divided into two examples. In Example 1, the set of reference pitch angle data has a square wave form:

$$y_{ref}(t) \equiv \theta_{ref}(t) = \begin{cases} 0 & 0 \le t < 24 \\ 0.2618 & 24 \le t < 48 \\ 0 & if \quad 48 \le t < 72 \\ -0.1745 & 72 \le t < 96 \\ 0 & 96 \le t < 120 \end{cases} \tag{5.1}$$

The time step is 0.01s generating a matrix in *Microsoft® Excel®* of 12000 rows (from $k=0$ to $k=11999$) and 2 columns (t, θ_{ref}).

In Example 2, the set of reference pitch angle data is the one from subsection 4.3.1. In each of these examples a comparison is made between the controllers presented in section 3.3, where the initial conditions assumed are shown in Table 5.1.

Table 5.1 - Initial conditions for longitudinal simulation.

	Example 1		**Example 2**	
	Controller 1	Controller 2	Controller 1	Controller 2
$u_p(0) \equiv \eta(0)$	0.1 rad		0.2 rad	
$y_p(0) \equiv \theta(0)$	0.6 rad		2 rad	
$F(0)$	$0.04I$		$0.01I$	
γ	---	0.3	---	0.85

The choice of $F(0)$ will be explained later only for the longitudinal motion, however the same concept is valid for the lateral-directional motion.

5.1.2 Lateral-Directional Motion

In this motion case, the set of reference output data used to test the extended/modified controller 2 has a square wave form according to (5.2) and (5.3), where the time step is 0.01s.

$$y_{ref}^{(1)}(t) \equiv \varphi_{ref}(t) = \begin{cases} 0 & 0 \le t < 24 \\ 0.8 & 24 \le t < 48 \\ 0 & if \quad 48 \le t < 72 \\ -0.5 & 72 \le t < 96 \\ 0 & 96 \le t < 120 \end{cases} \tag{5.2}$$

$$y_{ref}^{(2)}(t) \equiv v_{ref}(t) = \begin{cases} 0 & 0 \le t < 24 \\ 0.5 & 24 \le t < 48 \\ 0 & if \quad 48 \le t < 72 \\ -0.5 & 72 \le t < 96 \\ 0 & 96 \le t < 120 \end{cases} \tag{5.3}$$

The initial conditions assumed for this part of the simulation are shown in the next table, where the right choice of $F(0)$ is crucial due to instability problems.

Table 5.2 - Initial conditions for lateral-directional simulation.

Coefficients	Values
$F_{\varphi}(0)$	$0.5I$
$F_{v}(0)$	$0.01I$
γ_{φ}	0.95
γ_{v}	0.8
$u_p^{(1)}(0) \equiv \xi(0)$	0.1 rad
$u_p^{(2)}(0) \equiv \zeta(0)$	0.1 rad
$y_p^{(1)}(0) \equiv \varphi(0)$	0.1 rad
$y_p^{(2)}(0) \equiv v(0)$	1 m/s

5.2 Simulation Results

In this section, the results from the previous simulations are presented when the plant is subjected to the model reference adaptive control.

5.2.1 Longitudinal Motion

Example 1 with controller 1

In Figure 5.2, the classic control is used, and it can be seen in Figure 5.2(a) that initially there is a large error between the two graphs up to approximately $k=400$, this is due to the initial conditions assumed and the random values of the initial parameter vectors. In the first pitch angle transition at $k=2400$, there is a small difference between the graphs where the plant's output reaches a local maximum value of 0.3192 rad, this is because the controller is facing the first suddenly transition of reference signal after a period of constant values. However, this difference gradually decreases over k. The following transitions occur smoothly, the controller can adjust itself very well so that y_p follows y_{ref} as perfect as possible.

It can be seen in Figure 5.2(b) that initially there is a significant error up to $k=700$ (approximately), which occurs due to the initial conditions assumed and the random values of the initial parameter vectors that enter the control law.

The controller presents acceptable values, having an absolute maximum elevator angle of 0.6145 rad (35º). Although this peak has a high value relatively to 25º, the following peaks have less magnitude due to the decreasing reference output and the increasing accuracy of the adaptive parameters.

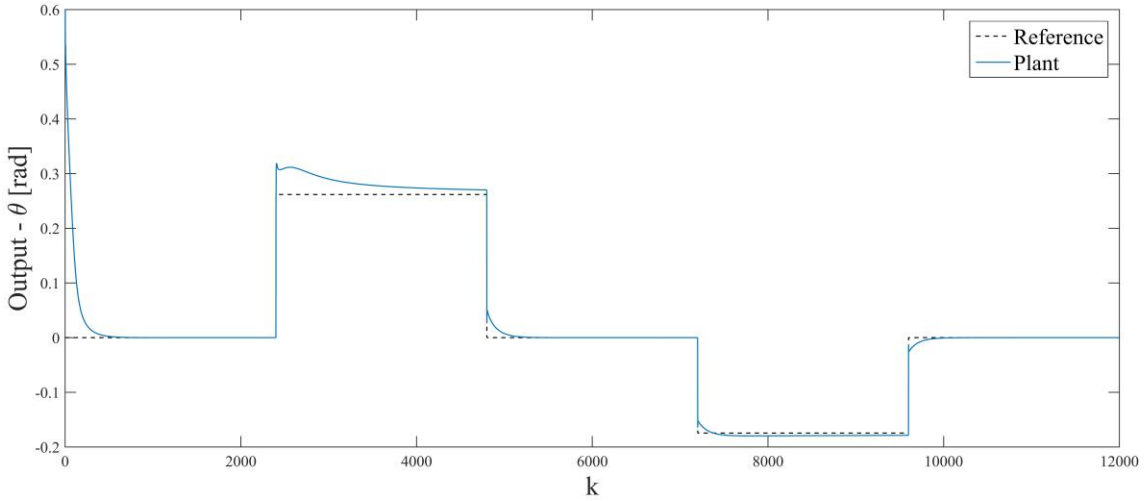

(a) Output

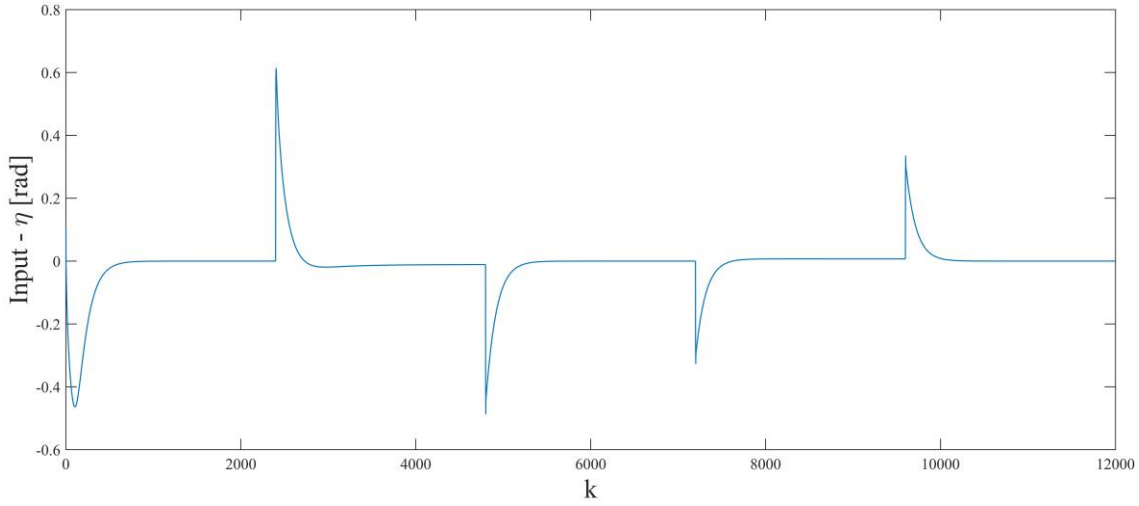

(b) Control Input

Figure 5.2 - Example 1 with classic control.

Example 1 with controller 2

In Figure 5.3, the penalized control is used, and it can be seen in Figure 5.3(a) that initially there is a significant error up to $k=1000$ (approximately), which occurs due to reasons already mentioned. The controller used was penalized with a weight coefficient, so it is observed that y_p does not follow perfectly y_{ref}, however it presents smooth transitions and advantages relatively to the values of u_p reached by this controller. The magnitude of the η peaks from controller 2 is smaller in comparison with the peaks from controller 1, having a local maximum elevator angle of 0.2708 rad (15.5º), as it can be observed in Figure 5.3(b).

The detailed analysis of the impulses/peaks shown in Figure 5.2(b) and Figure 5.3(b) is practically identical, since they are very similar in aspect and quantity, with only difference in magnitude (higher for classic control) and time duration (slightly higher for penalized control). One can say that the lack of tracking performance is compensated by efficient control signals, where magnitude values can be easier achieved by real actuators.

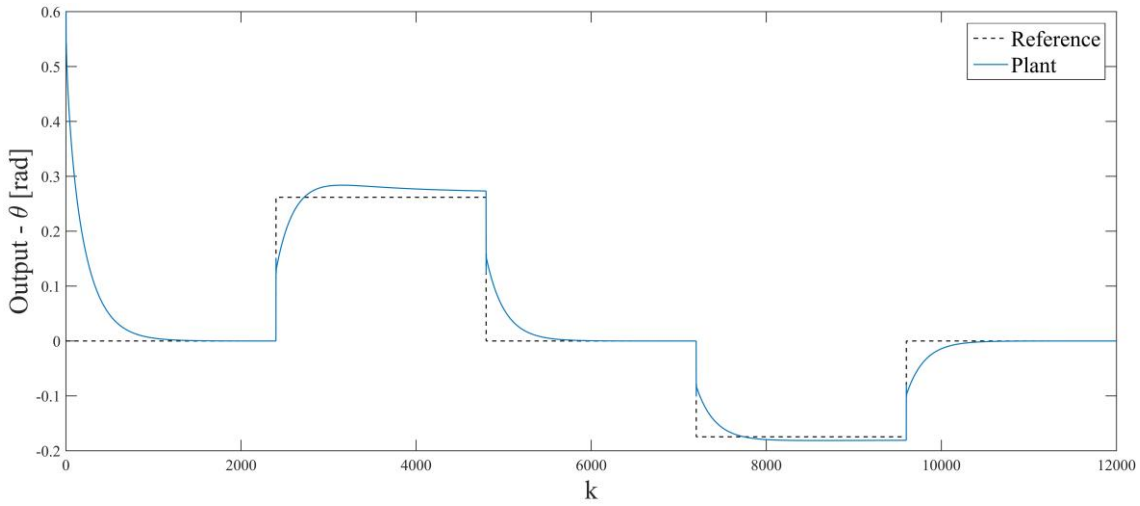

(a) Output

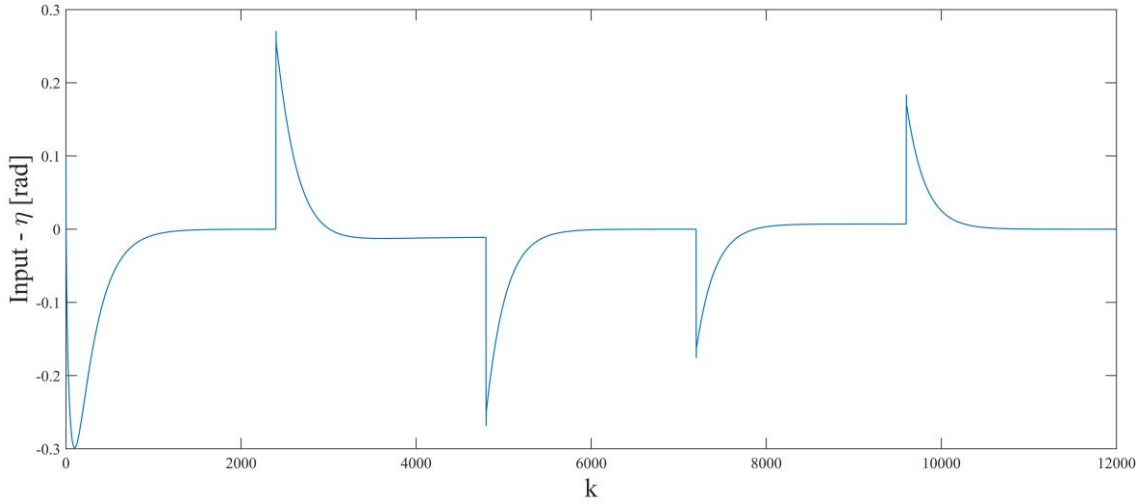

(b) Control Input

Figure 5.3 – Example 1 with penalized control.

The controller, after stabilizing the error due to the initial conditions, guarantees to the aircraft 0 rad of pitch angle. At $k=2400$ the reference requires a positive increase of θ, this is guaranteed with the deflection of the elevator that reaches a certain value, but quickly returns to 0 rad. The pitch angle remains at the same value due to manipulation of the airplane's thrust (provided by the propulsion system) and it only returns to 0 rad when the controller ensures the opposite deflection. During this time interval, the aircraft is climbing, increasing its altitude. At $k=7200$ a pitch angle transition occurs again but now with the opposite signal. In this case, the aircraft is diving, decreasing its altitude. After those transition intervals the airplane returns to $\theta=0\ rad$.

Example 2 with controller 1

Example 2 has data that produces a smooth graph that can be easily controlled. Thus, very pronounced tracking errors between y_p and y_{ref} are not to be expected. Also, this reference signal was used to obtain the plant's model through system identification.

In Figure 5.4, the classic control is used. From Figure 5.4(a), it can be seen that initially there is an error between the two graphs up to approximately $k=53$, this error quickly disappears. In $k=2000$ the first transition of η from 0 rad to 0.1745 rad occurs, which causes in $k=2170$ to $k=2540$ (approximately) a small tracking error between the two output graphs, nothing too excessive. In general, the plant output closely follows the reference output.

In Figure 5.4(b), there is initially a significant error up to $k=90$ (approximately) that is gradually stabilized. Although peaks occur, the controller presents acceptable values with magnitude lower than 0.281 rad (neglecting the initial peak), which is acceptable for the deflection of an airplane's control surface. Despite the existence of those peaks, the controller attempts to adapt in order to stabilize itself. The graph that shows the reference input that was used to generate the reference output is only represented to verify that when the square wave increases or decreases, the controller also tends to follow the same behavior.

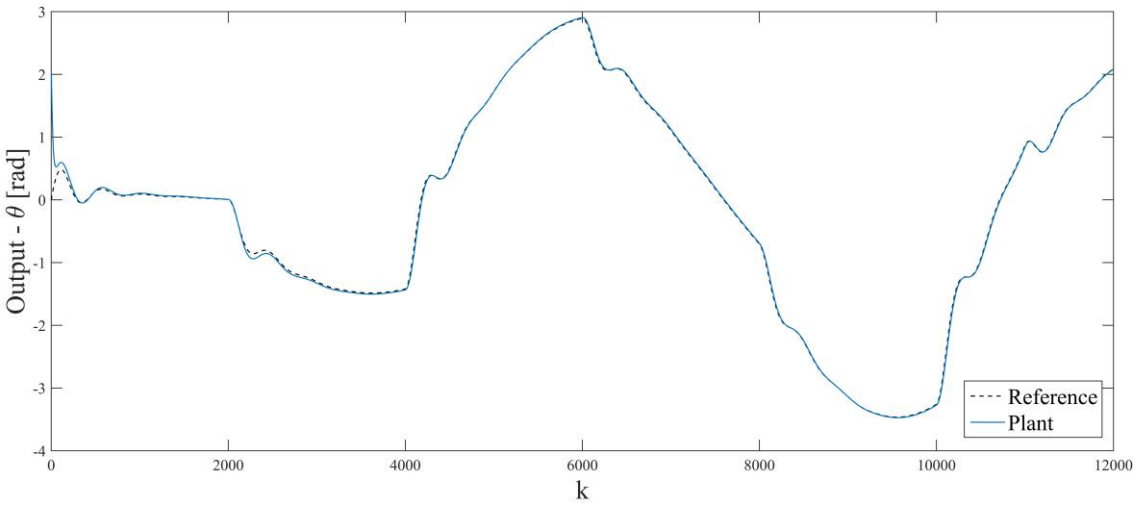

(a) Output

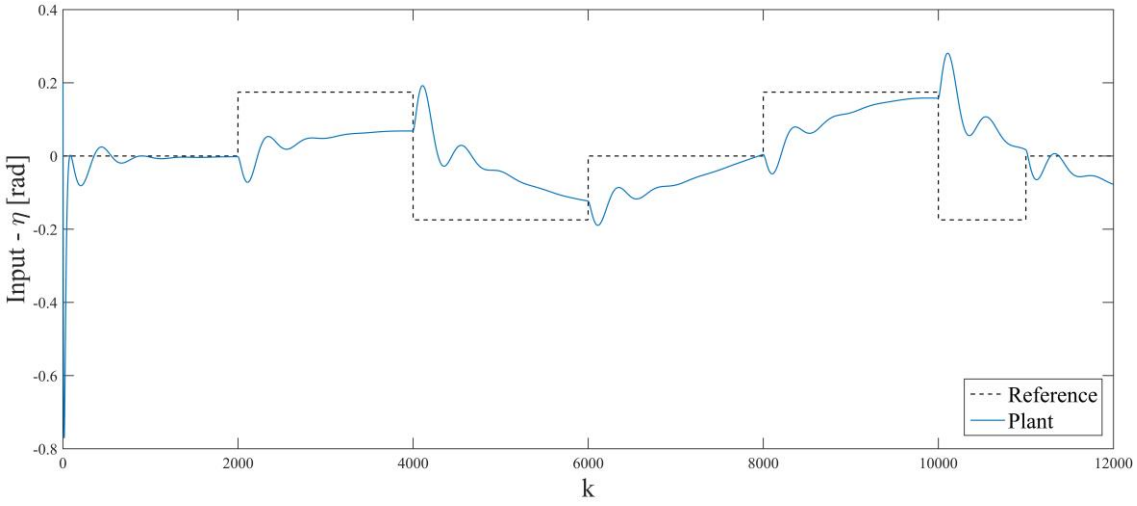

(b) Input

Figure 5.4 - Example 2 with classic control.

Example 2 with controller 2

In Figure 5.5, the penalized control is used. The analysis is very similar to Figure 5.4 except that, because of γ, this controller presents an y_p slightly deviated from y_{ref} which has the advantage of reducing the initial maximum η value from -0.7712 rad to -0.4739 rad.

It should be noted that also in Figure 5.5(b) the goal is not to see u_p following the reference input that was used to generate the reference output. The representation of this graph in the same plot as u_p is only to observe the ideal behavior of the reference input relatively to the controller.

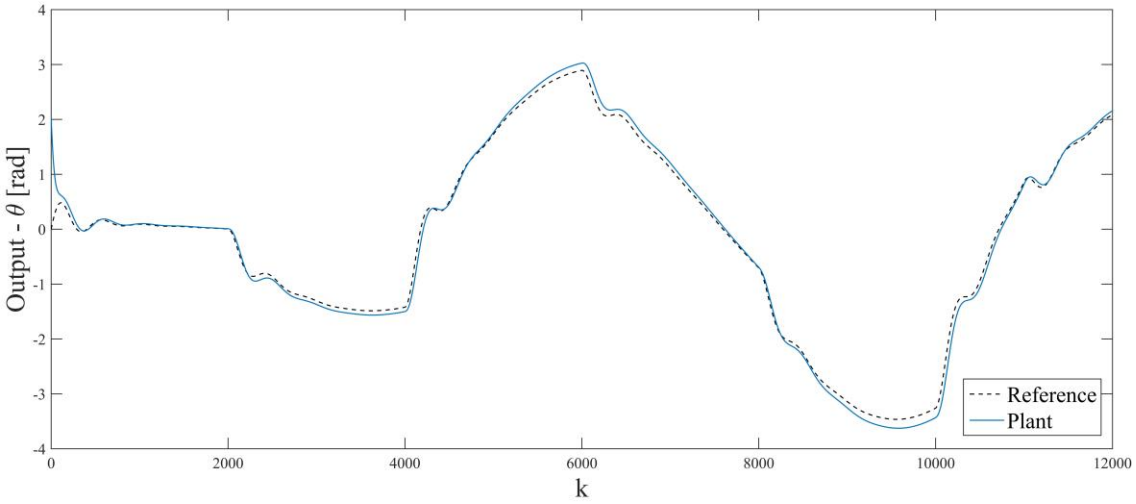

(a) Output

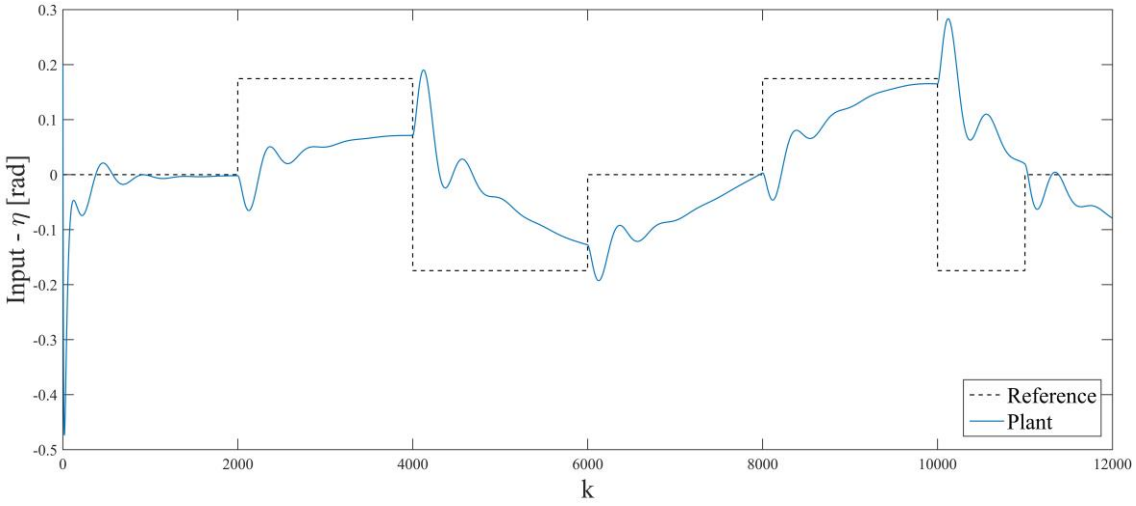

(b) Input

Figure 5.5 - Example 2 with penalized control.

In the MRAC, the convergence speed of the estimation of parameters increases as the initial value of the adaptation gain increases [34].

The longitudinal simulation was carried out with a value of $0.04I$ for example 1 and $0.01I$ for example 2, because although the increase of $F(0)$ causes an increase of convergence, it also increases the maximum magnitude of the peaks shown in the previous graphs to values not likely to be reached by the airplane's control surfaces. For values close to (bigger than) $0.06I$ both controllers, in the two examples, are unstable, $u_p(k) \to +\infty \ or \ -\infty$, once $\hat{b}_0(k) \to 0$.

5.2.2 Lateral-Directional Motion

In Figure 5.6, the modified controller 2 is subjected to the reference output of (5.2) and (5.3), and it can be seen in Figure 5.6(a) that it adjusts very well to the sudden changes in magnitude. In the roll angle graph, the tracking is almost perfect with only one initial error between the reference and the plant outputs due to the initial conditions assumed and the random values of the initial parameter vectors. The initial error occurs up to $k=150$ (approximately), where φ from the plant reaches 0.2026 rad.

In the lateral velocity graph, one of the initial conditions was assumed to be 1 m/s, this value is quickly stabilized by the controller after $k=155$ (approximately). A peak with value of 1.246 m/s appears with the variation of the reference's magnitude, however a quick adjustment by the controller is made against this change. It should be noted that a peak also appears (almost unnoticeable) on the roll angle graph, but with a smaller magnitude.

In Figure 5.6(b), the controller presents values for the aileron and rudder angles within the limits of ±0.4363 rad. There are small errors initially due to the simulation conditions assumed and the random values of the initial parameter vectors that enter the control law. The aileron angle graph shows maximum values between ±0.4215 rad, these signals are very short in time due to the Phantom's roll performance, which it can perform 1.571 rad of roll angle in 1.3s. The graph of the rudder angle shows maximum values between ±0.2780 rad, these signals are also short in time taking approximately 1.25s (first signal). This is normal for a military aircraft such as the F-4C.

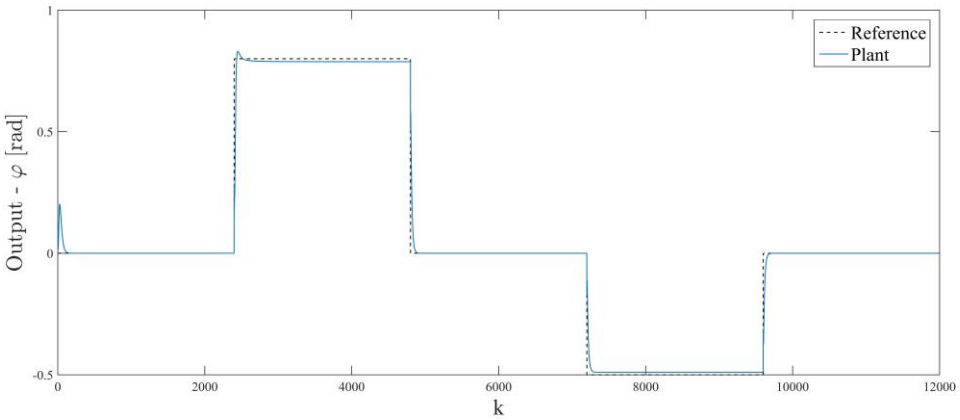

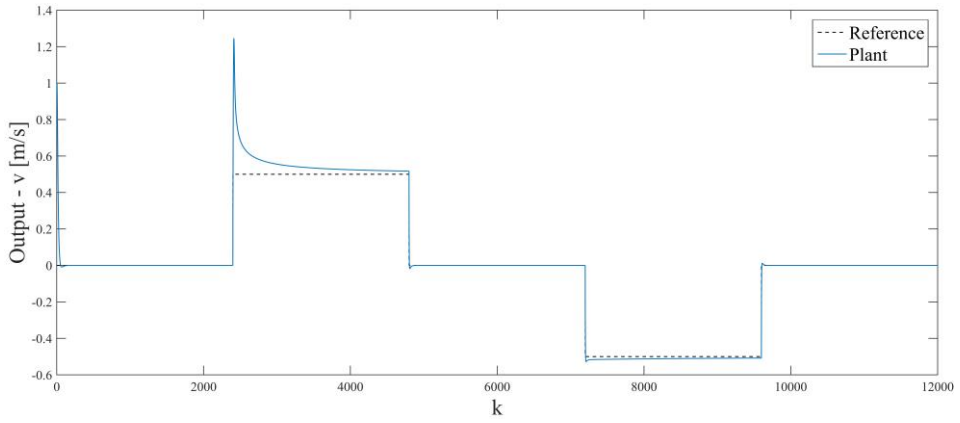

(a) Outputs

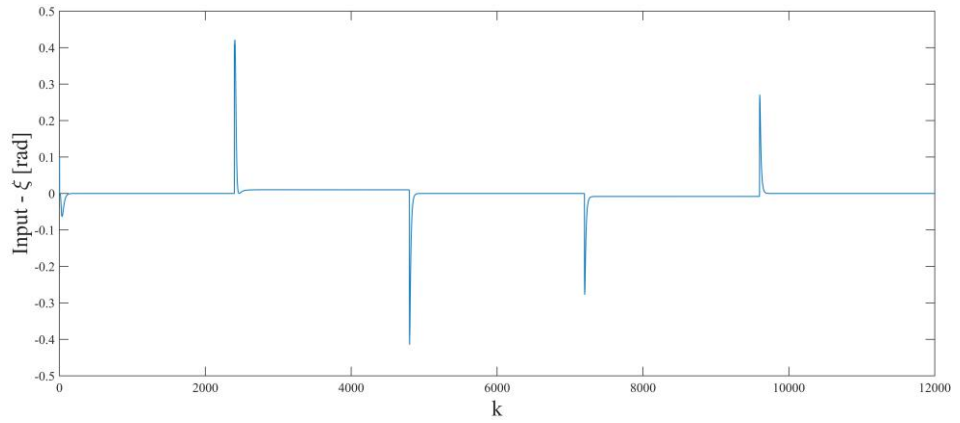

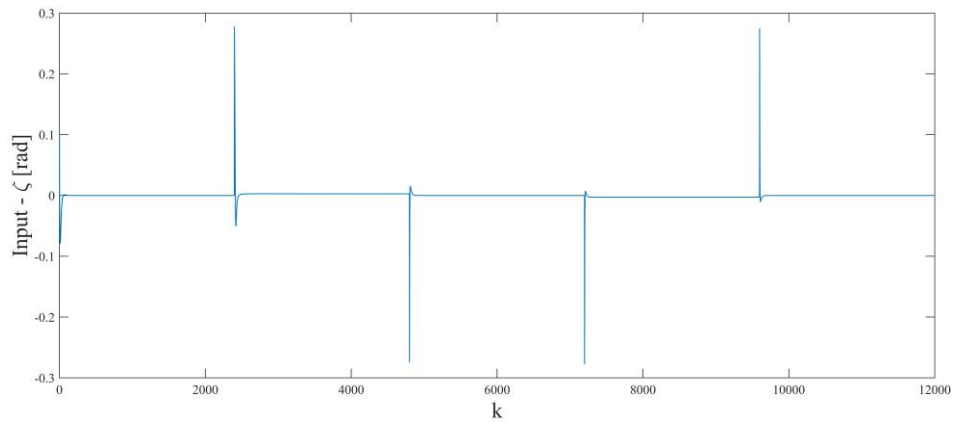

(b) Control Inputs

Figure 5.6 - Testing the controller with the reference data from (5.2) and (5.3).

As already mentioned, there is a coupling relation between the variables studied in the lateral-directional case, in which a decoupling process had to be done to control them independently. According to the Phantom's flight manual [56], the aileron-rudder interconnect system causes rudder deflection proportional to aileron deflection which provides coordinated turns at low airspeeds. To verify this relation between variables, the graphs from Figure 5.7 and Figure 5.8 present results where one of the reference outputs was maintained at 0 (neutral).

In Figure 5.7, the reference lateral velocity is maintained at 0 m/s. From Figure 5.7(a) one can say that the roll angle graphic is equal to the graph from Figure 5.6(a), however the first one presents a slightly better tracking performance. The lateral velocity graph has a very interesting behavior: although v_{ref} has been established as 0 m/s, the plant's output has peaks with magnitude near 0 m/s. These peaks suggest that v is related with the other variables, such as ξ.

In Figure 5.7(b), the ξ graphic is similar to the one from Figure 5.6(b), however the peaks have a lower magnitude between ±0.4097 rad. This happens because v_{ref} is zero and the contribution from the ailerons is no longer a big necessity to help changing the lateral velocity. However, the angle values of the ailerons are still quite significant since they depend directly on the roll angle that is not maintained at 0 rad in this part of the simulation.

Almost all values from the ζ graph are 0 rad, yet there are peaks with small magnitude that suggest a relation with the roll angle. That is, during the Phantom's roll maneuver, although the ailerons are the main control surfaces used, the rudder also helps.

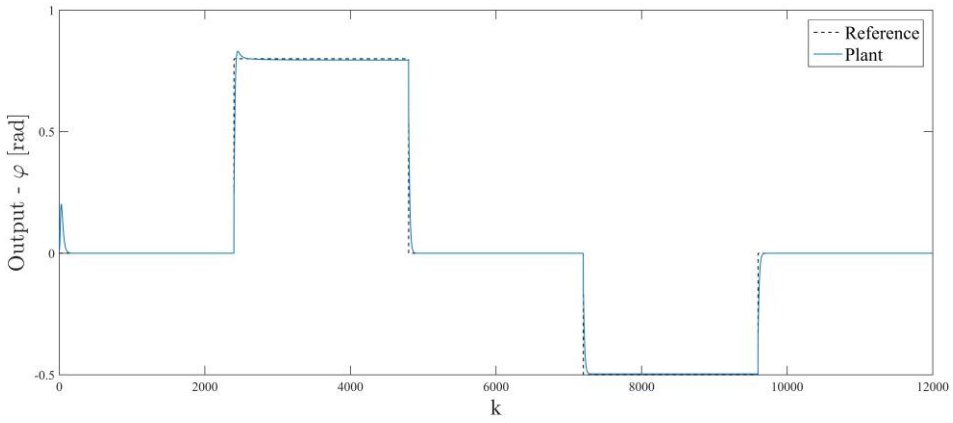

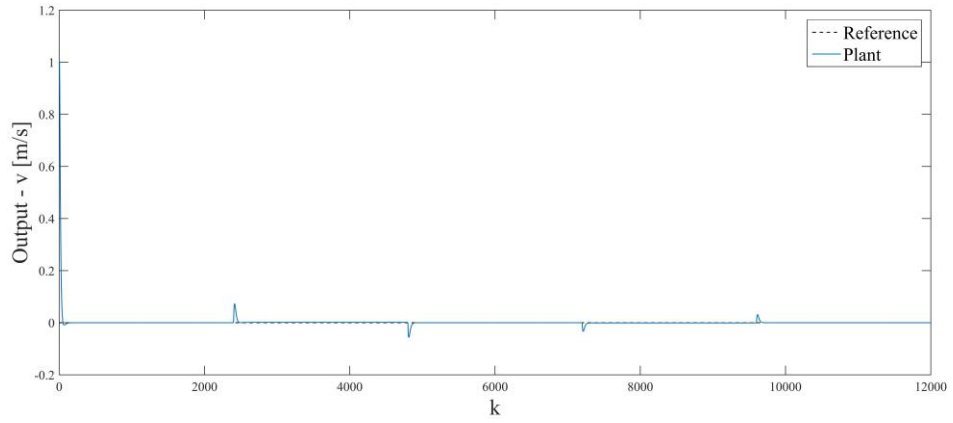

(a) Outputs

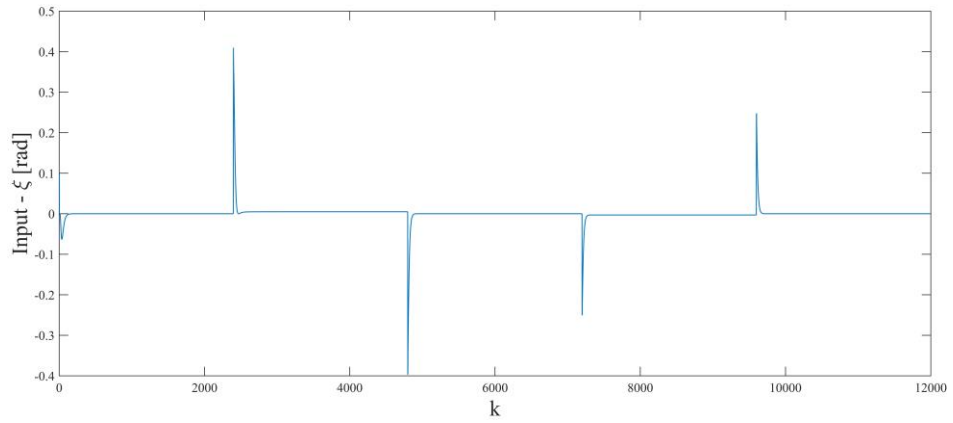

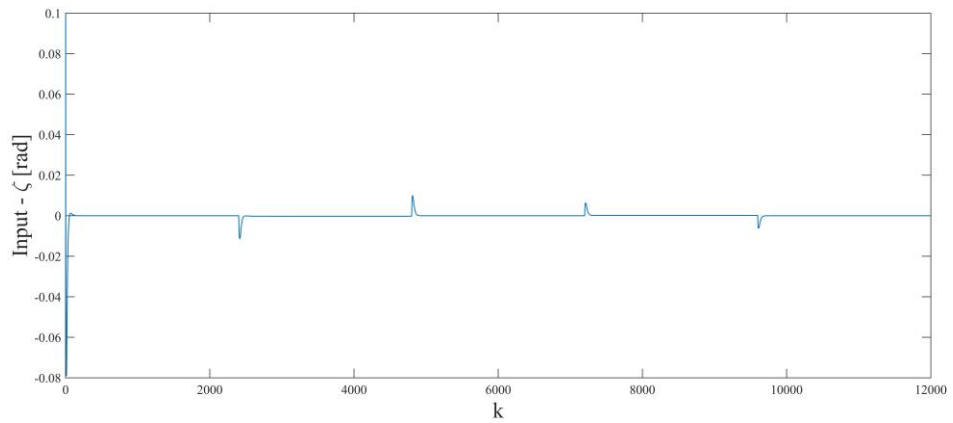

(b) Control Inputs

Figure 5.7 - Testing the controller with φ_{ref} from (5.2) and v_{ref} set to 0.

In Figure 5.8 the reference roll angle is maintained at 0 rad. In Figure 5.8(a), the graphic of the roll angle initially presents an error due to the initial conditions assumed and the parameter vectors, this error is stabilized after $k=170$ (approximately). These results are interesting: there are peaks with magnitude between ±0.2282 rad in which this value decreases over time, there are also time intervals in which φ is approximately ±0.0088 rad (negligible value). Again, these results suggest that φ is related to the other variables, such as ζ.

The values of the lateral velocity between the graphs from Figure 5.6(a) and Figure 5.8(a) at first sight are identical, however there is a slightly better tracking in the graph from Figure 5.8(a).

There is a significant decrease in the ξ magnitude in Figure 5.8(b) compared to the values in Figure 5.6(b). The values from Figure 5.8(b) lie between ±0.1197 rad which indicates that, given the chosen flight conditions, the F-4C ailerons contribute to the lateral velocity variation in addition to the roll angle. The rudder angle is very similar in the graphs of Figure 5.6(b) and Figure 5.8(b), there is only a decrease in the magnitude of the small peaks that guarantee return to the neutral position. This is because φ_{ref} is maintained at 0 rad.

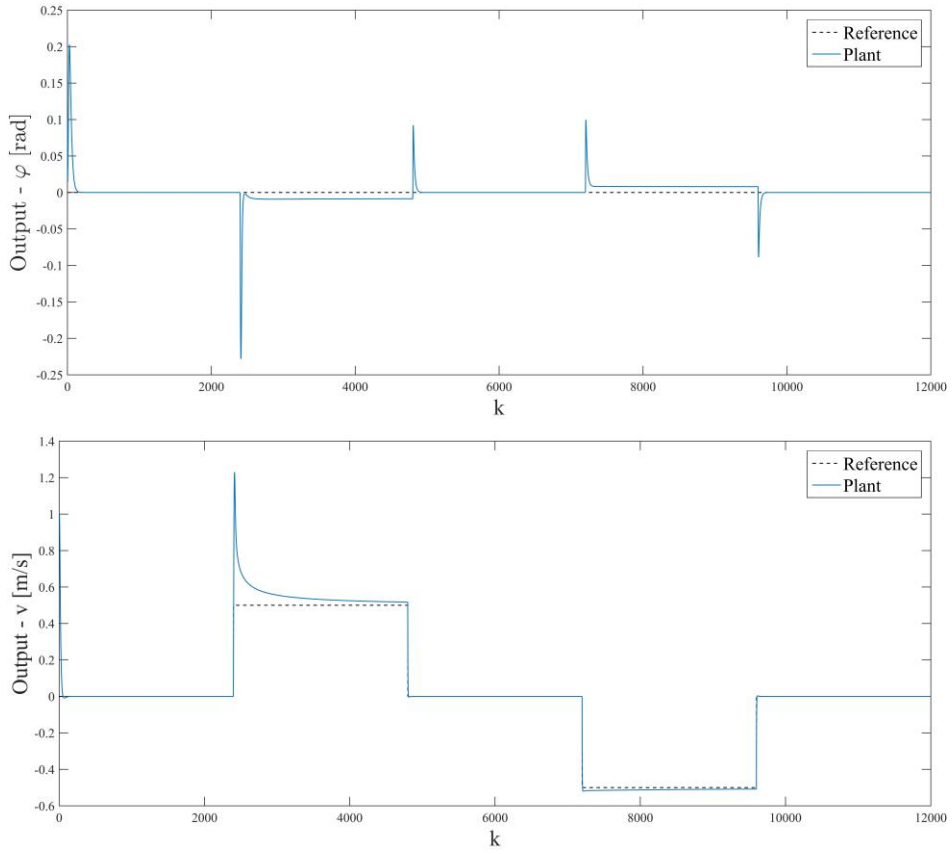

(a) Outputs

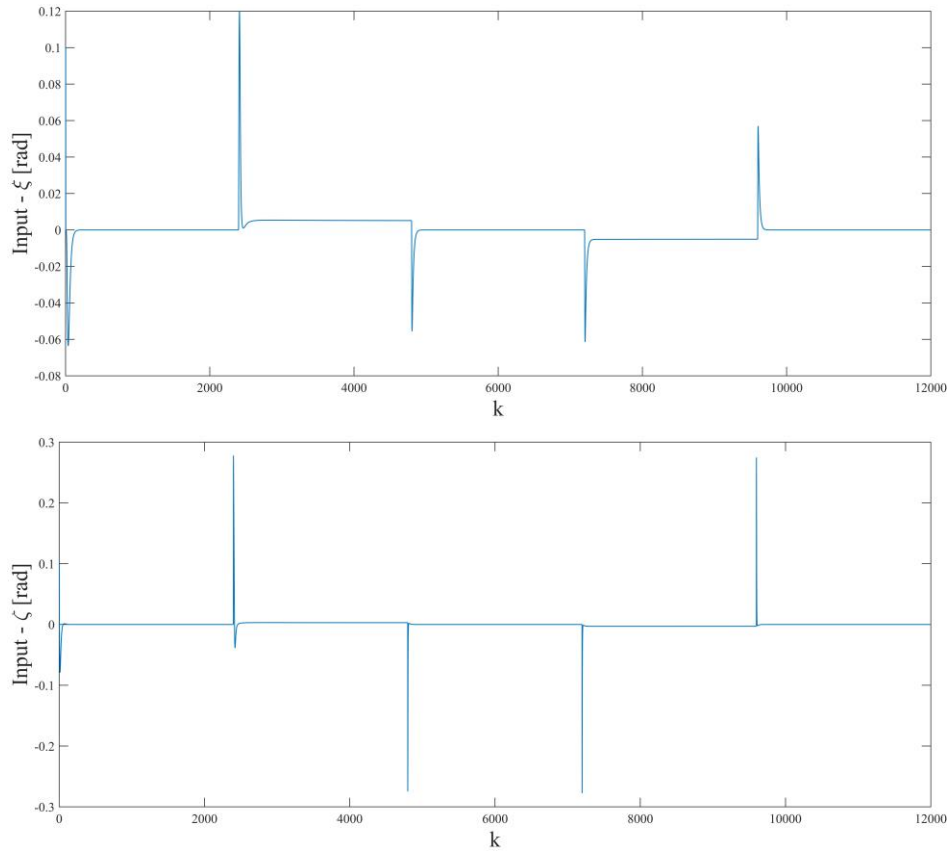

(b) Control Inputs

Figure 5.8 - Testing the controller with v_{ref} from (5.3) and φ_{ref} set to 0.

F-4C Phantom is designed with swept wings, which is the primary mechanism that gives the roll effect to an airplane that may only receive a rudder input. When yaw is introduced, one wing will extend more directly into the wind-stream increasing in airspeed, while the other wing will decrease in airspeed generating less lift than the other, introducing a rolling motion [57], [58].

Varying the angle of the ailerons causes the airplane to make a rolling motion and may also cause adverse yaw. For instance, as the airplane roll to the right, it may initially yaw to the left, varying the lateral velocity. This occurs in this example because the right aileron creates less lift and less drag than the left aileron that produces more drag and more lift [59].

It should be noted that all the peaks that appeared in the graphs until now are short in time, not damaging the actuators of a real F-4C airplane.

Chapter 6 - Conclusions

This dissertation presented a specific type of Model Reference Adaptive Control tested on an example aircraft. The theory of the MRAC that has been shown is applied to a linearized plant model of the F-4C Phantom during longitudinal and lateral-directional motion, where an extended/modified version of the controller is used in the second motion case to deal with MIMO decoupling. Since a linear model is used, there may exist some difference between the theory and the practical system, once an aircraft, manly a fighter-bomber like the F-4C, is a non-linear system.

Simulation results have shown the importance of choosing the right initial conditions, specifically the adaptation gain matrix. The choice of the type of adaptation algorithm is also essential to obtain the best results.

As verified in the longitudinal simulation, there has to be a compromise between the energy cost spent by the controller (visible in the graphs by the maximum magnitude of the peaks) and the precision of the plant output to follow the reference, this is verified in the comparison between the classic controller and the penalized one.

In the lateral-directional simulation, the controller yielded good tracking performance with results that showed the coupling relation between the flight variables studied. Although lateral-directional flight is simplified by stating that ailerons are only responsible for rolling movement and the rudder is the main responsible for lateral velocity, the truth is that ξ also influences the values of v, as well as ζ influences the values of φ.

In short, for both motion cases the MRAC proved to be very effective when applied to a simulated airplane, becoming a possible candidate for autopilots and future full autonomous UAVs comparatively to controllers such as gain-scheduling.

The challenge in designing an adaptive control that will be applied to a real aircraft is to deal with rate saturation and actuator magnitude. Since specific flight regimes with particular conditions were assumed in this dissertation, some further research topics should include:

- Development of a mechanism that prevents the controller from exceeding control actuation limits set by the airplane manufacturer;
- Application of the algorithm to real tests performed on unmanned aircraft;
- Application of the controller to other aircraft types, such as helicopters, and non-linear aircraft models.

Chapter 7 - Bibliography

[1] M. V. Cook, *Flight Dynamics Principles: A Linear Systems Approach to Aircraft Stability and Control*, Second. Butterworth-Heinemann, 2007.

[2] A. Zolghadri, "Modern Control Theory and Real-World Aerospace Applications: I love You, Nor do I?," *IFAC-PapersOnLine*, vol. 50, no. 1, pp. 6446–6451, Jul. 2017.

[3] H. Korul, D. Tosun, and Y. Isik, "A Model Reference Adaptive Controller Performance of an Aircraft Roll Attitude Control System," *Recent Adv. Syst. Signals, Control. Commun. Comput.*, 2015.

[4] K. J. Astrom and B. Wittenmark, *Adaptive Control*, Second. Dover Publications, 1994.

[5] S. G. Anavatti, F. Santoso, and M. A. Garratt, "Progress in adaptive control systems: past, present, and future," in *2015 International Conference on Advanced Mechatronics, Intelligent Manufacture, and Industrial Automation (ICAMIMIA)*, 2015, pp. 1–8.

[6] K. A. Wise, E. Lavretsky, and N. Hovakimyan, "Adaptive control of flight: theory, applications, and open problems," in *2006 American Control Conference*, 2006, p. 6.

[7] D. J. Wagg, "Adaptive Control of Nonlinear Dynamical Systems Using a Model Reference Approach," *Meccanica*, vol. 38, no. 2, pp. 227–238, 2003.

[8] K. P. Valavanis and G. J. Vachtsevanos, *Handbook of Unmanned Aerial Vehicles*. Dordrecht: Springer Netherlands, 2015.

[9] W. Black, P. Haghi, and K. Ariyur, "Adaptive Systems: History, Techniques, Problems, and Perspectives," *Systems*, vol. 2, no. 4, pp. 606–660, Nov. 2014.

[10] R. Mishkov and S. Darmonski, "Nonlinear adaptive control system design with asymptotically stable parameter estimation error," *Int. J. Control*, vol. 91, no. 1, pp. 181–203, Jan. 2018.

[11] P. A. Ioannou and J. Sun, *Robust Adaptive Control*. Prentice-Hall, 1995.

[12] D. McLean, *Automatic Flight Control Systems*, First. Prentice-Hall, 1990.

[13] I. D. Landau, R. Lozano, M. M'Saad, and A. Karimi, *Adaptive Control: Algorithms, Analysis and Applications*. Springer, 2011.

[14] N. T. Nguyen, *Model-Reference Adaptive Control*, First. Cham: Springer International Publishing, 2018.

[15] F. Ohkawa and M. Tomizuka, "Model Reference Adaptive Control of a Class of Nonlinear Systems," *IFAC Proc. Vol.*, vol. 24, no. 1, pp. 151–155, Jan. 1991.

[16] Y. Shin, A. J. Calise, and M. Johnson, "Adaptive Control of Advanced Fighter Aircraft in Nonlinear Flight Regimes," *J. Guid. Control. Dyn.*, vol. 31, no. 5, pp. 1464–1477, Sep. 2008.

[17] E. Lavretsky and K. A. Wise, *Robust and Adaptive Control with aerospace applications*. London: Springer London, 2013.

[18] K. Aström, “History of Adaptive Control,” in *Encyclopedia of Systems and Control*, London: Springer London, 2014, pp. 1–9.

[19] D. Cenciotti, “That Time An X-15 Rocket Plane Entered Hypersonic Spin At Mach 5 And Broke Apart Killing USAF Test Pilot.,” *The Aviationist*, 2017. [Online]. Available: https://theaviationist.com/2017/11/15/that-time-an-x-15-rocket-plane-entered-hypersonic-spin-at-mach-5-and-brought-apart-killing-usaf-test-pilot/. [Accessed: 03-Apr-2019].

[20] I. D. Landau and R. Lozano, “Unification of discrete time explicit model reference adaptive control designs,” *Automatica*, vol. 17, no. 4, pp. 593–611, Jul. 1981.

[21] M. Krstic, I. Kanellakopoulos, and P. V Kokotovic, *Nonlinear and Adaptive Control Design*, 1st ed. Wiley-Interscience, 1995.

[22] J. Ross, “X-36 Tailless Fighter Agility Research Aircraft,” *NASA*, 1997. [Online]. Available: https://www.nasa.gov/centers/dryden/multimedia/imagegallery/X-36/EC97-44121-40.html. [Accessed: 03-Apr-2019].

[23] M. Stefanovic and M. G. Safonov, *Safe Adaptive Control: Data-Driven Stability Analysis and Robust Synthesis*. Springer, 2011.

[24] J. I. Canelon, L. S. Shieh, and G. Song, “A new neural network-based approach for self-tuning control of nonlinear SISO discrete-time systems,” *Int. J. Syst. Sci.*, vol. 41, no. 12, pp. 1421–1435, 2010.

[25] S. Jafari, P. Ioannou, and L. Rudd, “What is L1 Adaptive Control,” *AIAA Guid. Navig. Control Conf.*, p. 9, 2013.

[26] S. Shan, Z. Hou, and W. Wang, “Aircraft longitudinal decoupling based on a singular perturbation approach,” *Adv. Mech. Eng.*, vol. 9, no. 9, pp. 1–8, Sep. 2017.

[27] Y. Liu, G. Tao, and S. M. Joshi, “Modeling and Model Reference Adaptive Control of Aircraft with Asymmetric Damage,” *J. Guid. Control. Dyn.*, vol. 33, no. 5, pp. 1500–1517, Sep. 2010.

[28] M. Bodson and J. E. Groszkiewicz, “Multivariable adaptive algorithms for reconfigurable flight control,” *IEEE Trans. Control Syst. Technol.*, vol. 5, no. 2, pp. 217–229, Mar. 1997.

[29] D. Wagner and M. Hromcik, “Robust pitch attitude hold with MRAC for a nonlinear light combat aircraft model,” in *2017 21st International Conference on Process Control (PC)*, 2017, pp. 71–75.

[30] K. G. Arvanitis, “Adaptive decoupling of linear systems using multirate generalized sampled-data hold functions,” *IMA J. Math. Control Inf.*, vol. 12, no. 2, pp. 157–177, 1995.

[31] M. M. Bayoumi and L. Mo, “Adaptive Decoupling Control of MIMO System,” *IFAC Proc. Vol.*, vol. 21, no. 9, pp. 109–113, Aug. 1988.

[32] B. Wittenmark, R. H. Middleton, and G. C. Goodwin, “Adaptive decoupling of multivariable systems,” *Int. J. Control*, vol. 46, no. 6, pp. 1993–2009, Dec. 1987.

[33] Y. A. Vershinin, “A method of separation of an aircraft motion on a roll and sideslip,”

Aircr. Eng. Aerosp. Technol., vol. 76, no. 2, pp. 179–184, Apr. 2004.

[34] K. Araki and A. Yamamoto, "Application of the Model Reference Adaptive Control with the Constant Trace Algorithm to a Pneumatic Servo," *Proc. JFPS Int. Symp. Fluid Power*, vol. 1989, no. 1, pp. 313–320, 1989.

[35] L. Dugard and I. Landau, "Stochastic model reference adaptive controllers," in *1980 19th IEEE Conference on Decision and Control including the Symposium on Adaptive Processes*, 1980, pp. 1132–1137.

[36] A. Alleyne and J. K. Hedrick, "Nonlinear adaptive control of active suspensions," *IEEE Trans. Control Syst. Technol.*, vol. 3, no. 1, pp. 94–101, Mar. 1995.

[37] E. A. Morelli, "Real-Time Parameter Estimation in the Frequency Domain," *J. Guid. Control. Dyn.*, vol. 23, no. 5, pp. 812–818, Sep. 2000.

[38] G. Tao, *Adaptive Control Design and Analysis*, First. Wiley-Interscience, 2003.

[39] G. C. Goodwin and R. L. Payne, *Dynamic System Identifications: Experiment Design and Data Analysis, Book series: Mathematics in Science and Engineering, vol.136*. Academic Press, 1977.

[40] A. Iggidr, "Controllability, Observability, and Stability of Mathematical Models," in *Encyclopedia of Life Support Systems (EOLSS)*, J. A. Filar, Ed. UNESCO, Eolss Publishers, 2004.

[41] D. A. Caughey, "Introduction to Aircraft Stability and Control Course Notes for M&AE 5070." Sibley School of Mechanical & Aerospace Engineering, Cornell University, Ithaca, New York, 2011.

[42] M. S. Beck and N. E. Gough, "A Model Reference Adaptive Control System using a Cost Function Criterion for Driers and other Dead-time Processes," *Int. J. Control*, vol. 5, no. 1, pp. 55–76, Jan. 1967.

[43] R. LOZANO and I. D. LANDAU, "Redesign of explicit and implicit discrete time model reference adaptive control schemes," *Int. J. Control*, vol. 33, no. 2, pp. 247–268, Feb. 1981.

[44] S. Bose, Y. V. Hote, and S. D. Hanwate, "Analysis of Practical Non-minimum Phase Systems by Transfer Function Approach," in *2018 4th International Conference on Electrical Energy Systems (ICEES)*, 2018, pp. 500–505.

[45] CornellUniversity, "Chapter 4 - Dynamical Equations for Flight Vehicles," *MAE 5070 Dynamics of Flight Vehicles*, 2011. [Online]. Available: https://courses.cit.cornell.edu/mae5070/. [Accessed: 29-Sep-2019].

[46] PearlHarborAviationMuseum, "McDonnell Douglas F-4C Phantom II." [Online]. Available: https://www.pearlharboraviationmuseum.org/exhibits/mcdonnell-douglas-f-4c-phantom-ii-fighter/. [Accessed: 11-Oct-2019].

[47] G. Swanborough and P. M. Bowers, *United States Navy Aircraft Since 1911*. Naval Institute Press, 1990.

[48] R. F. Dorr and C. Bishop, *Vietnam Air War Debrief*. Aerospace Publishing, 1996.

[49] R. K. Heffley and W. F. Jewell, "Aircraft Handling Qualities Data," Washington D.C.,

1972.

[50] U. S. Air Force, “MIL-F-8785C: Military Specification,” Washington D.C., 1980.

[51] M. H. Sadraey, “Design of Control Surfaces,” in *Aircraft Design: A Systems Engineering Approach*, Wiley, 2013.

[52] MathWorks, “System Identification Overview,” *Documentation*, 2019. [Online]. Available: https://www.mathworks.com/help/ident/gs/about-system-identification.html#bsguh6g-1. [Accessed: 14-Oct-2019].

[53] V. Klein and E. A. Morelli, *Aircraft System Identification: Theory and Practice*. AIAA, 2006.

[54] U. S. Air Force, “F-4C Phantom with AGM-12 Bullpups,” 1960. [Online]. Available: https://upload.wikimedia.org/wikipedia/commons/0/0e/F-4C_Phantom_with_AGM-12_Bullpups.jpg. [Accessed: 05-Jun-2019].

[55] I. Barkana, “Adaptive Control? But is so Simple!,” *J. Intell. Robot. Syst.*, vol. 83, no. 1, pp. 3–34, Jul. 2016.

[56] U. S. Air Force, *Flight Manual: USAF Series F-4E Aircraft*. 1979.

[57] L. LeQuella, “What causes an aircraft to roll when rudder is applied,” *StackExchange: Physics*, 2013. [Online]. Available: https://physics.stackexchange.com/questions/49905/what-causes-an-aircraft-to-roll-when-rudder-is-applied. [Accessed: 23-Jul-2019].

[58] M. Thomas, “Why does rudder cause roll?,” *StackExchange: Aviation*, 2016. [Online]. Available: https://aviation.stackexchange.com/questions/24114/why-does-rudder-cause-roll. [Accessed: 23-Jul-2019].

[59] C. Cutler, “How Adverse Yaw Affects Your Plane,” *boldmethod*, 2019. [Online]. Available: https://www.boldmethod.com/learn-to-fly/aerodynamics/how-adverse-yaw-affects-your-plane-during-a-turn/. [Accessed: 23-Jul-2019].

Appendix A - Obtaining the Penalized Control Law from the Cost Function

$$J\left(u_p\right)=\left(y_{ref}-\hat{p}^T\cdot\Phi\right)^2+\gamma\cdot u_p^2 \quad ,\ \gamma>0 \tag{A.1}$$

$$\frac{dJ\left(u_p\right)}{du_p}=0 \tag{A.2}$$

$$\left[\left(y_{ref}-\hat{p}^T\cdot\Phi\right)^2+\gamma\cdot u_p^2\right]'=0\Leftrightarrow$$

$$\left[\left(y_{ref}-\hat{p}^T\cdot\Phi\right)^2\right]'+\left[\gamma\cdot u_p^2\right]'=0\Leftrightarrow$$

$$2\cdot\left[y_{ref}-\hat{p}^T\cdot\Phi\right]'\cdot\left(y_{ref}-\hat{p}^T\cdot\Phi\right)+2\cdot\gamma\cdot u_p=0\Leftrightarrow$$

$$2\cdot\left(\left[y_{ref}\right]'-\left[\hat{p}^T\cdot\Phi\right]'\right)\cdot\left(y_{ref}-\hat{p}^T\cdot\Phi\right)+2\cdot\gamma\cdot u_p=0\Leftrightarrow$$

$$2\cdot\left(0-\left(\left[\hat{p}^T\right]'\cdot\Phi+\hat{p}^T\cdot\left[\Phi\right]'\right)\right)\cdot\left(y_{ref}-\hat{p}^T\cdot\Phi\right)+2\cdot\gamma\cdot u_p=0\Leftrightarrow$$

$$2\cdot\left(0-\left(0+\hat{b}_0\right)\right)\cdot\left(y_{ref}-\hat{p}^T\cdot\Phi\right)+2\cdot\gamma\cdot u_p=0\Leftrightarrow$$

$$\hat{b}_0\cdot\left(y_{ref}-\hat{p}^T\cdot\Phi\right)=\gamma\cdot u_p\Leftrightarrow$$

$$\hat{b}_0\cdot\left(y_{ref}-\left(\hat{b}_0\cdot u_p+\hat{p}_0^T\cdot\Phi_0\right)\right)=\gamma\cdot u_p\Leftrightarrow$$

$$y_{ref}-\hat{b}_0\cdot u_p-\hat{p}_0^T\cdot\Phi_0=\frac{\gamma\cdot u_p}{\hat{b}_0}\Leftrightarrow$$

$$\frac{\gamma\cdot u_p}{\hat{b}_0}+\hat{b}_0\cdot u_p=y_{ref}-\hat{p}_0^T\cdot\Phi_0\Leftrightarrow$$

$$u_p\left(\frac{\gamma}{\hat{b}_0}+\hat{b}_0\right)=y_{ref}-\hat{p}_0^T\cdot\Phi_0\Leftrightarrow$$

$$u_p\left(\frac{\gamma+\hat{b}_0^2}{\hat{b}_0}\right)=y_{ref}-\hat{p}_0^T\cdot\Phi_0\Leftrightarrow$$

$$u_p=\frac{\hat{b}_0\cdot\left(y_{ref}-\hat{p}_0^T\cdot\Phi_0\right)}{\gamma+\hat{b}_0^2} \tag{A.3}$$

To not overload the notation, the variable k is hidden.

Appendix B - Numerical Simulation of Differential Equations

I. Methods

The model of a controlled system is described by:

$\dot{x} = f(x,u)$ (not considering disturbances)

where $x \in \mathbb{R}^n$ is the state vector and $u \in \mathbb{R}^r$ is the control vector.

Notation:

h: simulation step.

$x_k \equiv x(t_k)$, k=0,1,2, …, $t_k = t_{k-1} + h$: time in k step;

$u_k \equiv u(t_k)$.

1. Euler Method

Assuming the given initial value x_0, the system states at t_1, t_2, …, t_k, … are determined by:

$$x_{k+1} = x_k + hf(x_k, u_k)$$

2. Modified Euler Method

Assuming the given initial value x_0, the system states at t_1, t_2, …, t_k, … are determined by:

$$x_{k+1} = x_k + \frac{h}{2}\left(f(x_k, u_k) + f\left(x_k + hf(x_k, u_k), u_k\right)\right)$$

3. Butcher's Algorithm

Assuming the given initial value x_0, the system states at t_1, t_2, …, t_k, … are determined by:

$$x_{k+1} = x_k + \frac{1}{90}(7k_1 + 32k_3 + 12k_4 + 32k_5 + 7k_6)$$

where:

$$k_1 = hf(x_k, u_k),$$
$$k_2 = hf(x_k + k_1/4, u_k),$$
$$k_3 = hf(x_k + k_1/8 + k_2/8, u_k),$$
$$k_4 = hf(x_k - k_2/2 + k_3, u_k),$$
$$k_5 = hf(x_k + 3k_1/16 + 9k_4/16, u_k),$$
$$k_6 = hf(x_k - 3k_1/7 + 2k_2/7 + 12k_3/7 - 12k_4/7 + 8k_5/7, u_k).$$

Appendix C - Papers

Aircraft Pitch Angle Tracking using a Model Reference Adaptive Control

Emanuel C. Castanho

Abstract – A *discrete time explicit Model Reference Adaptive Control (MRAC) with constant trace algorithm is applied to an airplane model in order to test the stability of this type of control during specific flight conditions. Simulations are performed for two examples of pitch angle data, in which two expressions for the control law (classic and penalized) are applied in each example to compare their performance. The adaptive controller shows excellent tracking behavior during all simulations. The choice of the initial simulation conditions is also analyzed, in order to prevent instability problems.*

Keywords*: Adaptive Control, Aircraft Attitude, Discrete Time, MRAC, Parameter Estimation*

Nomenclature

MRAC	Model Reference Adaptive Control
LTI	Linear Time-Invariant
t	Time
d	Time delay
k	Time instant
$\hat{p}$, $\hat{P}$	Estimation parameter vector
F	Adaptation gain matrix
ϕ	Plant variable vector
e^*	"Augmented" filtered plant-model error
y_p	Plant output
u_p	Plant input
y_{ref}	Reference output
u_{ref}	Reference input
γ	Weighting coefficient
$\hat{y}$	Estimated output
u	Longitudinal velocity perturbation
w	Vertical velocity perturbation
q	Pitch rate perturbation
θ	Pitch angle perturbation
η	Elevator angle perturbation

I. Introduction

An aircraft is a dynamic system that changes significantly with speed, altitude, angle of attack, among other factors and in some particular cases may be subject to structural damage and component failure. Control systems such as autopilots and stability augmentation systems were and are still used to correct those changes and eventual problems listed above [1]. These systems were initially based on linear feedback with constant gains that worked well when speeds and altitudes were low. With the implementation of jet engines into aircraft, flight envelopes increased significantly resulting in a wide range of operating conditions. During the 1950s existing autopilots were not able to provide good performance at supersonic flight, so the aerospace industry began experimenting the adaptive control, that would eventually lead to the MRAC by Whitaker [2], [3].

An adaptive control system can adjust its own operation behavior in response to the changes in the dynamics of the plant and the disturbances [1]. This type of controller differentiates from the other types because of its adaptation mechanisms, which mostly rely on the initial knowledge as well as previous and current measurements of the plant being controlled. It works to overcome slowly time varying changes of any parameters of a particular system, while fixed-gain controllers are only suitable for time-invariant systems. Furthermore, modern LTI robust controls, and other fixed-gain controls may decay in performance for large uncertainty. Also, robust controls performance may not be better than the performance of adaptive control when subjected to constant or slow-varying parameters [4].

When the dynamics of the system are not fully known, and their parameters may vary over time, adaptive control can be used to approximate, for instance, aerodynamic parameters. In some cases, when an aircraft is developed and modifications are necessary, a wind tunnel might be an expensive option in terms of schedule and budget, instead an adaptive control can be retrofitted into the existing production flight control system, reducing costs [5].

Gain scheduling is the most used adaptive control method for handling parameter variations in flight control systems since it is usual for an aircraft to have acceptable flying qualities at many points in its flight envelopes. There are, however, flight missions where gain scheduling cannot provide good performance, such as when an aircraft has just released a significant quantity of payload or when is performing rapid maneuvers [6].

MRAC is a possible new flight control technology for aerospace vehicles in the near future [7]. This controller was originally proposed to solve performance

specifications, which are given in terms of a reference model that determines how the process output ideally should respond to an external command signal. The structure of a MRAC system includes a plant with a known structure but unknown parameters, reference model, adaptive law (adjust parameters) and controller (parameterized and provides tracking) [1].

Different types of MRAC with different aeronautical applications, such as airplanes that suffered structural damage [8] or combat aircraft that are considered highly non-linear systems [9], [10], have already been addressed in several papers.

In this paper, it is used a discrete time explicit MRAC design based on the work of Landau and Lozano [11] and other authors [12], [13] in combination with longitudinal flight data, generated from an example aircraft, to compare the performance of a classic control and a penalized control. The plant parameters are unknown to the adaptive controller.

This paper is organized as follows: section II describes the MRAC algorithm in two parts using simple and intuitive notation. In section III, the case of study is presented and how the flight data was generated. In sections IV and V, the full simulation and their results are shown through graphics with the following analysis. Finally, the conclusions about this work are presented in section VI.

II. The MRAC Algorithm

The MRAC system has a feedback loop composed of the plant and the controller and another feedback loop that changes the controller parameters. The parameters are changed on the basis of feedback from the error, which is the difference between the output of the plant and the output of the reference [1]. Adaptive parameter estimation is dynamic, using updated plant signals to produce parameter estimates on-line, this is important where controller parameters need to be updated in real-time as the controlled system is operating [14]. The main advantage of this procedure is that there is no need to store the entire data set as additional measurements are added, thus reducing computational effort.

This section is divided into two parts, together they compose the general algorithm used in the simulation.

II.1. The Adaptation Mechanism

This subsection presents the equations that constitute the adaptation algorithm with time varying adaptation gains for updating the plant parameters. This adaptation mechanism was derived based on an asymptotic stability theorem which simplifies the design, as in [11].

$$\hat{p}(k) = \hat{p}(k-1) + F(k-1)\cdot\phi(k-d)\cdot e^{*}(k) \qquad (1)$$

with:

$$F(k) = \frac{1}{\lambda_1(k)} \times \left[F(k-1) - \frac{F(k-1)\cdot\phi(k-d)\cdot\phi^T(k-d)\cdot F(k-1)}{\lambda_1(k)/\lambda_2(k) + \phi^T(k-d)\cdot F(k-1)\cdot\phi(k-d)} \right]; \quad F(0) > 0 \qquad (2)$$

To make the algorithm implementable an expression for e^*, which depends on the parameters estimated up to *k-1*, is given as:

$$e^{*}(k) = \frac{y_p(k) - \hat{p}^T(k-1)\cdot\phi(k-d)}{1 + \phi^T(k-d)\cdot F(k-1)\cdot\phi(k-d)} \qquad (3)$$

The parameter vector $\hat{p}(k)$ has the following format:

$$\hat{p}_0^T(k) = [\hat{b}_1(k),...,\hat{b}_{n-1}(k),\hat{a}_0(k),...,\hat{a}_{n-1}(k)] \qquad (4)$$

$$\hat{p}^T(k) = [\hat{b}_0(k); \hat{p}_0^T(k)] \qquad (5)$$

The vector ϕ^T has the following format:

$$\phi_0^T(k) = [u_p(k-1),...,u_p(k-n+1), y_p(k),..., y_p(k-n+1)] \qquad (6)$$

$$\phi^T(k) = [u_p(k); \phi_0^T(k)] \qquad (7)$$

The variable *n* is the fixed length of the rectangular window method, having the same value as the system order. For example, a window of *n=2* includes *k=0* and *k=1*.

Each time a new data point is added, an old data point is discarded thus keeping the active number of points equal to *n*. Using the previous example, the window of the next step should include *k=1* and *k=2* to remain with a value of *n=2*. Because of this, the above algorithm requires that the last *n* data points be stored [15].

To complete the introduction of this algorithm, one has:

$$0 < \lambda_1(k) \le 1;\ 0 < \lambda_2(k) < 2 \quad \forall k \qquad (8)$$

The choice of $\lambda_1(k)$ and $\lambda_2(k)$ allows to obtain different types of adaptation algorithms, in this article the constant trace algorithm is used. $\lambda_1(k)/\lambda_2(k)$ is kept constant at value 1, while $\lambda_1(k)$ is adjusted at each time step so that:

$$\lambda_1(k) = \frac{tr\left[F(k-1) - \frac{F(k-1)\cdot\phi(k-d)\cdot\phi^T(k-d)\cdot F(k-1)}{1 + \phi^T(k-d)\cdot F(k-1)\cdot\phi(k-d)} \right]}{tr[F(0)]} \qquad (9)$$

This type of adaptation algorithm ensures better performance compared to others, ensuring better results [11], [12].

II.2. The controller

The type of the cost function and method of minimization determines the properties and performance of the adaptive scheme [16], [17].

Two types of controllers are introduced in this subsection. They will be later compared in terms of stability and operation.

The first control $u_p(k)$ in the adaptive case is given by:

$$u_p(k) = \frac{y_{ref}(k+d) - \hat{p}_0{}^T(k) \cdot \phi_0(k)}{\hat{b}_0(k)} \tag{10}$$

This control will be referred as a classic control (controller 1) in this paper.

In general, before carrying out any simulation, it is not known how the controller 1 will behave towards the initial conditions imposed, being able to present the following limitations:

- Inability to be applied to non-minimum phase systems, i.e. systems whose zeros have positive real parts [18];
- Instability, even if the system is a minimum phase system, the controller itself can provide signals in which the magnitude will increase, making it impossible for the aircraft actuators to reach such values [19].

The aircraft control study cannot be subject to problems due to the previous limitations, so the following cost function J is introduced:

$$J\left(u_p\right) = \left(y_{ref} - \hat{p}^T \cdot \phi\right)^2 + \gamma \cdot u_p^2 \ , \ \gamma > 0 \tag{11}$$

This cost function can be derived:

$$\frac{dJ\left(u_p\right)}{du_p} = 0 \tag{12}$$

To not overload the notation, the variable k is hidden.

The expression that minimizes the solution of (12) is the second control $u_p(k)$, which is given by:

$$u_p(k) = \frac{\hat{b}_0(k) \cdot \left[y_{ref}(k+d) - \hat{p}_0^T(k) \cdot \phi_0(k) \right]}{\gamma + \hat{b}_0^2(k)} \tag{13}$$

This control will be referred as a penalized control (controller 2) in this paper, since it presents a coefficient γ that allows to damp the magnitude of the control.

The aim of those previous algorithms is to generate a control input, by which the plant output measurements go to y_{ref} [12].

In [11], the full algorithm has a polynomial that does not appear in equation (10), because it was considered to be 1. The polynomial is called C_2-polynomial and when is equal to 1 it means that the plant-model error is cancelled d steps after the control input is applied. This C_2-polynomial plays a filtering role and the adaptive control performance will depend on its choice, since it smooths the adaptation process [20].

III. Data Generation

The longitudinal steady-level flight of the McDonnell F-4C Phantom (see Fig. 1) was the basis for generating the measurement data that would be later implemented in the simulation.

Fig. 1. McDonnell F-4C Phantom II [21]

The equations of motion for the aircraft where linearized and the longitudinal state equation is given according to example 4.3 in the Flight Dynamics Principles book, see [22] for more information.

$$\begin{bmatrix} \dot{u} \\ \dot{w} \\ \dot{q} \\ \dot{\theta} \end{bmatrix} = \begin{bmatrix} 7.181 \times 10^{-4} & 4.570 \times 10^{-3} & -29.072 & -9.678 \\ -0.0687 & -0.2953 & 174.868 & -1.601 \\ 1.73 \times 10^{-3} & -0.0105 & -0.4462 & 1.277 \times 10^{-3} \\ 0 & 0 & 1 & 0 \end{bmatrix} \cdot \begin{bmatrix} u \\ w \\ q \\ \theta \end{bmatrix} + \begin{bmatrix} 1.041 \\ -6.294 \\ -4.888 \\ 0 \end{bmatrix} \eta \tag{14}$$

The aircraft motion can be decomposed into a trim and a perturbed motion. The first one is when the aircraft is in an equilibrium for a steady-level flight. The perturbed motion is a small amplitude motion about the trim condition. Because the amplitudes are assumed to be small, linearization of the equations of motion can be performed [7].

With (14) and using the following variations in η over time (15) (square wave format), one can generate data to estimate a linear model through system identification.

In the Simulation Results section only the pitch angle perturbation is analyzed.

$$\eta(t) = \begin{cases} 0 & 0 \le t < 20 \\ 0.1745 & 20 \le t < 40 \\ -0.1745 & 40 \le t < 60 \\ 0 \quad if & 60 \le t < 80 \\ 0.1745 & 80 \le t < 100 \\ -0.1745 & 100 \le t < 110 \\ 0 & 110 \le t < 120 \end{cases} \tag{15}$$

The time step is 0.01s generating a matrix in *Excel* of 12000 rows (from *k=0* to *k=11999*) and 3 columns (*t* in seconds, η in radians, θ in radians).

IV. Simulation

The simulation was carried out considering the aircraft as a 3rd order system, which is equivalent to *n=3*. The initial values of the estimation parameter vector were set as $\hat{p}^T(0) = \begin{bmatrix} 1 & 0 & 0 & 0 & 0 & 0 \end{bmatrix}$ and the time delay was set as equal to 1.

In the first part of the simulation, it was used the values generated in the previous section and the adaptation mechanism introduced in II.1 is applied in order to obtain a vector of parameters, which the best estimation corresponds to *k=11999*. This vector will be used to translate the plant/aircraft behavior.

The previous description is shown schematically in Fig. 2, where u_p corresponds to η values and y_p corresponds to θ values.

In the second part of the simulation, the airplane model is applied to the full algorithm using the initial conditions shown in Table I. Here the parameter vector is updated in real-time so that the adaptive control can make the necessary changes to the control law in order to follow the reference (y_{ref}) to achieve stability and performance goals. In Fig. 3, it is shown the scheme that describes the second part of the simulation.

The second part of the simulation is divided into two examples. In the first example, the set of pitch angle values is a square wave:

$$\theta_{ref}(t) = \begin{cases} 0 & 0 \le t < 24 \\ 0.2618 & 24 \le t < 48 \\ 0 \quad if & 48 \le t < 72 \\ -0.1745 & 72 \le t < 96 \\ 0 & 96 \le t < 120 \end{cases} \tag{16}$$

The time step is 0.01s generating a matrix in *Excel* of 12000 rows (from *k=0* to *k=11999*) and 2 columns (*t* in seconds, θ_{ref} in radians).

In the second example, the set of pitch angle values is the one from the Data Generation section.

In each of those examples a comparison is made between the controllers presented in the subsection II.2.

The schemes from Fig. 2 and Fig. 3 are based on the ones present in [23], with the necessary changes.

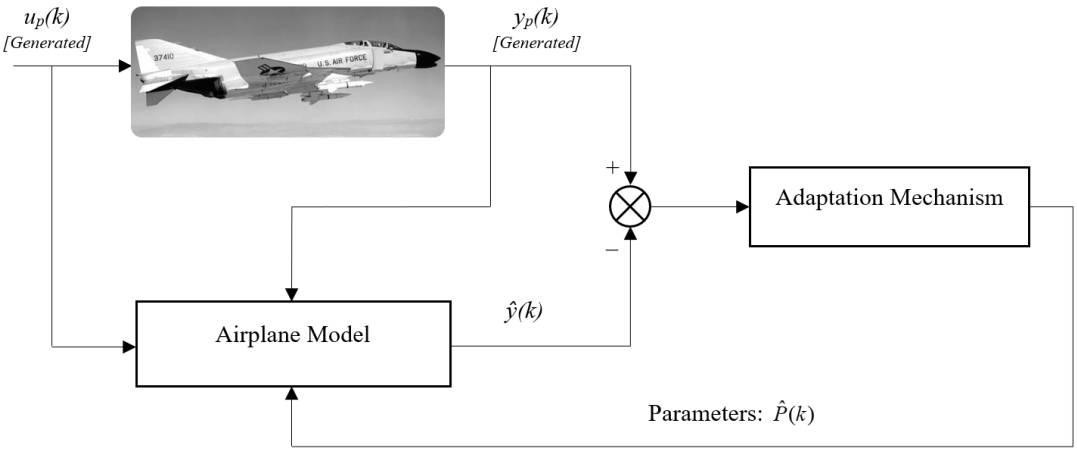

Fig. 2. Scheme to obtain the plant model using generated data

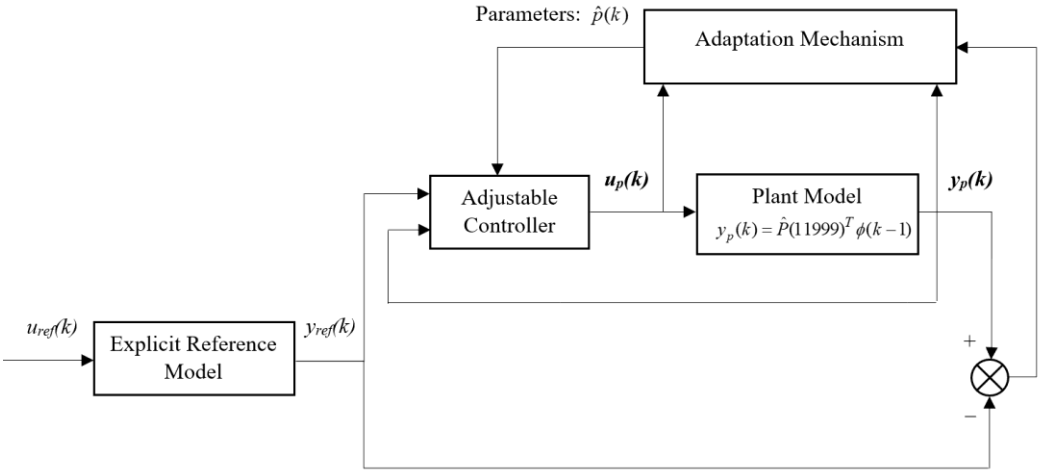

Fig. 3. MRAC scheme used in the simulation

TABLE I
INITIAL SIMULATION CONDITIONS

	Example 1		**Example 2**	
	Controller 1	Controller 2	Controller 1	Controller 2
$u_p(0)$	0.1 rad		0.2 rad	
$y_p(0)$	0.6 rad		2 rad	
$F(0)$	$0.04I$		$0.01I$	
γ	---	0.3	---	0.85

The choice of $F(0)$ will be explained in the next section.

V. Simulation Results

In this section, the simulation results are presented for the pitch angle perturbation when the plant/aircraft is subjected to the model reference adaptive control. These results are compared with the reference signals to check the good convergence performance of the controllers.

V.1. focuses on the first example, where the pitch angle data has a square wave format and V.2. focuses on the second example, where the pitch angle data follows [22].

V.1. Square wave example

In Fig. 4, the classic control is used, and it can be seen in Fig. 4(a) that initially there is a large error between the two graphs up to approximately $k=400$, this is due to the initial conditions assumed and the random values of the initial parameter vectors. In the first pitch angle transition at $k=2400$ there is a small difference between the graphs where y_p reaches a local maximum value of 0.3192 rad, this difference rapidly decreases. The following transitions occur smoothly, the controller can adjust itself very well so that y_p follows y_{ref} as perfect as possible.

It can be seen in Fig. 4(b) that initially there is a significant error up to $k=700$ (approximately), which occurs due to the initial conditions assumed and the random values of the initial parameter vectors that enter the control law.

The controller presents acceptable values, having an absolute maximum elevator angle of 0.6145 rad (35º), the following peaks have less magnitude due to the increased accuracy of the parameters.

In Fig. 5, the penalized control is used, and it can be seen in Fig. 5(a) that initially there is a significant error up to $k=1000$ (approximately), which occurs due to reasons already mentioned. The controller used was penalized with a weight coefficient, so it is observed that y_p does not follow perfectly y_{ref}, however it presents smooth transitions and advantages relatively to the values of u_p reached by this controller. The magnitude of the η peaks from controller 2 is smaller in comparison with the peaks from controller 1, having a local maximum elevator angle of 0.2708 rad (15.5º), as it can be observed in Fig. 5(b).

The detailed analysis of the impulses/peaks shown in Fig. 4(b) and Fig. 5(b) is practically identical, since they are very similar in aspect and quantity, with only differences in magnitude (higher for classic control) and time duration (slightly higher for penalized control).

The controller, after stabilizing the error due to the initial conditions, guarantees to the aircraft 0 rad of pitch angle. At $k=2400$ the reference requires a positive increase of θ, this is guaranteed with the deflection of the elevator that reaches a certain value, but quickly returns to 0 rad. The pitch angle remains at the same value due to manipulation of the aircraft thrust (provided by the propulsion system) and it only returns to 0 rad when the

controller guarantees the opposite deflection. During this time interval, the aircraft is climbing, increasing its altitude. At *k=7200* a pitch angle transition occurs again but now with the opposite signal. In this case, the aircraft is diving, decreasing its altitude. After this transition interval the aircraft returns to $\theta=0$ rad.

V.2. Flight Dynamics Principles book example

This example has data that produces a smooth graph that can be easily controlled. Thus, very pronounced tracking errors between y_p and y_{ref} are not to be expected.

In Fig. 6, the classic control is used. From Fig. 6(a), it can be seen that initially there is an error between the two graphs up to approximately *k=53*, this error quickly disappears. In *k=2000* the first transition of η from 0 rad to 0.1745 rad occurs, which causes in *k=2170* to *k=2540* (approximately) a small tracking error between the two output graphs, nothing too exaggerated. In general, the plant output closely follows the reference output.

In Fig. 6(b), there is initially a significant error up to *k=90* (approximately). The controller presents acceptable values, since although peaks occur, they have a value lower than 0.281 rad (neglecting the initial peaks up to *k=90*) which is acceptable for the deflection of an aircraft control surface. Despite the existence of those peaks, the controller attempts to adapt in order to stabilize itself. The u_{ref} graph is only represented to verify that when the square wave increases or decreases, the controller also tends to follow this behavior.

In Fig. 7, the penalized control is used. The analysis is very similar to Fig. 6 except that, because of γ, this controller presents an y_p slightly deviated from y_{ref} which has the advantage of reducing the initial maximum η value from -0.7712 rad to -0.4739 rad.

It should be noted that in Fig. 6(b) and Fig. 7(b) the goal is not to see u_p following u_{ref}. The representation of u_{ref} in the same plot as u_p is only to observe the ideal behavior of the input relative to the controller.

In the MRAC, the convergence speed of the estimation of parameters increases as the initial value of the adaptation gain increases [12].

The simulation was carried out with a value of $0.04I$ for example 1 and $0.01I$ for example 2, because although the increase of *F(0)* causes an increase of convergence, it also increases the maximum magnitude of the peaks shown in the previous graphs to values not likely to be reached by the aircraft control surfaces. For values close to (bigger than) $0.06I$ both controllers, in both the examples, are unstable, $u_p(k) \to +\infty \; or \; -\infty$, once $\hat{b}_0(k) \to 0$.

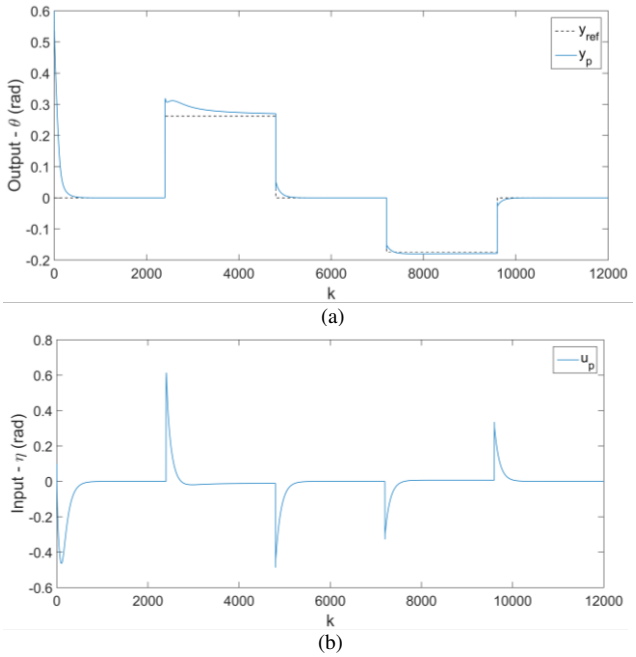

Fig. 4. Example 1 with classic control: (a) Output $y_p(k)$ and $y_{ref}(k)$ (b) Control input $u_p(k)$

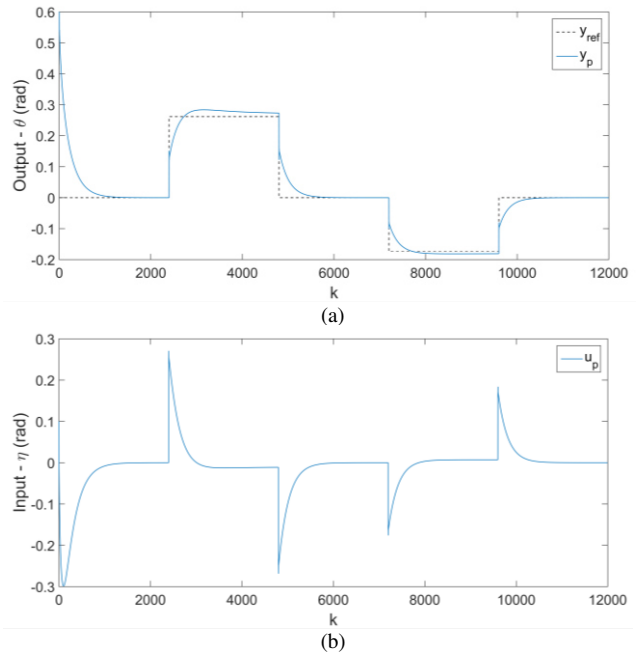

Fig. 5. Example 1 with penalized control: (a) Output $y_p(k)$ and $y_{ref}(k)$ (b) Control input $u_p(k)$

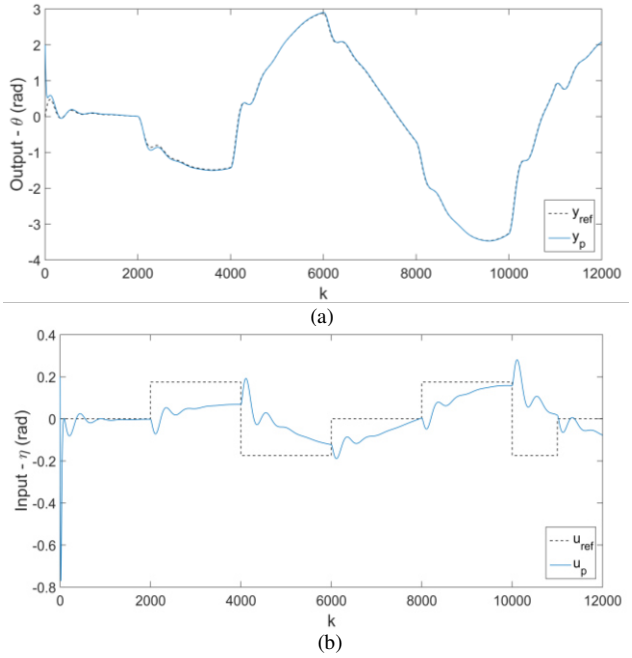

Fig. 6. Example 2 with classic control: (a) Output $y_p(k)$ and $y_{ref}(k)$ (b) Control input $u_p(k)$ and input $u_{ref}(k)$

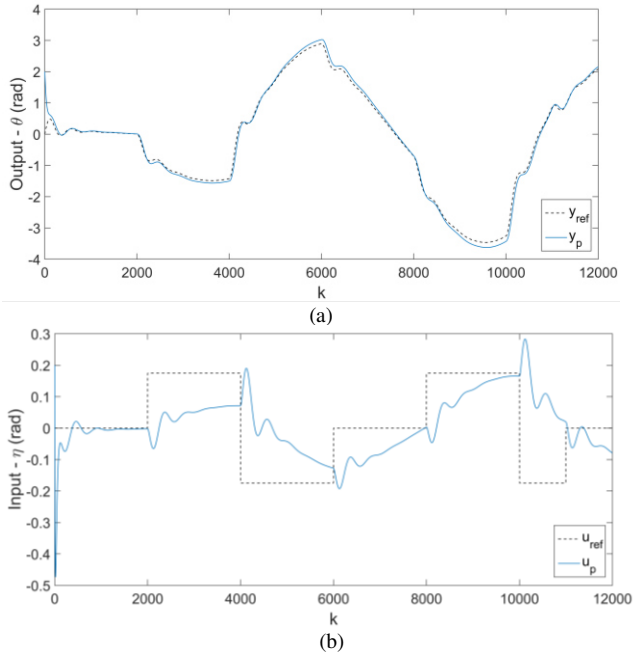

Fig. 7. Example 2 with penalized control: (a) Output $y_p(k)$ and $y_{ref}(k)$ (b) Control input $u_p(k)$ and input $u_{ref}(k)$

VI. Conclusion

This article presented a Model Reference Adaptive Control tested on an example aircraft. The theory of the MRAC that has been shown is applied to a linear plant. So, there may exist some difference between the theory and the practical system, once an aircraft, mainly a fighter-bomber like the F-4C Phantom, is a non-linear system. However, under certain flight conditions, the aircraft can be considered as a linear plant, such as steady-level flight.

Simulation results have shown the importance of choosing the right initial conditions, specifically the adaptation gain matrix. The choice of the type of adaptation algorithm is also essential to obtain the best results.

There has to be a compromise between the energy cost spent by the controller (visible in the graphs by the maximum magnitude of the peaks) and the precision of the plant output to follow the reference, this is verified in the comparison between the classic controller and the penalized one.

The MRAC proved to be very effective when applied in the simulated airplane, becoming a possible candidate for autopilots comparatively to controllers such as gain scheduling.

Some further research topics should include the use of lateral-directional data, the application of the controller to real tests performed on unmanned aircraft, as well as their extension to fully non-linear analysis.

Acknowledgements

This research work was conducted in the Laboratory of Avionics and Control of the university of Beira Interior (Covilhã, Portugal) and supported by the Portuguese Foundation for Sciences and Technology (FCT) and the Aeronautics and Astronautics Research Center (AeroG) of the Associated Laboratory for Energy, Transports and Aeronautics (LAETA).

References

[1] K. J. Astrom and B. Wittenmark, *Adaptive Control* (Dover Publications, 1994). ISBN: 0486462781

[2] W. Black, P. Haghi, and K. Ariyur, Adaptive Systems: History, Techniques, Problems, and Perspectives, *Systems, Vol. 2* (Issue 4): *606–660, November 2014.* https://doi.org/10.3390/systems2040606

[3] K. Aström, Encyclopedia of Systems and Control (Springer London, 2014, pp. 1-9). https://doi.org/10.1007/978-1-4471-5102-9_120-1

[4] S. G. Anavatti, F. Santoso, and M. A. Garratt, Progress in adaptive control systems: past, present, and future, in *2015 International Conference on Advanced Mechatronics, Intelligent Manufacture, and Industrial Automation (ICAMIMIA)*, pp. 1-8. https://doi.org/10.1109/ICAMIMIA.2015.7537196

[5] K. A. Wise, E. Lavretsky, and N. Hovakimyan, Adaptive control of flight: theory, applications, and open problems, in *2006 American Control Conference*, pp. 6. https://doi.org/10.1109/ACC.2006.1657677

[6] D. McLean, *Automatic Flight Control Systems* (Prentice-Hall, 1990). ISBN: 0130540080

[7] N. T. Nguyen, *Model-Reference Adaptive Control: A Primer*

(Springer, 2018).
https://doi.org/10.1007/978-3-319-56393-0

[8] Y. Liu, G. Tao, and S. M. Joshi, Modeling and Model Reference Adaptive Control of Aircraft with Asymmetric Damage, *J. Guid. Control. Dyn.*, *Vol. 33* (Issue 5): *1500-1517, September 2010.*
https://doi.org/10.2514/1.47996

[9] D. Wagner and M. Hromcik, Robust pitch attitude hold with MRAC for a nonlinear light combat aircraft model, in *2017 21st International Conference on Process Control (PC)*, pp. 71-75.
https://doi.org/10.1109/PC.2017.7976191

[10] Y. Shin, A. J. Calise, and M. Johnson, Adaptive Control of Advanced Fighter Aircraft in Nonlinear Flight Regimes, *J. Guid. Control. Dyn.*, *Vol. 31* (Issue 5): *1464-1477, September 2008.*
https://doi.org/10.2514/1.30213

[11] I. D. Landau and R. Lozano, Unification of discrete time explicit model reference adaptive control designs, *Automatica*, *Vol. 17* (Issue 4): *593-611*, *July 1981*.
https://doi.org/10.1016/0005-1098(81)90031-5

[12] K. Araki and A. Yamamoto, Application of the Model Reference Adaptive Control with the Constant Trace Algorithm to a Pneumatic Servo, *Proc. JFPS Int. Symp. Fluid Power*, *Vol. 1989* (Issue 1): *313-320, 1989*.
https://doi.org/10.5739/isfp.1989.313

[13] L. Dugard and I. Landau, Stochastic model reference adaptive controllers, in *1980 19th IEEE Conference on Decision and Control including the Symposium on Adaptive Processes*, pp. 1132-1137.
https://doi.org/10.1109/CDC.1980.271980

[14] G. Tao, *Adaptive Control Design and Analysis* (Wiley-Interscience, 2003).
ISBN: 0471274526

[15] G. C. Goodwin and R. L. Payne, *Dynamic System Identifications: Experiment Design and Data Analysis,* Book series: Mathematics in Science and Engineering, (Academic Press, 1977).
ISBN: 0122897501

[16] P. A. Ioannou and J. Sun, *Robust Adaptive Control* (Prentice-Hall, 1995).
ISBN: 9780134391007

[17] M. S. Beck and N. E. Gough, A Model Reference Adaptive Control System using a Cost Function Criterion for Driers and other Dead-time Processes, *Int. J. Control*, *Vol. 5* (Issue 1): *55-76, January 1967*.
https://doi.org/10.1080/00207176708921743

[18] S. Bose, Y. V. Hote, and S. D. Hanwate, Analysis of Practical Non-minimum Phase Systems by Transfer Function Approach, in *2018 4th International Conference on Electrical Energy Systems (ICEES)*, pp. 500-505.
https://doi.org/10.1109/ICEES.2018.8442413

[19] K. P. Valavanis and G. J. Vachtsevanos, *Handbook of Unmanned Aerial Vehicles* (Springer Netherlands, 2015).
https://doi.org/10.1007/978-90-481-9707-1

[20] R. Lozano and I. D. Landau, Redesign of explicit and implicit discrete time model reference adaptive control schemes, *Int. J. Control*, *Vol. 33* (Issue 2): *247-268, February 1981*.
https://doi.org/10.1080/00207178108922922

[21] U.S. AirForce (public domain), *F-4C Phantom with AGM-12 Bullpups*, 1960. [Online] Available: https://upload.wikimedia.org/wikipedia/commons/0/0e/F-4C_Phantom_with_AGM-12_Bullpups.jpg [Accessed: 05-Jun-2019].

[22] M. V. Cook, *Flight Dynamics Principles: A Linear Systems Approach to Aircraft Stability and Control* (Butterworth-Heinemann, 2007).
ISBN: 9780750669276

[23] I. D. Landau, R. Lozano, M. M'Saad, and A. Karimi, *Adaptive Control: Algorithms, Analysis and Applications* (Springer, 2011).
ISBN: 9780857296641

Authors' information

Department of Aerospace Sciences,
Faculty of Engineering,
University of Beira Interior.
Calçada Fonte do Lameiro, 6201-001, Covilhã, Portugal.
E-mail: emanuelcastanho@hotmail.com

To be submitted

Aircraft lateral-directional motion decoupling using a MIMO Model Reference Adaptive Control

Emanuel C. Castanho*

Department of Aerospace Sciences, University of Beira Interior,
Calçada Fonte do Lameiro, Covilhã 6201-001, Portugal

(Received keep as blank , Revised keep as blank , Accepted keep as blank)

Abstract. Aircraft flight control is an important and interesting subject in which a wide range of engineering skills and efforts are aligned in order to achieve a control design. This paper describes a decoupling adaptive control scheme for a linearized Multi-Input-Multi-Output (MIMO) plant with equal number of inputs and outputs. A modified Model Reference Adaptive Control (MRAC) with constant trace algorithm is the type of adaptive control studied and it is applied to a linearized F-4C Phantom model during specific flight conditions. Simulations are performed in order to verify if the controller is able to handle the coupling relation between some variables in the lateral-directional case, such as lateral velocity, roll angle, aileron angle and rudder angle. The adaptive controller, for the chosen initial conditions, showed good tracking behavior when following the reference output, presenting no drift problems.

Keywords: adaptive control; aircraft; decoupling; lateral-directional attitude; MIMO; MRAC

1. Introduction

An aircraft is a system that changes significantly with fuel consumption, speed, altitude, among other factors (Astrom and Wittenmark 1994; Anavatti, Santoso, and Garratt 2015). Depending on the mission requirements, the non-linear flight dynamics are generally linearized at the operation point, ensuring local stability i.e. satisfactory results close to an equilibrium regime (Valavanis and Vachtsevanos 2015). The linearized equations obtained can be divided into longitudinal and lateral-directional motion (Shan, Hou, and Wang 2017).

In the lateral-directional motion, the yaw and roll axis are always coupled with each other, so one needs to design a multivariable control law that can decouple the various outputs from each other (Bajodah, Mibar, and Ansari 2018; Snell 1998). This is a Multi-Input-Multi-Output (MIMO) problem with high coupling, in which a PID (Proportional-Integral-Derivative) and classical control methods are impractical to yield acceptable results, although being very effective when dealing with Single-Input-Single-Output (SISO) systems (Valavanis and Vachtsevanos 2015; Korul, Tosun, and Isik 2015).

*Corresponding author, M.Eng. Student, E-mail: emanuelcastanho@hotmail.com

In the 1970s and 1980s, the question of robust stability and performance was raised, and modern control methods emerged. This progress over the years provided the theory required for optimizing the controller design for MIMO systems. Since the early 1980s, engineers have been focused upon determining the stability and robustness of MIMO designs in the presence of parameter uncertainties, leading to new methods that complemented and, in some cases, replaced the classical methods (Lavretsky and Wise 2013).

Adaptive systems measure their own performance and operating environment to perform an online estimation of the uncertainties, adapting their own parameters to produce a control input to anticipate, minimize, or overcome the undesirable deviations from the targeted specifications (Valavanis and Vachtsevanos 2015; Black, Haghi, and Ariyur 2014). The time variation of the parameters can account for changes in the flight condition, aircraft configuration changes or various types of failures (Astrom and Wittenmark 1994).

Adaptive controllers are normally designed using methods based on Lyapunov stability theory (Mishkov and Darmonski 2018). Their design for MIMO plant models is more complex than in the SISO case, because of the coupling between inputs and outputs. However, as in the SISO case, the design of an adaptive controller for a MIMO plant can be achieved by combining a control law with an adaptive law that estimates the unknown parameters (Ioannou and Sun 1995).

There are several types of adaptive controllers, the Model Reference Adaptive Control (MRAC) is one of the most popular (Ohkawa and Tomizuka 1991) and it is used in this article avoiding the gain scheduling process, which although it is widely applied in the aeronautical field (McLean 1990), in certain situations might be costly, time consuming and labor intensive (Shin, Calise, and Johnson 2008).

In the MRAC the desired performance of the system is specified by a reference model, and the controller's parameters are adjusted based on the error between the outputs of the plant and the model to ensure good tracking (Astrom and Wittenmark 1994). This control technique allows to easily incorporate considerations of tracking and decoupling in the adaptive design (Bodson and Groszkiewicz 1997).

Several articles have been published over the years addressing adaptive decoupling control of MIMO plants, some examples are the works from Arvanitis (1995), Bayoumi and Mo (1988), and Wittenmark, Middleton and Goodwin (1987). Some authors have applied adaptive decoupling to aeronautic studies. According to Shan, Hou and Wang (2017) there are many researchers who published papers studying the longitudinal dynamics of an aircraft and this type of control problem.

In this paper, it is used a discrete time explicit MRAC design based on the work of Landau and Lozano (1981) in combination with lateral-directional flight data, generated from an example airplane. The MRAC design was modified to decouple the link between the inputs and outputs of the aircraft plant, and the data generated was subjected to sensor noise. The purpose of using decoupling is to control each output of the MIMO system independently (Bayoumi and Mo 1988). Applying the adaptive controller, one will verify how it behaves towards a system with multiple sensors and actuators, and how those variables interact with each other.

To the best knowledge of the authors, there are very few results in the literature about adaptive decoupling applied to a MIMO aircraft plant, using MRAC and during lateral-directional flight. Some close examples include the works from Korul, Tosun and Isik (2015) with the use of MRAC, and Vershinin (2004) with lateral-directional analysis.

This paper is organized as following: in section 2 the problem is identified and explained, section 3 is divided into two parts and presents the MIMO MRAC algorithm used in the

decoupling process. Section 4 describes how the flight data was generated. In sections 5 and 6, the simulation using the flight data and the adaptive controller is carried out and results and their analysis are given. Final remarks are concluded in section 7.

2. Problem statement

The ideal situation in terms of aircraft control during lateral-directional flight is that ailerons are only responsible for rolling and the rudder is only responsible for yaw, consequently changing the lateral velocity. However, in reality there is a coupling relation between those variables.

Most control systems for industrial processes are designed for SISO plants, this is acceptable only if the coupling relations between inputs and outputs are weak (Wittenmark, Middleton, and Goodwin 1987).

Nevertheless, there are many MIMO processes that have strong coupling relations that cannot be disregarded when designing a controller. Thus, it may be desirable to design a controller with decoupling to control the multiple outputs individually (Wittenmark, Middleton, and Goodwin 1987).

Usually, for study and research purposes, a plant can be described by a set of linear time-invariant differential equations with the following state-space form (Bodson and Groszkiewicz 1997)

$$\begin{aligned} \dot{x}(t) &= Ax(t) + Bu(t) \\ y(t) &= Cx(t) + N(t) \end{aligned} \tag{1}$$

where t is the time in seconds, A is the system matrix, B is the input matrix, C is the output matrix, $N(t)$ is the sensor noise vector, $x(t)$ is the state vector, $u(t)$ is the input vector and $y(t)$ is the output vector.

In this study, the plant is an airplane with inputs ($u_p \in \mathbb{R}^2$): aileron angle (ξ) and rudder angle (ζ); and outputs ($y_p \in \mathbb{R}^2$): lateral velocity (v) and roll angle (φ). In Fig. 1 it can be seen the coupling relation between the different variables of the plant.

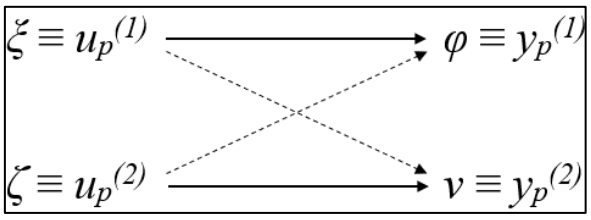

Fig. 1 Coupling relation between variables

where, at each time instant k, the lateral-directional model is given as

$$y_p^{(1)}(k) = \hat{p}^{(1)T}(k-1) \cdot \Phi^{(1)}(k-1) \tag{2}$$

$$y_p^{(2)}(k) = \hat{p}^{(2)T}(k-1) \cdot \Phi^{(2)}(k-1) \tag{3}$$

The parameter vector $\hat{p}(k)$ and the plant variable vector $\Phi(k)$ must translate the decoupling procedure of the strong relation between the multi-variables of the plant.

Therefore, one has the following formats

$$\hat{p}_0^{(1)T}(k) = [\hat{b}_1(k),...,\hat{b}_{n-1}(k),\hat{c}_0(k),...,\hat{c}_{n-1}(k),\hat{a}_0(k),...,\hat{a}_{n-1}(k)] \tag{4}$$

$$\hat{p}^{(1)T}(k) = [\hat{b}_0(k); \hat{p}_0^{(1)T}(k)] \tag{5}$$

$$\Phi_0^{(1)T}(k) = [\xi(k-1),...,\xi(k-n+1),\zeta(k-1),...,\zeta(k-n), y_p^{(1)}(k),..., y_p^{(1)}(k-n+1)] \tag{6}$$

$$\Phi^{(1)T}(k) = [\xi(k); \Phi_0^{(1)T}(k)] \tag{7}$$

$$\hat{p}_0^{(2)T}(k) = [\hat{e}_1(k),...,\hat{e}_{n-1}(k),\hat{f}_0(k),...,\hat{f}_{n-1}(k),\hat{d}_0(k),...,\hat{d}_{n-1}(k)] \tag{8}$$

$$\hat{p}^{(2)T}(k) = [\hat{e}_0(k); \hat{p}_0^{(2)T}(k)] \tag{9}$$

$$\Phi_0^{(2)T}(k) = [\zeta(k-1),...,\zeta(k-n+1),\xi(k-1),...,\xi(k-n), y_p^{(2)}(k),..., y_p^{(2)}(k-n+1)] \tag{10}$$

$$\Phi^{(2)T}(k) = [\zeta(k); \Phi_0^{(2)T}(k)] \tag{11}$$

The set of parameters $\hat{a}$, $\hat{b}$, $\hat{c}$, $\hat{d}$, $\hat{e}$ and $\hat{f}$ are time-varying, and the variable n is the fixed length of the rectangular window method.

Given the measurements ($\Phi_0^{(1)}$ and $\Phi_0^{(2)}$), the parameter vectors should be estimated, and the appropriate controls determined so that they track the desired references. The following section presents the algorithm that intends to solve the referred problem.

3. The modified MRAC algorithm

The first design of a MRAC for discrete time SISO plant was proposed by Ionescu and Monopoli (1977), and the work from Landau and Lozano (1981) is highly based on this type of MRAC.

The general algorithm used in this article has a time delay equal to 1 and it is divided into two parts in this section. Here, the MRAC scheme for SISO plants from Landau and Lozano (1981) is extended to a MIMO plant, applying a decoupling method.

3.1 The adaptive law

The adaptation mechanism is described in this subsection by a set of equations that estimate process parameters. The parameter estimation problem, also referred as system identification

(Valavanis and Vachtsevanos 2015), is done on-line using a collection of available system signals (Astrom and Wittenmark 1994).

Therefore, the estimation parameter vector $\hat{p}$ at each time instant is

$$\hat{p}(k) = \hat{p}(k-1) + F(k-1) \cdot \Phi(k-1) \cdot \varepsilon^*(k) \tag{12}$$

where the adaptation gain matrix is described by

$$F(k) = \frac{1}{\lambda_1(k)} \times \left[F(k-1) - \frac{F(k-1) \cdot \Phi(k-1) \cdot \Phi^T(k-1) \cdot F(k-1)}{\lambda_1(k) / \lambda_2(k) + \Phi^T(k-1) \cdot F(k-1) \cdot \Phi(k-1)} \right]; \tag{13}$$
$$F(0) > 0$$

and the "augmented" filtered plant-model error is given as

$$\varepsilon^*(k) = \frac{y_p(k) - \hat{p}^T(k-1) \cdot \Phi(k-1)}{1 + \Phi^T(k-1) \cdot F(k-1) \cdot \Phi(k-1)} \tag{14}$$

The parameter estimates are calculated at each time sample when new measured data are available, thus the above algorithm requires that some of the data points be stored. This recursive nature avoids reprocessing old data, ensuring an efficient real-time operation and better results (Goodwin and Payne 1977; Astrom and Wittenmark 1994).

To complete the introduction of this algorithm, one needs to choose $\lambda_1(k)$ and $\lambda_2(k)$ in order to obtain different types of adaptation algorithms. In this paper the constant trace algorithm from Araki and Yamamoto (1989) is used, where the ratio between $\lambda_1(k)$ and $\lambda_2(k)$ is maintained equal to 1, while λ_1 is adjusted at each time step according to

$$\lambda_1(k) = \frac{tr\left[F(k-1) - \dfrac{F(k-1) \cdot \Phi(k-1) \cdot \Phi^T(k-1) \cdot F(k-1)}{1 + \Phi^T(k-1) \cdot F(k-1) \cdot \Phi(k-1)} \right]}{tr\left[F(0) \right]} \tag{15}$$

with

$$0 < \lambda_1(k) \leq 1; \;\; 0 < \lambda_2(k) < 2 \quad \forall k \tag{16}$$

Real-time parameter estimation involves iterative adjustment of some variables, such as the variable n, to decide how long into the past the data memory will extend. This is important because, in the context of aircraft flight, there are periods of low or no excitation where the control and state variables are almost constant, leading to numerical problems for some methods (Astrom and Wittenmark 1994).

3.2 The control law

The adaptive control logic presented in the previous subsection will make the necessary changes to the control law to achieve tracking stability and performance goals, matching the plant output with the reference output (y_{ref}) (Astrom and Wittenmark 1994; Araki and Yamamoto 1989).

The type of cost function determines the properties of the adaptive control scheme (Ioannou and Sun 1995; Beck and Gough 1967). The following cost function J is used

$$J\left(u_p(k)\right) = \left(y_{ref}(k+1) - \hat{p}^T(k)\cdot\Phi(k)\right)^2 + \gamma\cdot u_p^2(k) \tag{17}$$

and can be derived as

$$\frac{dJ\left(u_p(k)\right)}{du_p(k)} = 0 \tag{18}$$

The expression that minimizes the solution of Eq. (18) is the controller used in this study, which is given by two different variations for the two inputs

$$u_p^{(1)}(k) = \frac{\hat{b}_0(k)\cdot\left[\, y_{ref}^{(1)}(k+1) - \hat{p}_0^{(1)T}(k)\cdot\Phi_0^{(1)}(k)\right]}{\gamma^{(1)} + \hat{b}_0^2(k)} \tag{19}$$

$$u_p^{(2)}(k) = \frac{\hat{e}_0(k)\cdot\left[\, y_{ref}^{(2)}(k+1) - \hat{p}_0^{(2)T}(k)\cdot\Phi_0^{(2)}(k)\right]}{\gamma^{(2)} + \hat{e}_0^2(k)} \tag{20}$$

Being γ the weighting coefficient and greater than zero.

This is a penalized controller and the aim is to generate a control input for the aircraft plant, that will be further analyzed.

During the execution of the algorithm one must use the two variations of the control law, Eq. (19) to update ξ and Eq. (20) to update ζ, since Φ uses both set of updated values.

4. Case of study

The kinematic behavior of an airplane is translated by a set of non-linear differential equations that can be effectively approximated, during some flight conditions, by a set of equations as Eq. (1).

In this paper, the study was conducted with the linearized motion equations of the McDonnell F-4C Phantom, see Fig. 2. This fighter-bomber and twin engine supersonic jet (Swanborough and Bowers 1990) was the basis for generating the set of measurement data that would be later implemented in the simulation.

Fig. 2 McDonnell F-4C Phantom II (Air Force 1960)

According to the MIL-F-8785C (1980) specification, the F-4 Phantom II can be included in Class IV since it is a fighter/interceptor (high maneuverability airplane). The flight conditions that will be presented in this section have been chosen to provide the Phantom with Category A and Level 1 requirements. Thus, the roll performance of this aircraft is 90º (1.571 rad) of roll angle in 1.3s (US Air Force 1980; Cook 2007).

The lateral-directional state equation for the above airplane is given according to example 4.4 in the Flight Dynamics Principles book

$$\begin{bmatrix} \dot{v} \\ \dot{p} \\ \dot{r} \\ \dot{\varphi} \\ \dot{\psi} \end{bmatrix} = \begin{bmatrix} -0.0565 & 29.072 & -175.610 & 9.6783 & 1.6022 \\ -0.0601 & -0.7979 & -0.2996 & 0 & 0 \\ 9.218\times10^{-3} & -0.0179 & -0.1339 & 0 & 0 \\ 0 & 1 & 0 & 0 & 0 \\ 0 & 0 & 1 & 0 & 0 \end{bmatrix} \cdot \begin{bmatrix} v \\ p \\ r \\ \varphi \\ \psi \end{bmatrix} + \begin{bmatrix} -0.2678 & 2.0092 \\ 4.6982 & 0.7703 \\ 0.0887 & -1.3575 \\ 0 & 0 \\ 0 & 0 \end{bmatrix} \cdot \begin{bmatrix} \xi \\ \zeta \end{bmatrix} \tag{21}$$

where v is in meters per second, p is the roll rate in radians per second, r is the yaw rate in radians per second, φ is in radians, ψ is the yaw angle in radians, ξ is in radians and ζ is in radians.

This equation is simplified, since it is assumed that longitudinal and lateral motion is fully decoupled, which is valid for the majority of airplanes when small perturbation transient motion is only considered (Cook 2007).

Using Eq. (21) with the following variations in ξ and ζ over time shown in Eq. (22) and the initial conditions in Eq. (23), one can apply the Butcher's algorithm with time step equal to 0.01s generating data to simulate the plant's behavior.

$$\xi(t)=\begin{cases}0 & 0\le t<20\\ 0.08727 & 20\le t<30\\ -0.08727 & 30\le t<40\\ 0 & if\quad 40\le t<60\\ -0.08727 & 60\le t<80\\ 0.08727 & 80\le t<100\\ 0 & 100\le t<120\end{cases};\quad \zeta(t)=\begin{cases}0 & 0\le t<20\\ 0.04363 & 20\le t<30\\ -0.04363 & 30\le t<40\\ 0 & if\quad 40\le t<60\\ -0.04363 & 60\le t<80\\ 0.04363 & 80\le t<100\\ 0 & 100\le t<120\end{cases} \tag{22}$$

$$x(0)=\begin{bmatrix}1\\0\\0\\0\\0\end{bmatrix} \tag{23}$$

In the results and discussion section only the lateral velocity and roll angle perturbations are analyzed, so one has

$$\begin{bmatrix}v\\ \varphi\end{bmatrix}=\begin{bmatrix}1 & 0 & 0 & 0 & 0\\ 0 & 0 & 0 & 1 & 0\end{bmatrix}\cdot\begin{bmatrix}v\\ p\\ r\\ \varphi\\ \psi\end{bmatrix}+\begin{bmatrix}N_v\\ N_\varphi\end{bmatrix} \tag{24}$$

In order to obtain a more realistic simulation, the output data is corrupted with sensor noise (Valavanis and Vachtsevanos 2015). N_v is 20% and N_φ is 1% of a Gaussian distribution with 0 mean and variance 1, which according to the original data set, allow to obtain graphics (Figs. 3-4) with slightly noise enough to test the controller.

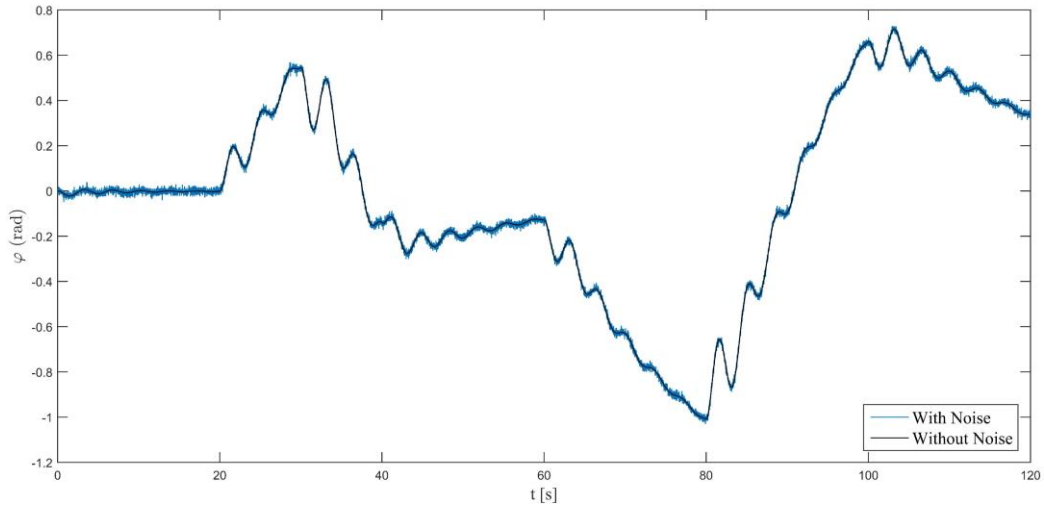

Fig. 3 Roll angle perturbation with and without noise

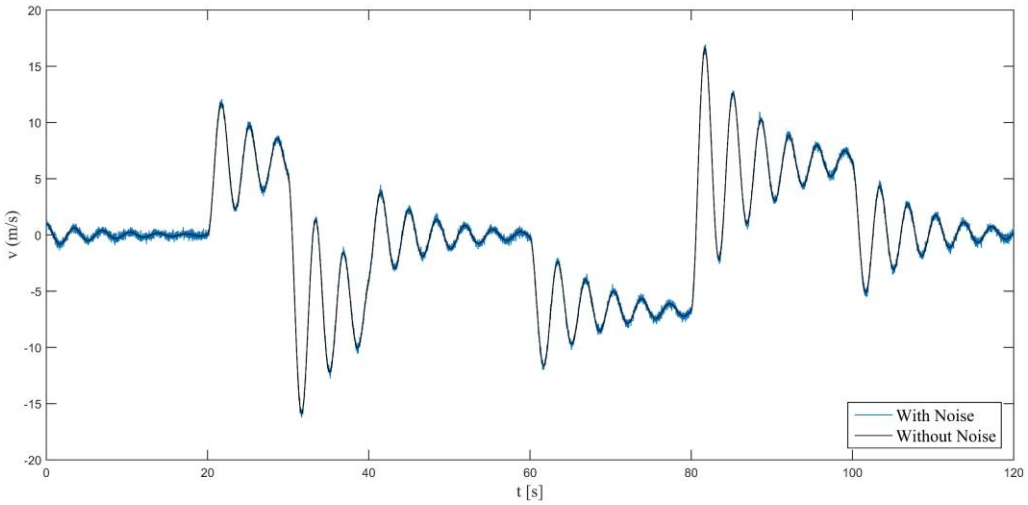

Fig. 4 Lateral velocity perturbation with and without noise

5. Simulation

The aircraft behaves well as a 3rd order system (*n=3*) for the simulation's flight conditions. In order to prevent $\hat{b}_0(k) \to 0$ and $\hat{e}_0(k) \to 0$, the initial values for the estimation vectors, $\hat{p}^{(1)T}(0)$ and $\hat{p}^{(2)T}(0)$, were set as $\begin{bmatrix} 1 & 0 & 0 & 0 & 0 & 0 & 0 & 0 & 0 \end{bmatrix}$.

The data measurement generated in section 4 together with the adaptive law from section 3 are applied in order to obtain a vector of parameters $\hat{P}$, which the best estimation that translates the aircraft behavior, corresponds to *k=11999*. This description is shown schematically in Fig. 5.

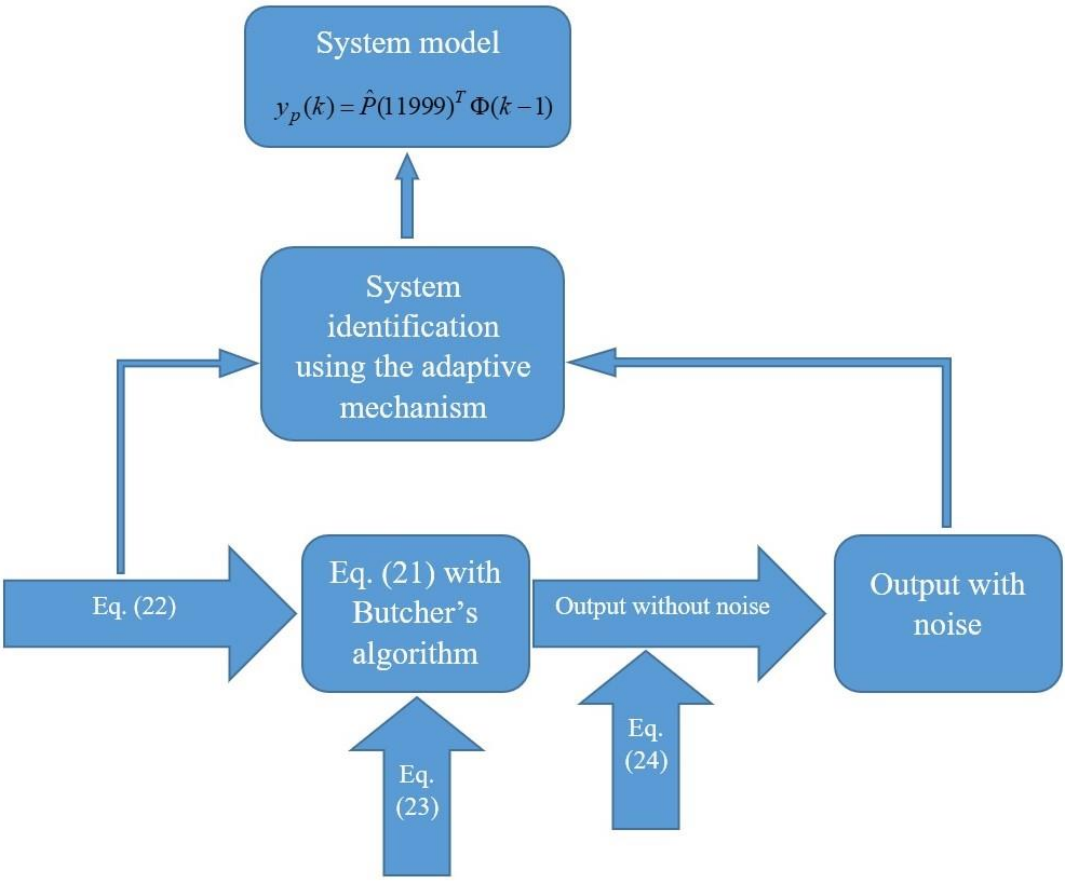

Fig. 5 System identification scheme

The plant model is then used in the MRAC algorithm to behave like an approximation of the real F-4C Phantom, where the initial conditions from Table 1 are essential for the correct operation of the controller. In the full algorithm the parameter vectors are updated in real-time so that the adaptive control can adjust the control law in order to track the reference with acceptable performance. Fig. 6 describes schematically the full MRAC simulation algorithm, where u_{ref} is the reference input, y_{ref} is the reference output and the subscript p indicates a plant variable. This scheme is based on the work from Landau et al. (2011).

Table 1 Initial conditions

Coefficients	Values
$F_{\varphi}(0)^{*}$	$0.5I$
$F_{v}(0)^{*}$	$0.01I$
γ_{φ}	0.95
γ_{v}	0.8
$\xi_{p}(0)$	0.1 rad
$\zeta_{p}(0)$	0.1 rad
$\varphi_{p}(0)$	0.1 rad
$v_{p}(0)$	1 m/s

*The right choice of $F(0)$ is crucial due to instability problems

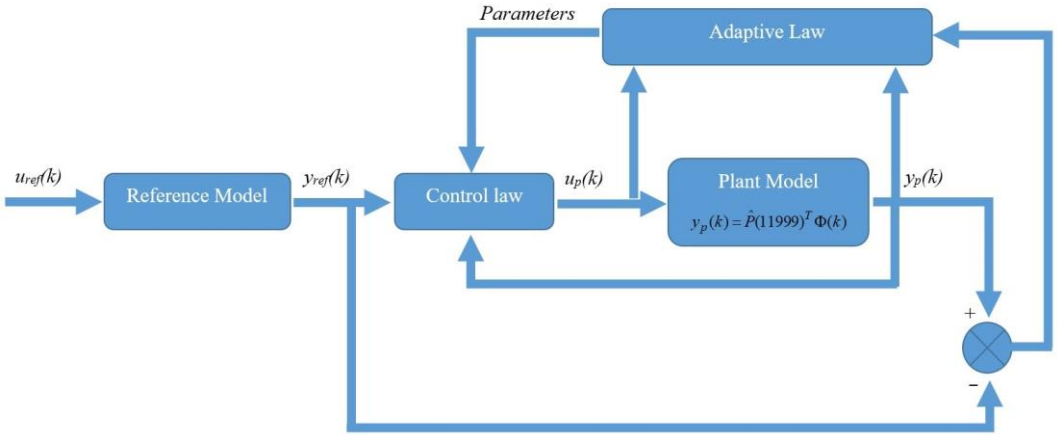

Fig. 6 MRAC scheme

The reference output used to test the controller has a square wave form according to Eq. (25), where the time step is 0.01s.

$$\varphi_{ref}(t) = \begin{cases} 0 & 0 \le t < 24 \\ 0.8 & 24 \le t < 48 \\ 0 & 48 \le t < 72 \\ -0.5 & 72 \le t < 96 \\ 0 & 96 \le t < 120 \end{cases} \quad if \quad ; \quad v_{ref}(t) = \begin{cases} 0 & 0 \le t < 24 \\ 0.5 & 24 \le t < 48 \\ 0 & 48 \le t < 72 \\ -0.5 & 72 \le t < 96 \\ 0 & 96 \le t < 120 \end{cases} \quad if \qquad (25)$$

6. Results and discussion

In this section, the results from the previous simulation are presented for the roll angle and lateral velocity perturbations when the plant is subjected to the modified model reference adaptive control. For an accurate analysis of the results, the positive notation of the angles used in the simulation is represented in Fig. 7.

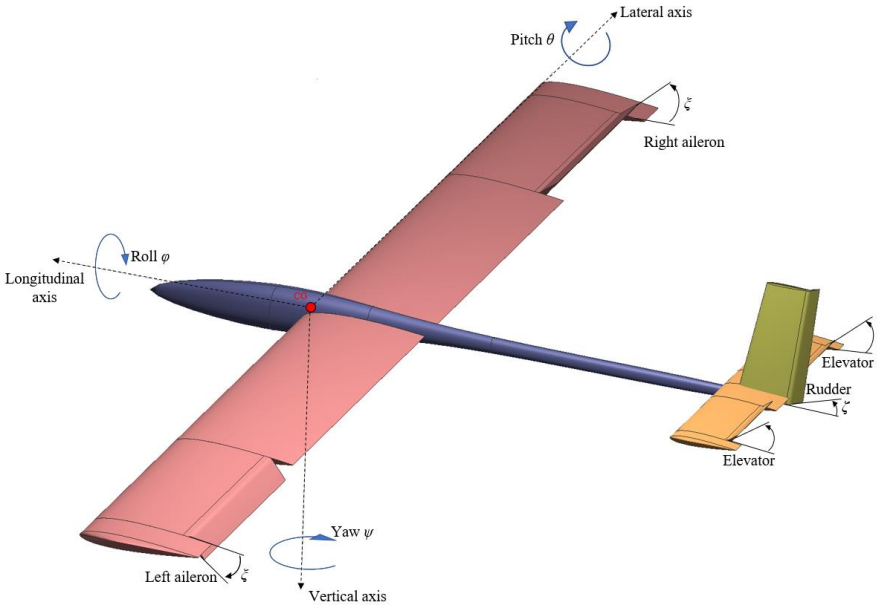

Fig. 7 Positive notation

Since the ailerons act differentially, ξ is considered as the mean value of the two surface angles (Cook 2007).

Due to the lack of data in the literature concerning the maximum deflection values for the Phantom's aileron and rudder control surfaces, it is assumed ±25º (±0.4363 rad). This is an acceptable value for most airplanes, because when the control surfaces are deflected more than 20-25 degrees, flow separation tends to occur (Sadraey 2013).

In Fig. 8, the controller is subjected to the reference output of Eq. (25) and it can be seen in Fig. 8(a) that it adjusts very well to the sudden changes in magnitude. In the roll angle graph, the tracking is almost perfect, with only one initial error between the reference and the plant outputs due to the initial conditions assumed and the random values of the initial parameter vectors. The initial error occurs up to $k=150$ (approximately), where φ_p reaches 0.2026 rad.

In the lateral velocity graph one of the initial conditions was assumed to be 1 m/s, this value is quickly stabilized by the controller after k = 155 (approximately). A peak with value of 1.246 m/s appears with the first variation of the reference's magnitude, however a quick adjustment by the controller is made against this change. It should be noted that a peak also appears on the roll angle graph, but with a smaller magnitude.

In Fig. 8(b) the controller presents values for the aileron and rudder angles within the limits of ±0.4363 rad. There are small errors initially due to the initial conditions assumed and the random

values of the initial parameter vectors that enter in the control law. The aileron angle graph shows maximum values between ±0.4215 rad, these signals are very short in time due to the Phantom's roll performance, which it can perform 1.571 rad of roll angle in 1.3s. The graph of the rudder angle shows maximum values between ±0.2780 rad, these signals are also short in time taking 1.25s (first signal, approximately). This is normal for a military aircraft such as the F-4C Phantom II.

As already mentioned, there is a coupling relation between the variables studied in this article, in which a decoupling process had to be done to control them independently. According to the Phantom's flight manual (US Air Force 1979), the aileron-rudder interconnect system causes rudder deflection proportional to aileron deflection which provides coordinated turns at low airspeeds. To verify this relation between variables, the graphs from Figs. 9-10 present results where one of the reference outputs was maintained at 0 (neutral).

In Fig. 9 the reference lateral velocity is maintained at 0 m/s. From Fig. 9(a) one can say that the roll angle graphic is equal to the graph from Fig. 8(a), however the first one presents a slightly better tracking performance. The lateral velocity graph has a very interesting behavior: although v_{ref} has been established as 0 m/s, the plant's output has peaks with magnitude near to 0 m/s. These peaks suggest that v is related with the other variables, such as ξ.

In Fig. 9(b), the ξ_p graphic is similar to the one from Fig. 8(b), however the peaks have a lower magnitude between ±0.4097 rad. This happens because v_{ref} is zero and the contribution from the ailerons is no longer a big necessity to help changing the lateral velocity. However, the angle values of the ailerons are still quite significant since they depend directly on the roll angle that is not maintained at 0 rad in this part of the simulation.

Almost all values from the ζ_p graph are 0 rad, yet there are peaks with small magnitude that suggest a relation with the roll angle. That is, during the Phantom's roll maneuver, although the ailerons are the main control surfaces used, the rudder also helps.

In Fig. 10 the reference roll angle is maintained at 0 rad. In Fig. 10(a), the graphic of the roll angle initially presents an error due to the initial conditions assumed and the parameter vectors, this error is stabilized after $k=170$ (approximately). These results are interesting: there are peaks with magnitude between ±0.2282 rad in which this value decreases over time, there are also time intervals in which φ_p is approximately ±0.0088 rad (negligible value). Again, these results suggest that φ is related to the other variables, such as ζ.

The values of the lateral velocity between the graphs from Figs. 8(a)-10(a) at first sight are identical, however there is a slightly better tracking in the graph from Fig. 10(a).

There is a significant decrease in the ξ_p magnitude in Fig. 10(b) compared to the values in Fig. 8(b). The values from Fig. 10(b) lie between ±0.1197 rad which indicates that, given the chosen flight conditions, the F-4C ailerons contribute to the lateral velocity variation in addition to the roll angle. The rudder angle is very similar in the graphs of Figs. 8(b)-10(b), there is only a decrease in the magnitude of the small peaks that guarantee return to the neutral position. This is because φ_{ref} is maintained at 0 rad.

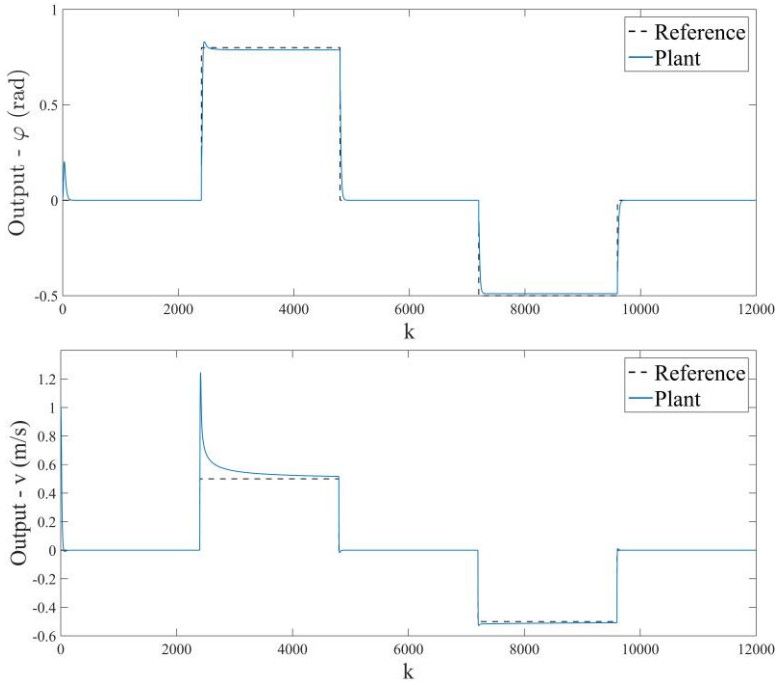

a) Outputs

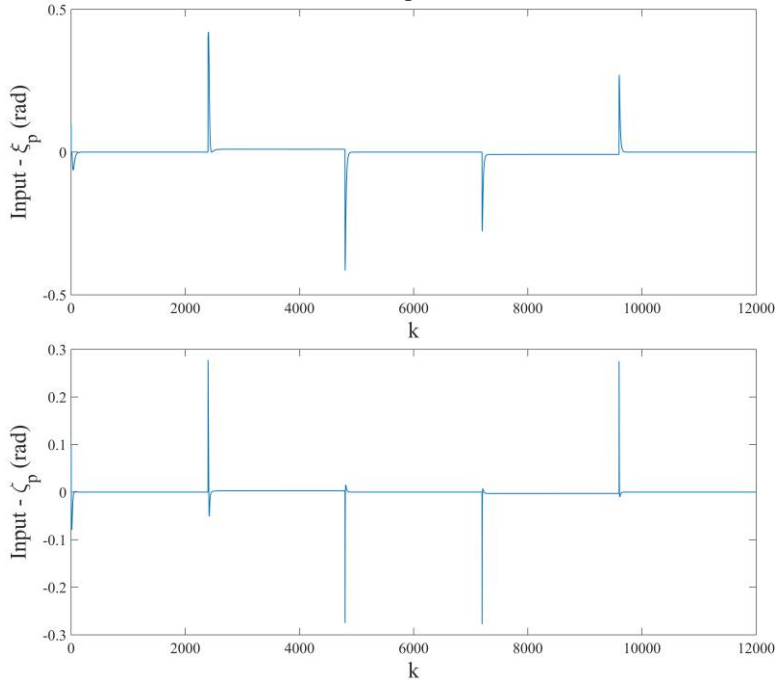

b) Inputs

Fig. 8 Testing the controller with the reference data from Eq. (25)

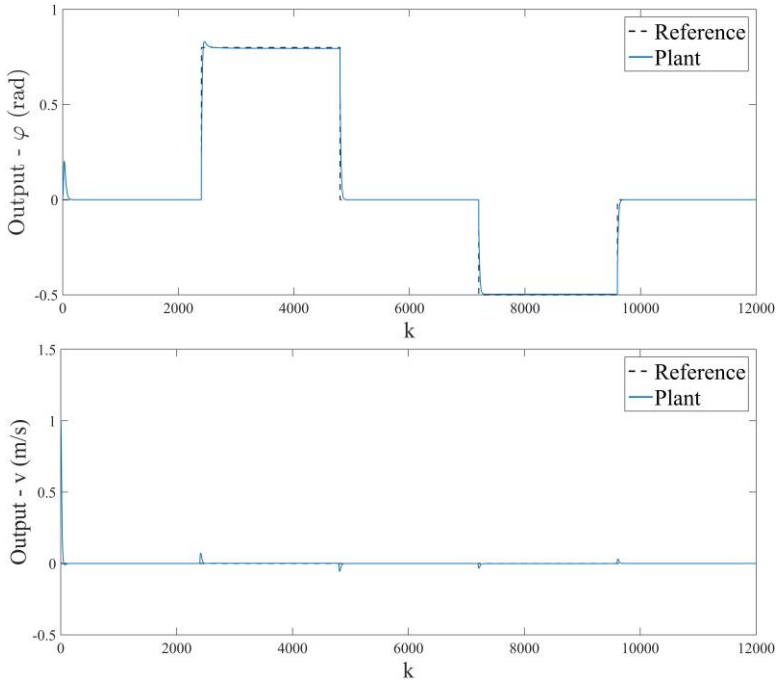

a) Outputs

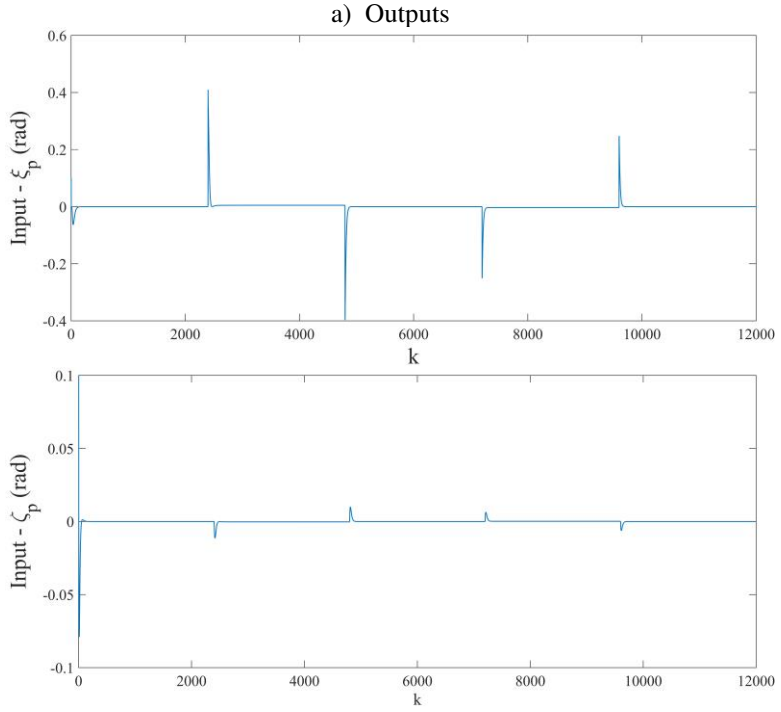

b) Inputs

Fig. 9 Testing the controller with φ_{ref} from Eq. (25) and v_{ref} set to 0

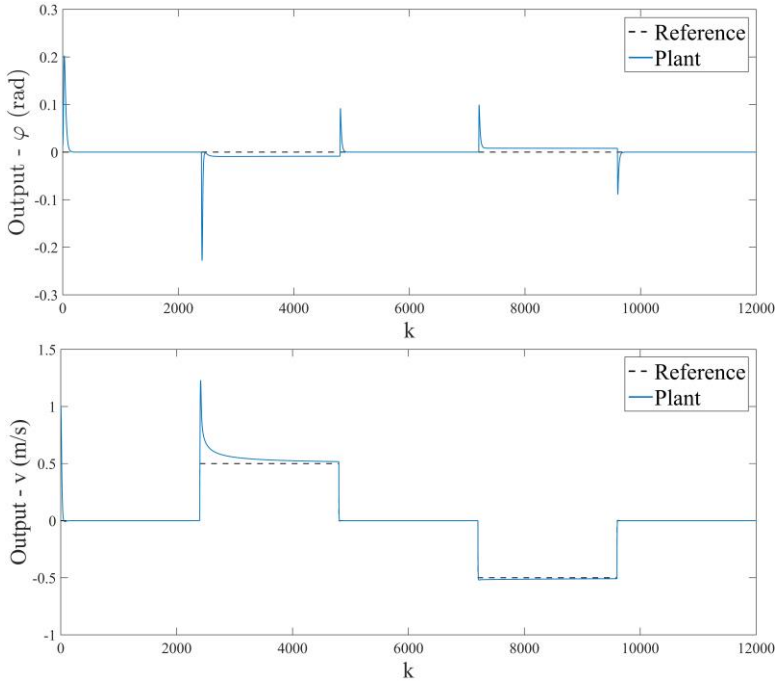

a) Outputs

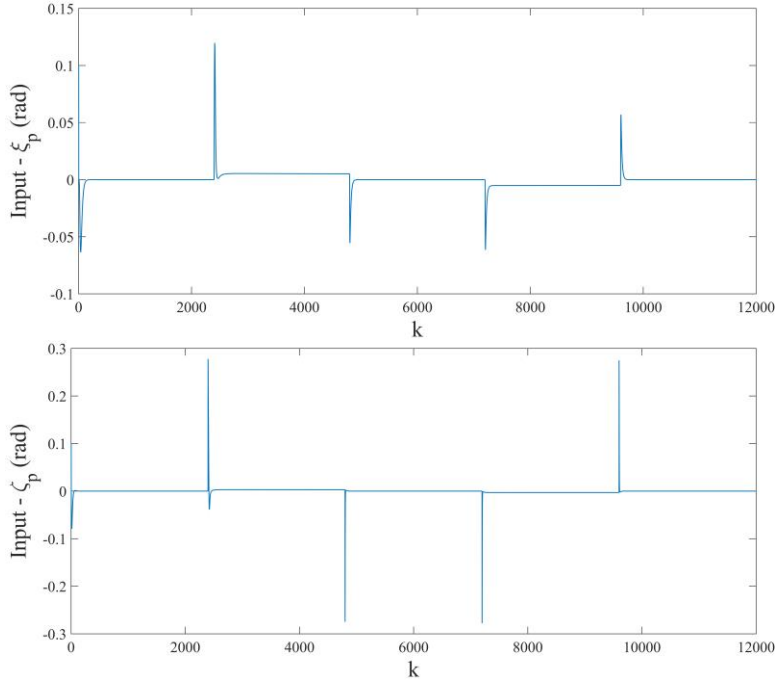

b) Inputs

Fig. 10 Testing the controller with v_{ref} from Eq. (25) and φ_{ref} set to 0

The F-4C Phantom is designed with swept wings, which is the primary mechanism that gives the roll effect to an airplane that may only receive a rudder input. When yaw is introduced, one wing will extend more directly into the wind-stream increasing in airspeed, while the other wing will decrease in airspeed generating less lift than the other, introducing a rolling motion (LeQuella 2013; Thomas 2016).

Varying the angle of the ailerons causes the aircraft to make a rolling motion and may also cause adverse yaw. For instance, as the airplane roll to the right, it may initially yaw to the left, varying the lateral velocity. This occurs in this example because the right aileron creates less lift and less drag than the left aileron that produces more drag and more lift (Cutler 2019).

7. Conclusions

An extended/modified Model Reference Adaptive Control for MIMO plants using decoupling has been presented in this article. The control algorithm has been applied to a linearized plant model of the F-4C Phantom during specific flight conditions, yielding a good tracking performance during the simulation with results that showed the coupling relation between the lateral-directional flight variables studied.

Although lateral-directional flight is simplified by stating that ailerons are responsible for rolling movement and the rudder is the main responsible for lateral velocity, the truth is that ξ also influences the values of v, as well as ζ influences the values of φ.

The challenge in designing an adaptive control that will be applied to a real aircraft is to deal with rate saturation and actuator magnitude. Since a specific flight regime was used in this paper, the authors suggest, as a future research topic, the development of a mechanism that prevents the controller from exceeding control actuation limits set by the aircraft manufacturer. Future works should also include the application of the presented controller to other aircraft types, such as helicopters, and non-linear aircraft models.

Acknowledgments

This research work was conducted in the Laboratory of Avionics and Control of the university of Beira Interior (Covilhã, Portugal) and supported by the Portuguese Foundation for Sciences and Technology (FCT) and the Aeronautics and Astronautics Research Center (AeroG) of the Associated Laboratory for Energy, Transports and Aeronautics (LAETA).

References

Air Force, U.S. (1979), *Flight Manual: USAF Series F-4E Aircraft*.

Anavatti, S., Santoso, F. and Garratt, M. (2015), "Progress in adaptive control systems: past, present, and future", *International Conference on Advanced Mechatronics, Intelligent Manufacture, and Industrial Automation (ICAMIMIA)*, 1-8. https://doi.org/10.1109/ICAMIMIA.2015.7537196.

Araki, K. and Yamamoto, A. (1989), "Application of the model reference adaptive control with the constant trace algorithm to a pneumatic servo", *Proceedings of the JFPS International Symposium on Fluid Power*, **1989**(1), 313-320. https://doi.org/10.5739/isfp.1989.313.

Arvanitis, K.G. (1995), "Adaptive decoupling of linear systems using multirate generalized sampled-data hold functions", *IMA Journal of Mathematical Control and Information*, **12**(2), 157-177. https://doi.org/10.1093/imamci/12.2.157.

Astrom, K.J. and Wittenmark, B. (1994), *Adaptive Control*, (2nd Edition), Dover Publications.

Bajodah, A.H., Mibar, H. and Ansari, U. (2018), "Aircraft motion decoupling of roll and yaw dynamics using generalized dynamic inversion control", *26th Mediterranean Conference on Control and Automation (MED)*, 1-9. https://doi.org/10.1109/MED.2018.8442505.

Bayoumi, M.M. and Mo, L. (1988), "Adaptive decoupling control of mimo system", *IFAC Proceedings Volumes*, **21**(9), 109-113. https://doi.org/10.1016/S1474-6670(17)54711-4.

Beck, M.S. and Gough, N.E. (1967). "A model reference adaptive control system using a cost function criterion for driers and other dead-time processes", *International Journal of Control*, **5**(1), 55-76. https://doi.org/10.1080/00207176708921743.

Black, W., Haghi, P. and Ariyur, K. (2014), "Adaptive systems: history, techniques, problems, and perspectives", *Systems*, **2**(4), 606-660. https://doi.org/10.3390/systems2040606.

Bodson, M. and Groszkiewicz, J.E. (1997), "Multivariable adaptive algorithms for reconfigurable flight control", *IEEE Transactions on Control Systems Technology*, **5**(2), 217-229. https://doi.org/10.1109/87.556026.

Boldmethod (2019), How Adverse Yaw Affects Your Plane; Cutler, C.. https://www.boldmethod.com/learn-to-fly/aerodynamics/how-adverse-yaw-affects-your-plane-during-a-turn/

Cook, M.V. (2007), *Flight Dynamics Principles: A Linear Systems Approach to Aircraft Stability and Control*, (2nd Edition), Butterworth-Heinemann.

F-4C Phantom with AGM-12 Bullpups (1960); Air Force, U.S.. https://upload.wikimedia.org/wikipedia/commons/0/0e/F-4C_Phantom_with_AGM-12_Bullpups.jpg

Goodwin, G.C. and Payne, R.L. (1977), *Dynamic System Identifications: Experiment Design and Data Analysis*, Academic Press.

Ioannou, P.A. and Sun, J. (1995), *Robust Adaptive Control*, Prentice-Hall.

Ionescu, T. and Monopoli, R. (1977), "Discrete model reference adaptive control with an augmented error signal", *Automatica*, **13**(5), 507-517. https://doi.org/10.1016/0005-1098(77)90071-1.

Korul, H., Tosun, D. and Isik, Y. (2015), "A model reference adaptive controller performance of an aircraft roll attitude control system", *Recent Advances on Systems, Signals, Control, Communications and Computers*, https://www.semanticscholar.org/paper/A-Model-Reference-Adaptive-Controller-Performance-Korul-TOSUN/5ca4bef2be5ecce22faff04cd8710a61f3412bee.

Landau, I.D. and Lozano, R. (1981), "Unification of discrete time explicit model reference adaptive control designs", *Automatica*, **17**(4), 593–611. https://doi.org/10.1016/0005-1098(81)90031-5.

Landau, I.D., Lozano, R., M'Saad, M. and Karimi, A. (2011), *Adaptive Control: Algorithms, Analysis and Applications*, Springer.

Lavretsky, E. and Wise, K.A. (2013), *Robust and Adaptive Control with Aerospace Applications*, Springer, London. https://doi.org/10.1007/978-1-4471-4396-3.

McLean, D. (1990), *Automatic Flight Control Systems*, (1st Edition), Prentice-Hall.

MIL-F-8785C: Military Specification. (1980); Air Force, U.S., Washington D.C. http://everyspec.com/MIL-SPECS/MIL-SPECS-MIL-F/MIL-F-8785C_5295/

Mishkov, R. and Darmonski, S. (2018), "Nonlinear adaptive control system design with asymptotically stable parameter estimation error", *International Journal of Control*, **91**(1), 181-203. https://doi.org/10.1080/00207179.2016.1276631.

Ohkawa, F. and Tomizuka, M. (1991), "Model reference adaptive control of a class of nonlinear systems", *IFAC Proceedings Volumes*, **24**(1), 151-155. https://doi.org/10.1016/S1474-6670(17)51312-9.

Sadraey, M.H. (2013), *Aircraft Design: A Systems Engineering Approach*, Wiley.

Shan, S., Hou, Z. and Wang, W. (2017), "Aircraft longitudinal decoupling based on a singular perturbation approach", *Advances in Mechanical Engineering*, **9**(9), 1-8. https://doi.org/10.1177/1687814017727474.

Shin, Y., Calise, A.J. and Johnson, M. (2008), "Adaptive control of advanced fighter aircraft in nonlinear flight regimes", *Journal of Guidance, Control, and Dynamics*, **31**(5), 1464-1477.

https://doi.org/10.2514/1.30213.
Snell, A. (1998), “Decoupling control design with applications to flight”, *Journal of Guidance, Control, and Dynamics*, **21**(4), 647–655. https://doi.org/10.2514/2.4284.
StackExchange: Aviation (2016), Why Does Rudder Cause Roll?; Thomas, M.. https://aviation.stackexchange.com/questions/24114/why-does-rudder-cause-roll
StackExchange: Physics (2013), What Causes an Aircraft to Roll When Rudder Is Applied; LeQuella, L.. https://physics.stackexchange.com/questions/49905/what-causes-an-aircraft-to-roll-when-rudder-is-applied
Swanborough, G. and Bowers, P.M. (1990), *United States Navy Aircraft Since 1911*, Naval Institute Press.
Valavanis, K.P. and Vachtsevanos, G.J. (2015), *Handbook of Unmanned Aerial Vehicles*, Springer, Dordrecht, Netherlands.
Vershinin, Y.A. (2004), “A method of separation of an aircraft motion on a roll and sideslip”, *Aircraft Engineering and Aerospace Technology*, **76**(2), 179-184. https://doi.org/10.1108/00022660410526042.
Wittenmark, B., Middleton, R.H. and Goodwin, G.C. (1987), “Adaptive decoupling of multivariable systems”, *International Journal of Control*, **46**(6), 1993-2009. https://doi.org/10.1080/00207178708934029.